CLEAN WATER WATER POLLUTION CONTROL RESEARCH SERIES ● 16130 DJU 02/71

AN ANALYTICAL AND EXPERIMENTAL INVESTIGATION OF SURFACE DISCHARGES OF HEATED WATER

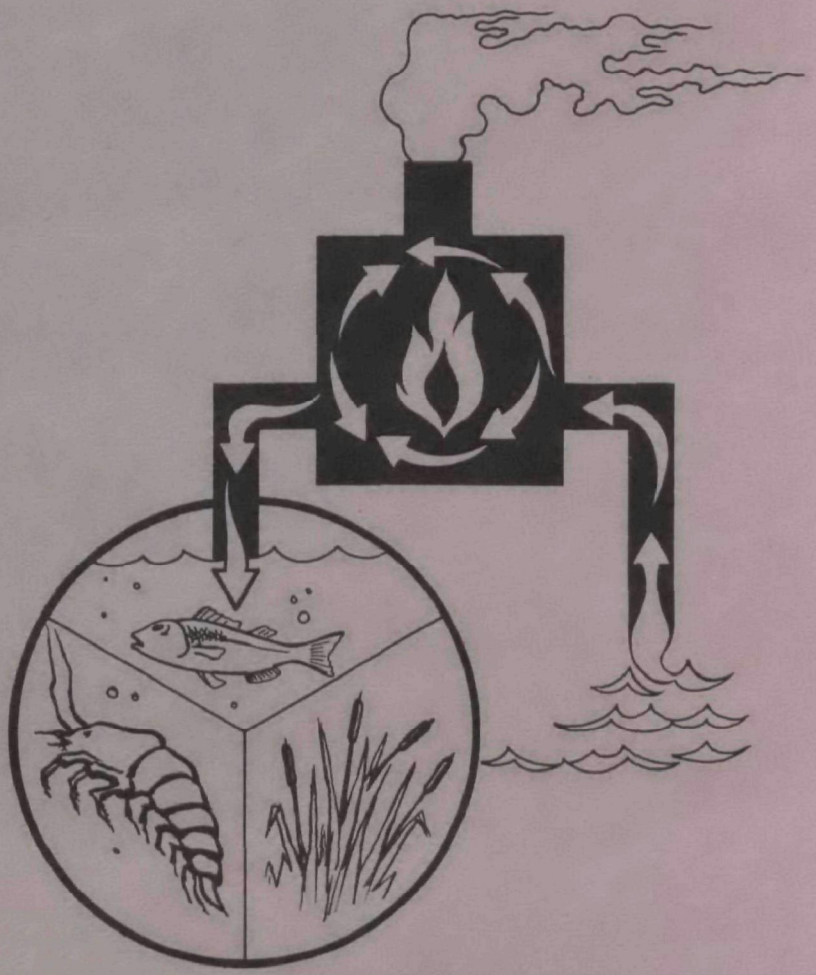

ENVIRONMENTAL PROTECTION AGENCY ● WATER QUALITY OFFICE

WATER POLLUTION CONTROL RESEARCH SERIES

The Water Pollution Control Research Series describes the results and progress in the control and abatement of pollution of our Nation's waters. They provide a central source of information on the research, development, and demonstration activities of the Water Quality Office, Environmental Protection Agency, through inhouse research and grants and contracts with Federal, State, and local agencies, research institutions, and industrial organizations.

Inquiries pertaining to the Water Pollution Control Research Reports should be directed to the Head, Project Reports System, Office of Research and Development, Water Quality Office, Environmental Protection Agency, Washington, D.C. 20242.

AN ANALYTICAL AND EXPERIMENTAL INVESTIGATION OF SURFACE DISCHARGES OF HEATED WATER

by

Keith D. Stolzenbach

and

Donald R. F. Harleman

RALPH M PARSONS LABORATORY

FOR WATER RESOURCES AND HYDRODYNAMICS

Department of Civil Engineering

Massachusetts Institute of Technology

Cambridge, Massachusetts 02139

for the

WATER QUALITY OFFICE

ENVIRONMENTAL PROTECTION AGENCY

Research Grant No. 16130 DJU

February, 1971

For sale by the Superintendent of Documents, U.S. Government Printing Office
Washington, D.C., 20402 - Price $1.75

EPA Review Notice

This report has been reviewed by the Water Quality Office, EPA, and approved for publication. Approval does not signify that the contents necessarily reflect the views and policies of the Environmental Protection Agency, nor does mention of trade names or commercial products constitute endorsement or recommendation for use.

ABSTRACT

The temperature distribution induced in an ambient body of water by a surface discharge of heated condenser cooling water must be determined for evaluation of thermal effects upon the natural environment, for prevention of recirculation of the heated discharge into the cooling water intake, for improved design of laboratory scale models and for insuring that discharge configurations meet legal temperature regulations.

An analytical and experimental study of discharges of heated water is conducted. The discharge is a horizontal, rectangular open channel at the surface of a large ambient body of water which may have a bottom slope or a cross flow at right angles to the discharge. Of interest is the dependence of the temperature distribution in the receiving water as a function of the initial temperature difference between the heated discharge and the ambient water, the initial discharge velocity, the geometry of the discharge channel, the bottom slope, the ambient cross flow, and the transfer of heat to the atmosphere through the water surface.

The theoretical development assumes that the discharge is a three-dimensional turbulent jet with an unsheared initial core and a turbulent region in which the velocity and temperature distributions are related to centerline values by similarity functions. Horizontal and vertical entrainment of ambient water into the jet is proportional to the jet centerline velocity by an entrainment coefficient. The vertical entrainment is a function of the local vertical stability of the jet and the buoyancy of the discharge increases lateral spreading. A cross flow deflects the jet by entrainment of lateral momentum and a bottom slope inhibits vertical entrainment and buoyant lateral spreading.

Experiments are performed in a laboratory basin in which all of the relevant parameters, including the cross flow and the bottom slope, are varied and three-dimensional temperature measurements are taken in the heated discharge.

The experiments verify that the theoretical model predicts the behavior of heated discharges. The theory contains no undetermined parameters and the comparison of the experimental and theoretical results does not involve any fitting of the theory to data. The rate of temperature decrease in the jet and the vertical and lateral spreading are controlled by the initial densimetric Froude number, the ratio of channel depth to width, and the bottom slope. A cross flow deflects the jet but does not greatly affect the temperature distribution. Heat loss does not significantly affect the temperature distribution in the heated discharge within the region treated by the theory.

Application of the theory to prediction of temperatures in an actual heated discharge is possible if the temperatures, velocities, and the geometry of the discharge may be schematized by representative steady state temperatures

and velocities and by an equivalent rectangular channel. If a model study is necessary the theory indicates that temperature similarity requires an undistorted model.

The theoretical model developed in this study may be extended by treating a stratified ambient condition, by considering recirculation of the heated jet in a finite enclosure and by development of a theory for the transition of the heated discharge jet into a buoyant plume.

This report was submitted in fulfillment of Research Grant No. 16130 DJU between the Water Quality Office, Environmental Protection Agency and the Massachusetts Institute of Technology.

Key words: thermal pollution; turbulent, buoyant jets; stratified flow; temperature prediction; heated surface discharges.

ACKNOWLEDGEMENT

This investigation was supported by the Water Quality Office, Environmental Protection Agency, under Research Grant No. 16130 DJU as part of a research program entitled "Prediction and Control of Thermal Pollution". The project officer was Mr. Frank Rainwater, Chief, National Thermal Pollution Research Program, Pacific Northwest Water Laboratory, at Corvallis, Oregon. The cooperation of Mr. Rainwater is gratefully acknowledged.

Stone and Webster Engineering Corporation of Boston, Massachusetts, supported the purchase of experimental equipment in conjunction with another research project.

The research program was administered at M.I.T. under DSR 71335 and 72324. The staff and students at the Ralph M. Parsons Laboratory for Water Resources and Hydrodynamics gave valuable suggestions throughout the study. The experimental work could not have been performed without the particular help of Mr. Umit Unluata, Miss Alician Quinlan, Mr. Edward McCaffrey and Mr. Roy Milley. Typing was done by Miss Kathleen Emperor. All computer work was done at the M.I.T. Information Processing Center.

The material contained in this report was submitted by Mr. Stolzenbach in partial fulfillment of the requirements for the degree of Doctor of Philosophy at M.I.T.

TABLE OF CONTENTS

I. Introduction

1.1 Why Heated Discharges?

The discharge of heated water into rivers, lakes and coastal regions has its roots in the growth of demand for electric power and in the economics of power production. The demand for power generating capacity in the United States is expected to continue doubling each decade. As hydro power plant sites are developed to their full capacity, the demand will be met increasingly by fossil fuel and nuclear steam plants. Regional economics and economics of scale result in an increase in plant size; often fuel costs make nuclear plants more economic than coal or oil facilities (6).

The heat rejected by a steam power plant is related to the thermodynamic efficiency of the power production process. Present levels of efficiency are about 40% for coal and oil plants and about 30% for nuclear plants. The nuclear plants reject significantly larger amounts of heat: 10,000 BTU/kwh vs. 6,000 BTU/kwh (10). Present levels of efficiency are determined by the economics of power plant design and are mostly a function of the cost of capital items such as turbines and condensers. Water is the only economic cooling fluid for large power plants and at present the costs of its supply and of the heat disposal system do not greatly influence the choice of economic efficiency. Significant technological improvements in the efficiency of conventional steam cycles or the development of more efficient thermal power generating methods are not foreseen in the near future (6).

The total volume of cooling water used for all industries in

the United States is fifty percent of all water use; the power industry accounts for all but ten of that fifty percent (19). The large volumes are dictated by the economic design of the cooling systems which require low operating temperatures and high flows.

Thus the amount of heat rejected, the volume of water required, and the temperature rise in the cooling system necessary to satisfy the demand for power are determined largely by in-plant technological and economic considerations not related to the ultimate heat disposal process or its effect upon the environment.

The choice of heat disposal systems for a given power plant site reflects the relatively fixed constraints on temperatures and flows. Economic re-use of waste heat for domestic or industrial purposes is inhibited by the low temperature uses and the large flows dictated by the plant design. The rejected heat must in most cases be returned to the natural environment. The present methods for heat disposal are cooling towers, cooling ponds, and once-through cooling. For a 1000 MW power plant unit the cost of cooling towers may be $10,000,000 and the cost of purchasing land for a cooling pond as high as $5,000,000. The once-through cooling method, in which water is withdrawn from an adjacent waterway and returned after being heated, is the most economical assuming the availability of the natural water (6).

1.2 Effects of Heated Discharges

Balancing the economic benefits of once-through cooling is the impact which the discharge has upon the natural environment and how this in turn affects the power plant directly and the users of the

power plant indirectly.

The most immediate undesirable effect of the heated discharge upon the power plant is the recirculation of the heated water into the intake, creating a feedback of heat which significantly raises the temperature of the cooling water. The resulting reduction in plant efficiency is considered as a cost to the power company. Prevention of recirculation was the major concern in the design of a discharge system before the era of large nuclear plants and public concern over thermal effects. Separation of the intake and discharge structures or the design of the intake as a selective withdrawal device are the most common techniques of preventing recirculation. A knowledge of the flow and temperature distribution in the receiving waters near the heated discharge is necessary for proper location and design of the intake for the prevention of recirculation.

The indirect effects of heated discharges are related to the changes in physical and chemical properties of water resulting from a temperature rise. As the temperature of water increases the density, viscosity and ability to dissolve gases decrease while the vapor pressure of water increases. The effects of these changes may be striking: density differences, although small, may produce stable stratified flows which differ markedly from natural flow patterns; and evaporative water losses are increased as vapor pressure rises. Dissolved oxygen, a prime indicator of water quality, may decrease. Biochemical reactions which consume oxygen and produce undesirable tastes and odors are promoted by increases in water temperature. Higher level species such as fish or

shellfish may not survive exposure to high temperatures or may have vital life cycles inhibited by temperature rises (19).

The above effects have been lumped together under the title of "thermal pollution" since the undesirable changes in the environment are the result of discharges of heat. Prediction of the response of the environment to increases in temperature is still at a very basic level; a fundamental requirement for such an evaluation is always a knowledge of the temperature distribution induced in the receiving water by the heated discharge.

1.3 Temperature Prediction

Once-through cooling systems are characterized by an intake and a discharge structure. The water velocity at the intake, for a given pumping rate, is a function of intake design since converging flow structures are not complicated by extreme flow separation. The minimum possible discharge velocity, however, is usually closely related to the in-plant velocity since special efforts must be made to de-accelerate a water flow. Economic power plant design velocities are typically of the order of 5 to 10 ft. per second. Thus even for a designed area increase of ten times the discharge velocity is near 1 ft. per second. This is in general higher than many ambient flow velocities in rivers and coastal areas. At the point of discharge the momentum of the discharge is significantly greater than that of the receiving fluid and jet-like mixing of the heated and ambient water occurs. Ambient water is entrained into the discharge jet and the average temperature and velocity of the heated flow are reduced. Further from the discharge

point the jet velocity is reduced to the magnitude of the ambient currents. In this region, entrainment does not occur and the temperature distribution is determined by natural turbulent diffusion and convection. Ultimately, all of the rejected heat is passed to the atmosphere through the water surface, a process driven by the elevation of the water surface temperature. The density difference between the heated discharge and the ambient water may inhibit mixing in the initial jet region and may promote spreading of the discharge as a heated layer.

The temperature distribution induced by a heated discharge is thus determined near the outlet by jet-like diffusion and in an outer region by natural processes. Surface heat loss and density effects occur throughout the flow. The interrelationship of these processes is very complex. Some basic understanding of each phenomena alone has been achieved: turbulent jet theory and solutions to convective diffusion equations are well established and predictions of surface heat loss rates are now possible. The effects of stratification are the least understood. Analytical predictions of temperatures in the vicinity of heated discharges are possible under the assumption that the flow is either a pure jet, a plume, or a stagnant cooling region.

Often it is not possible to isolate the dominant physical process and the flow may be significantly affected by density gradients or the presence of solid boundaries. It is customary in such cases to construct a physical model of the discharge and ambient waterway. Unfortunately model scaling laws must be based on an understanding of the very process which the model is supposed to reproduce. It is

often impossible, at the present level of knowledge about heated discharges, to build a model which accurately replicates all of the important features of the temperature distribution.

For a given cooling water flow the performance of the discharge structure is a function of its location, size and shape. Submerged jets achieve greater mixing than surface discharges. The presence of an ambient cross current increases natural heat dispersion while solid boundaries inhibit mixing. Several small orifices of high velocity produce more mixing than a single large one. The cost of the discharge structure varies widely from the case of a simple pipe ending at the water surface to a deeply submerged multiple port diffuser. Economical design of the discharge requires the least expensive configuration which will meet the restrictions imposed on the temperature distribution for prevention of recirculation and thermal pollution. In particular federal and state standards are presently expressed in terms of the permissible area in which a certain temperature rise, usually from 1.5 to 5°F, is permitted. The power company must prove before construction permits are granted that the design of the discharge structure will meet the legal standard. The pressing demand for new power facilities requires that accurate methods for relating discharge design to the temperature distribution induced by the heated discharge be developed.

1.4 Objectives of this Study

This investigation is motivated by the need, as discussed in previous sections, for accurate temperature prediction techniques which consider the effect of power plant condenser water discharge design upon the temperature distribution in the ambient water. Prevention

of recirculation, evaluation of thermal effects, construction of reliable scale models, and economical design of discharge structures require an understanding of the physics of heated discharges.

The following general problem is considered: A horizontal surface discharge of heated water from a rectangular open channel of arbitrary width and depth into a large unstratified body of water which may be stagnant or flowing with an arbitrary velocity distribution at right angles to the direction of discharge and which may be infinitely deep or may have a sloping bottom. The temperature and velocity distribution in the discharge are considered as functions of the discharge channel geometry, the initial velocity and temperature rise, the magnitude of the ambient cross flow and bottom slope, and the surface heat transfer rate. The discharge is considered only to the point where jet-like behavior ceases and natural turbulence and convection dominate the temperature and velocity distributions.

Figure 1-1 shows a schematic of the discharge scheme and the relevant parameters. This problem is chosen because:

1) Often the allowable mixing zone, as defined by temperature standards, is within the initial jet region.
2) Turbulent diffusion, density gradients, and surface heat loss may be studied within the defined region.
3) The number of controlling factors is relatively few.
4) The discharge may be studied on a laboratory scale, thereby allowing accurate measurements and close control of all parameters.

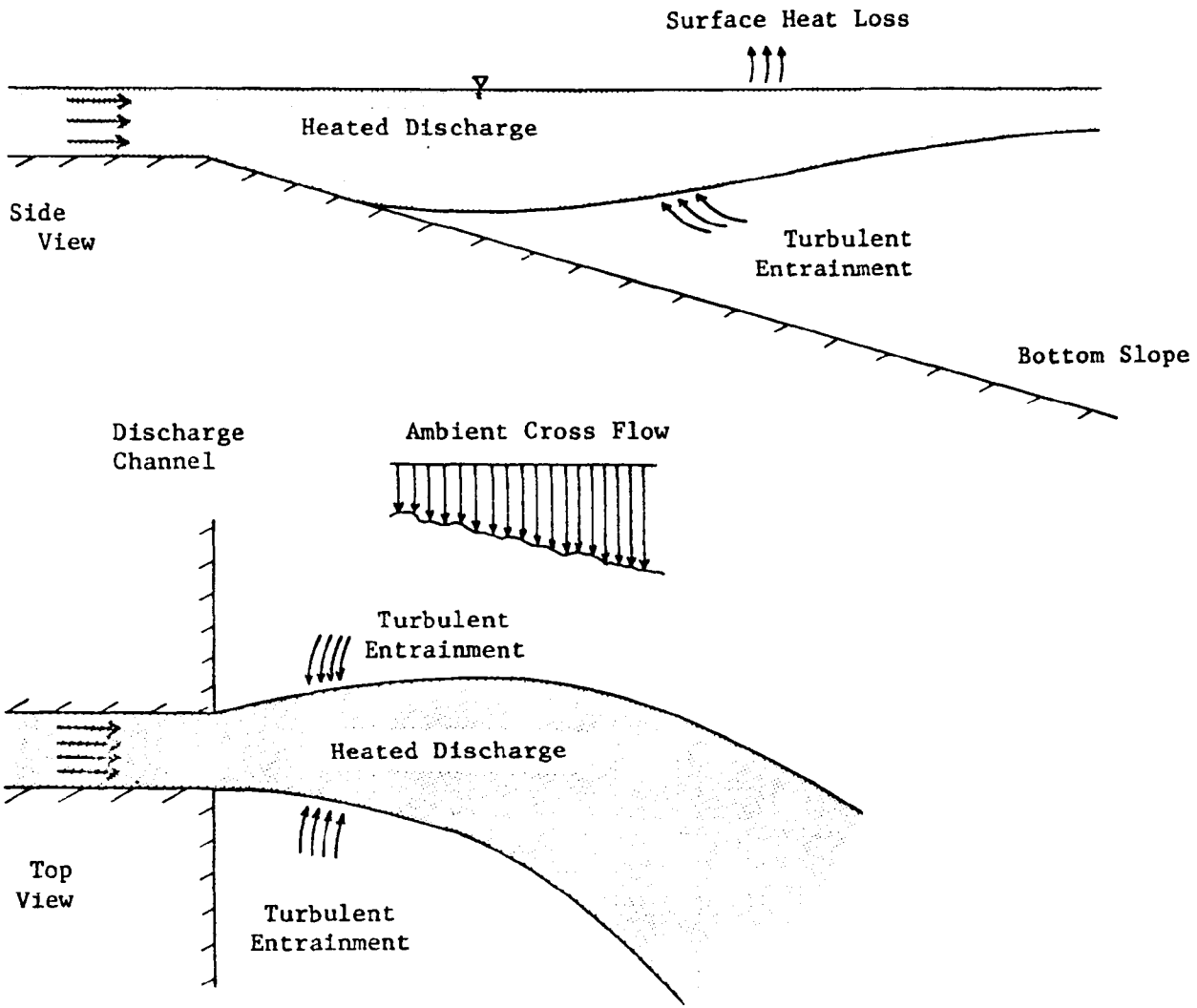

Figure 1-1. Schematic of Heated Discharge

The region dominated by natural processes, commonly called the "far field", is excluded because of the infinite number of possible conditions and because of the difficulty in modeling natural phenomena on a laboratory scale.

1.5 Summary of the Study

A guiding principle of this investigation is that an increased understanding of the problem as defined is to be found in a synthesis of existing knowledge of the physical phenomena of turbulent jets, stratified flows, and surface heat loss. A review of the scientific literature in these fields provides the framework for a three-dimensional theory based on a turbulent jet model with modifications introduced to include density gradients and surface heat loss. The theory is developed carefully from the basic governing equations to a set of integrated equations which may be solved numerically.

The discharge is modeled in a laboratory basin. All of the parameters of interest are varied and three-dimensional temperature measurements are taken. Comparisons of theory and experiment verify the validity of the theoretical model.

The application of the theory to temperature prediction in actual power plant discharges is discussed. The implications of the theoretical results for the design of scale models are illustrated by a case study. Finally, some suggestions for future work are made.

II. Review of Previous Investigations

2.1 Scope of the Review

The literature in the fields of turbulence and flows of non-homogeneous fluids is vast. This review discusses those works which are the major contributors to the theoretical analysis of this study. Analytical and experimental investigations of turbulent jets, flows with stable density gradients, and heat transfer in turbulent fluids are examined. Whenever possible reference is made to the best available summary rather than to original publications.

Several recent investigations treat horizontal surface discharges of heated water. These efforts are examined.

2.2 Turbulent Jets

2.2.1 Physical Properties

Abramovich (1) and Townsend (34) discuss the general characteristics of various kinds of submerged turbulent jets: (see Figure 2-1)

1) A turbulent shear flow region which increases in size away from the jet origin. There is a distinct boundary between the turbulent flow and a potential flow outside the jet. The jet width, b, is defined as the mean distance from the jet centerline to this boundary. In practice, however, a half width $b_{1/2}$ is often defined as the point where the mean x velocity, u, is one half the centerline mean velocity, u_c. For isolated submerged jets both b and $b_{1/2}$ are observed to grow linearly with x. In plane and axisymmetric jets, $b = .22\ x$.

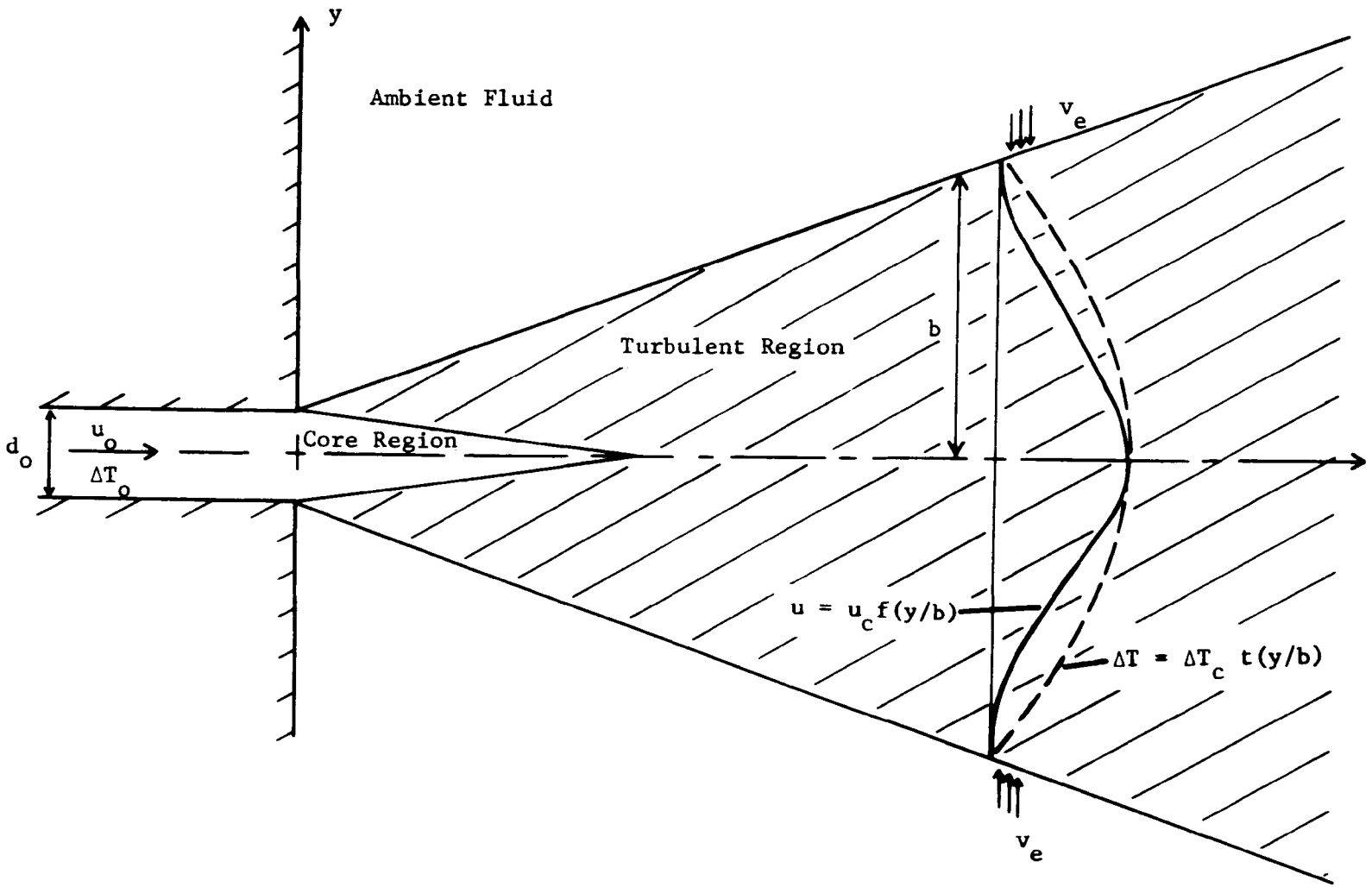

Figure 2-1. Structure of a Submerged Turbulent Jet

2) An initial core region of unsheared fluid which is gradually engulfed by the spread of the turbulent region.

3) Entrainment of ambient fluid into the turbulent region. The entrainment process is characterized by small scale eddies near the jet boundary under the overall control of larger scale features such as the mean shear. The entrained fluid velocity normal to the jet is v_e.

4) Heat, mass, momentum and kinetic energy are transported within the jet by convective and diffusive processes. The nature of the transport is different for each quantity.

5) Similarity of lateral profiles of velocity in the turbulent region. The velocity may be expressed by:

$$u = u_c f(y/b) \tag{2.1}$$

where u_c is the centerline velocity and f is a similarity function.

In heated jets, the lateral temperature profiles are similar to each other but have a shape different from the velocity profiles.

$$\Delta T = \Delta T_c t(y/b) \tag{2.2}$$

where ΔT_c is the centerline temperature difference and t is a similarity function.

Pearce (26) investigates the dependence of the jet characteristics on the Reynolds number of the jet. For circular jets the Reynolds

number is

$$\mathbb{R} = \frac{u_o d_o}{\nu} \tag{2.3}$$

where u_o = initial velocity

d_o = initial diameter

ν = kinematic viscosity

Pearce summarizes the changes in the structure of a circular water jet as $\mathbb{R}$ increases:

$\mathbb{R} < 500$ - A long laminar cylindrical column, expanding slightly. Some small stable wave instability but no turbulence for $x/d_o < 100$.

$500 < \mathbb{R} < 1500$ - Instability of the wave disturbances at some point distant from the orifice.

$1500 < \mathbb{R} < 2500$ - Complete breakdown into turbulence beyond a point which approaches the origin as $\mathbb{R}$ increases.

$2500 < \mathbb{R} < 3000$ - The whole jet is turbulent. The spread of the turbulent zone decreases with increasing $\mathbb{R}$.

$3000 < R$ - The fully turbulent jet structure is maintained for all higher values of $\mathbb{R}$. No further change in the angle of spread of the turbulent zone occurs.

Abramovich (1), Pai (24), and Hinze (17) discuss the turbulent properties of jets. The significant findings are:

1) The turbulent fluctuations in the shear regions are nearly isotropic. The fluctuating components of velocity are

the same magnitude in all directions.

2) The magnitudes of the turbulent fluctuations are small compared to the maximum mean velocity at any section.

2.2.2 Analytical Solutions

The equations governing free turbulent jets are derived by Schlichting (29). The assumptions common to all the cases considered are:

1) Molecular transport terms are negligible.

2) Longitudinal diffusion is negligible with respect to longitudinal advection.

3) Constant pressure throughout the jet.

The equations expressing conservation of mass, momentum, and heat energy for a steady state, two-dimensional flow are:

$$\frac{\partial u}{\partial x} + \frac{\partial v}{\partial y} = 0 \tag{2.4}$$

$$\frac{\partial u^2}{\partial x} + \frac{\partial uv}{\partial y} = \frac{\partial \overline{u'v'}}{\partial y} \tag{2.5}$$

$$\frac{\partial Tu}{\partial x} + \frac{\partial Tv}{\partial y} = \frac{\partial \overline{v'T'}}{\partial y} \tag{2.6}$$

where the quantities $\overline{u'v'}$ and $\overline{v'T'}$ are the time averaged fluxes of momentum and heat in the y direction due to turbulent motions. A similar set of equations may be formulated for axisymmetric flow.

The analytical solution of Equations 2.4 - 2.6 proceeds as follows:

1) The velocity and temperature distributions are assumed to be given by similarity functions f and t as in Equations 2.1 and 2.2. The functions f and t are not specified, but boundary conditions are stated. The most common boundary conditions are that the jet is symmetrical about the center-line axis, that the velocity is zero, the temperature constant, and all turbulent transfer is zero at the jet boundary.

2) The turbulent terms are related to the mean variables. Abramovich (1), Pai (24), Schlichting (29), and Hinze (17) discuss the well-known assumptions:

Prandtl's mixing length

$$\overline{u'v'} = \ell^2 \frac{\partial u}{\partial y}\left|\frac{\partial u}{\partial y}\right| \qquad \overline{u'T'} = \ell^2 \frac{\partial T}{\partial y}\left|\frac{\partial u}{\partial y}\right| \tag{2.7}$$

Taylor's vorticity transfer

$$\overline{u'v'} = \ell^2 \frac{\partial u}{\partial y}\left|\frac{\partial u}{\partial y}\right| \qquad \overline{u'T'} = 2\ell^2 \frac{\partial u}{\partial y}\left|\frac{\partial T}{\partial y}\right| \tag{2.8}$$

Reichardt's inductive theory

$$\overline{u'v'} = \ell \frac{\partial (u^2)}{\partial y} \tag{2.9}$$

Prandtl's new theory

$$\overline{u'v'} = e_v \frac{\partial u}{\partial y} \qquad \overline{u'T'} = e_T \frac{\partial T}{\partial y} \tag{2.10}$$

In the above relationships the quantities ℓ, e_v, and e_T are functions

of x only. The x dependence of these parameters is related to the jet structure on dimensional grounds:

$$\ell \sim b$$

$$e_v \sim e_T \sim u_c b \tag{2.11}$$

Careful experimental investigation has shown that none of the local relationships between turbulent transfer and mean gradients (Equations 2.7 - 2.10) are valid (34). For many cases, however, the solutions based on these assumptions do predict the gross behavior of the jet reasonably well.

3) The similarity functions (2.1 & 2.2) and the turbulent hypotheses (one of Equations 2.7 - 2.10) are substituted into the equations of motion (2.4 - 2.6). For jets, the sufficient criteria that unique equations for the similarity functions f and t exist, is found to be (34):

$$\frac{db}{dx} = \text{const.} = \varepsilon \tag{2.12}$$

where ε is determined later by comparison of the solution with experimental data. The functions f and t are determined subject to the stated boundary conditions. A particular failing of the mixing length hypothesis is that it results in the same similarity function for both velocity and temperature. Taylor's theory predicts that heat is diffused

laterally faster than momentum and that:

$$t = \sqrt{f} \tag{2.13}$$

Prandtl's new theory gives the same result if $e_T = 2e_v$ (see Figure 2.2) (29).

4) The behavior of u_c and ΔT_c is determined by integrating the equations of motion (2.4 - 2.6) over the jet cross section to yield expressions of constant momentum and heat flux in the x direction. This completes the analytical solution. A property of the solutions for plane and axisymmetric jets is that

$$v_e = \alpha u_c \tag{2.14}$$

i.e. the entrainment velocity is proportional to the centerline velocity with the coefficient of proportionality called an entrainment coefficient.

Analytical solutions which describe the jet behavior as accurately as those derived by the above process may be obtained by a considerably less complicated procedure (24):

1) A specific form for the similarity functions, f and t, is assumed.
2) Either the jet is assumed to spread linearly (Equation 2.12) or the entrainment relationship (2.14) is assumed. The appropriate constant, ε or α, is determined empirically.
3) The integrated equations of motion are used as in (4) above.

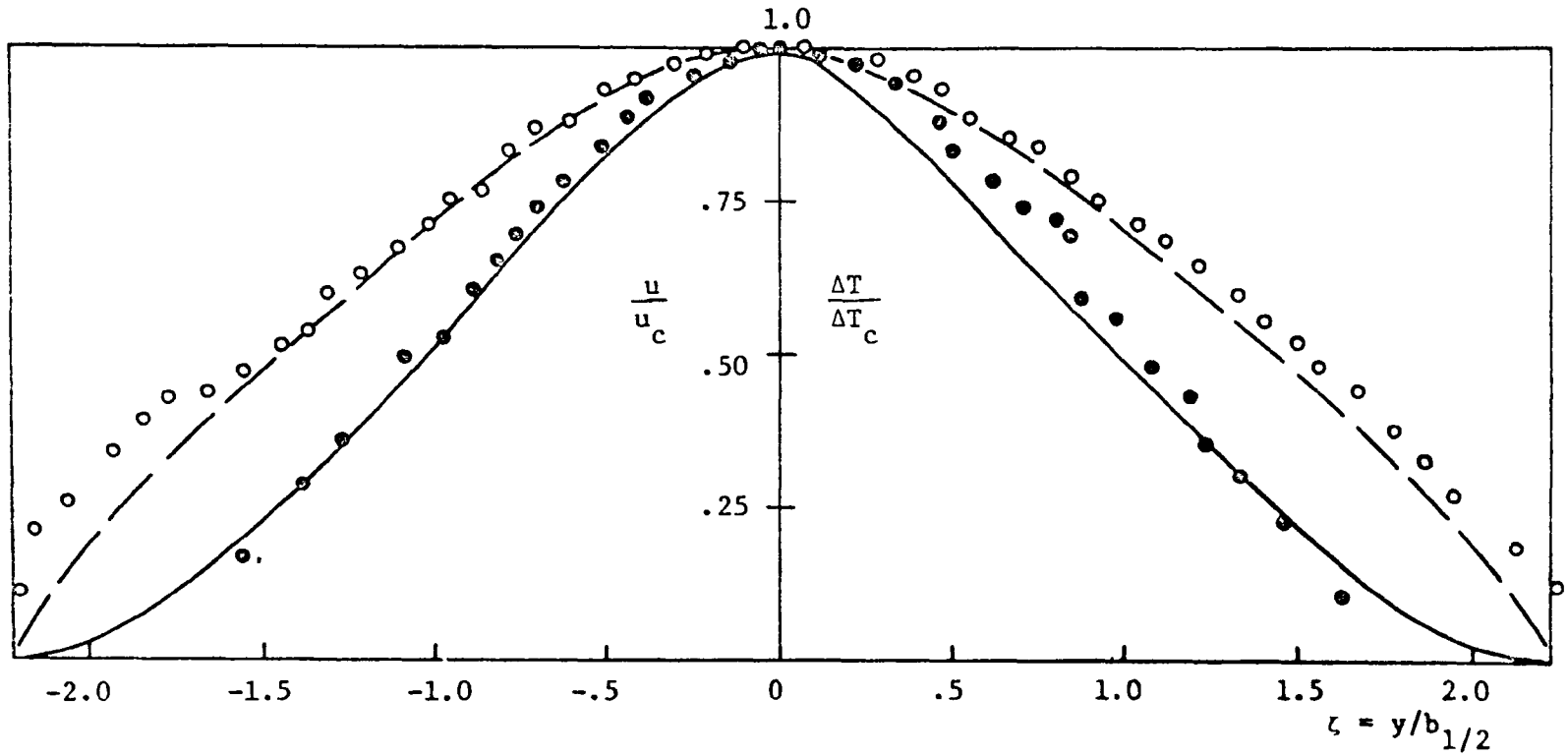

Figure 2-2. Velocity and Temperature Distributions in Submerged Jets

Reichardt's Data: Velocity ○ $u/u_c = (1 - .29\ \zeta^{3/2})^2$ ———

Temperature ○ $\Delta T/\Delta T_c = 1 - .29\ \zeta^{3/2}$ — — —

2.2.3 Deflected Jets

The case of turbulent jets discharged into a cross flow is discussed by Abramovich. The literature on the subject is well reviewed by Fan (11). In all the cases considered the jet is deflected by two processes:

1) Entrainment of the lateral cross flow momentum. The resulting force per unit length on the jet in the direction of the cross flow is:

$$F_e = \rho V q_e \tag{2.15}$$

where V is the cross flow velocity and q_e is the total entrainment per unit length of jet.

2) A net pressure force caused by eddying of the ambient fluid in the lee of the jet and by the distortion of the jet boundaries. This force per unit length is:

$$F_D = C_D \rho \frac{V^2}{2} D \tag{2.16}$$

where C_D is a drag coefficient and D is the jet diameter.

2.2.4 Confined Jets

The problem of jets discharging over a solid boundary is related to diffuser flow as discussed by Schlichting (29). Abramovich (1) also discusses the confined half jet. The effects of the boundary are:

1) Pressure gradients in the lateral and longitudinal direction. Adverse longitudinal pressure gradients result in

separation and eddying. For turbulent flows the point of separation is determined only empirically.

2) A viscous boundary layer near the solid boundary. Longitudinal momentum is decreased by wall shear.

2.3 Turbulent Flows with Density Gradients

2.3.1 Reduction of Turbulence

A discussion of turbulence in the presence of stable density gradients is given by Phillips (27). Deissler (7) formulates a simplified model of initially isotropic turbulence in the presence of a vertical density gradient. Experimental work with turbulent, density-stratified flow is reported by Webster (36). In all discussions the parameter controlling the effect of the density gradient upon the flow is the Richardson number given by:

$$R_i = \frac{\frac{g}{\rho}\left|\frac{\partial \rho}{\partial z}\right|}{\left[\frac{\partial u}{\partial z}\right]^2} \qquad (2.17)$$

As R_i increases from 0 to 1 the vertical turbulent fluctuations diminish; vertical transfer of mass, heat and momentum decrease, mass and heat transfer more so than momentum transfer. The region of maximum density gradient becomes an "interface" between two layers of different densities. Kato and Phillips (22) investigate the entrainment of mass across such an interface, using a surface shear to generate turbulence. They find the entrainment to be inversely proportional to the Richardson number. Ippen and Harleman (20) report that viscous underflows are stable for $IF < 1.0$ where IF is the densimetric Froude number

given by

$$\mathbb{F} = \frac{V}{\sqrt{\frac{\Delta\rho}{\rho} gh}} \tag{2.18}$$

V is the average flow velocity, h is the flow depth and $\Delta\rho$ is the density difference across the interface. Underflows of moderate turbulence are experimentally evaluated by Lofquist (23). Experiments over a large range of Richardson numbers for fully turbulent shear flows are treated by Ellison and Turner (9). Their determination of entrainment as a function of a gross Richardson number expressed as $R_i = 1/\mathbb{F}^2$ is given in Figure 2.3. The entrainment coefficient α is defined as the ratio of the velocity across the interface, v_e, to the average velocity parallel to the interface, u. For $R_i = 0$ the entrainment coefficient is equal to α_o, the value observed in homogeneous fluids.

Phillips (27) proposes a model for vertical transport of momentum in a shear flow, u(z). The model is based upon a wind wave generation theory; after considerable manipulation the eddy viscosity, e, defined by

$$\tau = \rho\, e \frac{\partial u}{\partial z} \tag{2.19}$$

is given by

$$e \sim \overline{w'^2}\, G_o \tag{2.20}$$

where

$$G_o = \int_0^\infty \frac{\overline{w'(t)w'(t+\xi)}}{\overline{w'^2}}\, d\xi = \int_0^\infty R(\xi)\, d\xi \tag{2.21}$$

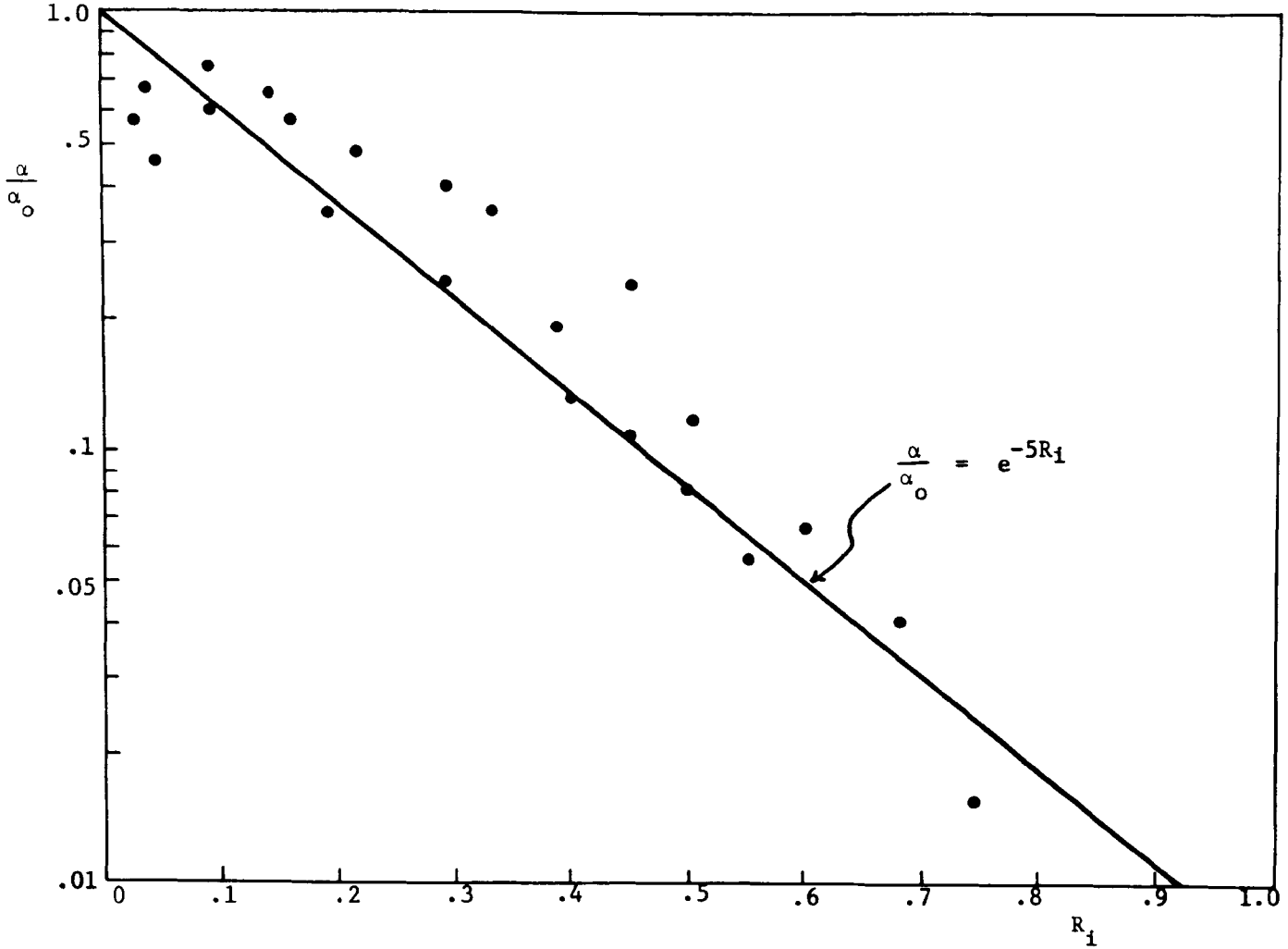

Figure 2-3. Reduction of Entrainment as a Function of Richardson Number

● - Data from Ellison & Turner

is the integral time scale of the turbulent vertical velocity fluctuations. The more persistent the vertical turbulent fluctuations, the greater the vertical momentum transfer. Phillips suggests that in a stratified flow the vertical velocity spectrum reflects the frequency of the natural oscillation associated with the density gradient, the Brunt-Vaisala frequency, N:

$$N = \left[-\frac{g}{\rho} \frac{\partial \rho}{\partial z} \right]^{1/2} \tag{2.22}$$

and that in the stratified flow.

$$G_s = \int_0^\infty R(\xi) \cos N \xi d\xi \leq G_o \tag{2.23}$$

Assuming that the Richardson number is not so large that vertical turbulence has been completely damped i.e. that w' is still the same magnitude as the other components of the turbulent velocity fluctuations, then the ratio of stratified shear to unstratified shear.

$$\frac{\tau_s}{\tau_o} = \frac{e_s}{e_o} = \frac{G_s}{G_o} \tag{2.24}$$

The vertical shear is related to the vertical entrainment by

$$\tau \sim u v_e \sim \alpha u^2 \tag{2.25}$$

Thus it must be that for a given shear flow u,

$$\frac{\alpha_s}{\alpha_o} = \frac{\int_0^\infty R(\xi) \cos N\xi d\xi}{\int_0^\infty R(\xi) d\xi} \leq 1 \tag{2.26}$$

providing a relationship between the reduction in entrainment and the vertical density gradient.

2.3.2 Submerged Buoyant Jets

A number of analytical and experimental investigations have been done for the case of submerged jets in which buoyancy acts on the jet as a whole, producing a vertical acceleration but in which the turbulent structure of the jet is not significantly altered by the density gradients. Fan (11) gives a review of the investigations which include stratified and non-stratified environments, cross flows, and plane or axisymmetric jets.

A major difference between the analysis of the buoyant and the non-buoyant jets is that the linear spread of the turbulent region is no longer generally valid because of the addition of buoyant forces. In place of a linear spread assumption it is usually assumed that the entrainment coefficient is constant along the jet. This assumption is correct for non-buoyant jets as previously discussed, and gives generally good results for the buoyant jets considered. The value of the entrainment coefficient is determined by comparison with experiment.

2.3.3 Two Layer Flow

If the local Richardson number is high or the overall densimetric Froude number low, two layer flows of different densities may exist. Harleman (12) discusses the equations of motion governing two layer flow in open channels. Of particular interest is the case of a flow issuing from a channel into a large body of denser fluid. If the densimetric Froude number based on the upstream depth, h_o, and velocity,

u_o, is less than one, a "stagnant wedge" of dense water extends upstream from the end of the channel beneath the flow of lighter fluid (see Fig. 2-4). The length of the wedge is given by:

$$L = \frac{2h_o}{\bar{f}_i}\left[\frac{1}{5}\,\frac{1}{\mathbb{F}^2} - 2 + 3\,\mathbb{F}^{2/3} - \frac{6}{5}\,\mathbb{F}^{4/3}\right] \tag{2.27}$$

where $\mathbb{F} = \dfrac{u_o}{\sqrt{\frac{\Delta\rho}{\rho}\,gh_o}}$ and $\bar{f}_i$ is a friction factor for interfacial shear stress, averaged over the length L. Harleman and Stolzenbach (13) estimate the friction factor by using smooth turbulent friction laws in which $\bar{f}_i$ is a function only of the Reynolds number of the flow. At the junction of the channel and the reservoir the interface rises rapidly. The upper flow densimetric Froude number, based on the actual layer depth and velocity, is unity at this point.

2.4 Surface Heat Exchange

A comprehensive review of surface heat exchange processes and predictive equations is given by Brady (3). The prediction of natural water temperatures requires a determination of all the natural heat inputs to the water body. The steady state natural water temperature for fixed heat inputs is referred to as the equilibrium temperature, T_e. In a large body of water the response time for temperature changes is longer than the characteristic oscillations in heat inputs. The actual water temperature is never exactly equal to T_e for this reason. In rivers, lakes, and reservoirs the difference between the actual and equilibrium temperatures is usually less than 5°F. In the ocean it may be as high as 10° - 20°F.

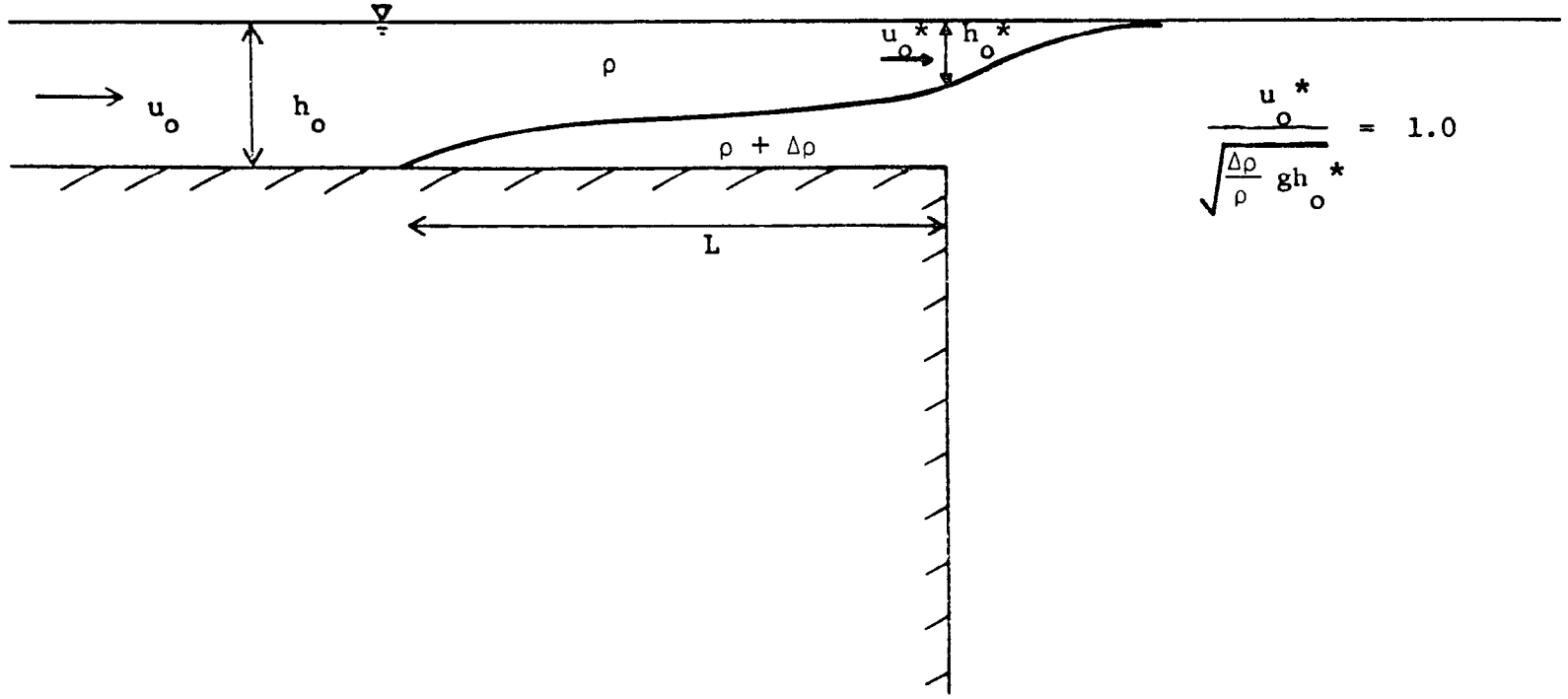

Figure 2-4. Two Layer Flow in the Discharge Channel

The "excess" temperature rise induced by the addition of power plant heat rejection may be calculated by assuming that the "excess" heat flux through the surface, q_s, is proportional to the difference between the heated water surface temperature, T_s and the equilibrium temperature, T_e.

$$q_s = \rho c_p K (T_s - T_e) \tag{2.28}$$

where the coefficient of proportionality is a function of the water surface temperature and meteorological conditions. Brady gives formulas and graphs for determining the value of K given wind speed and dewpoint temperature.

2.5 Surface Discharge of Heated Water

Experimental studies of three-dimensional surface discharges of heated water have been done by Hayashi (16), Wiegel (37), Jen (21), Stefan (31) and Tamai (32). Discussion of the experiments is presented in Chapter 4 and some of the results given in Chapter 5. Previous attempts to treat the problem analytically are presented in this section. Figure 2-5 shows the physical problem considered by each study.

Edinger and Polk present analytical solutions which assume that the heated discharge is a point source of heat at the water surface on the boundary of a uniform stream which is infinitely wide and deep.(8) No lateral or vertical convection occurs, the temperature distribution being determined entirely by vertical and lateral eddy diffusivities and by convection in the direction of the uniform stream. Buoyant

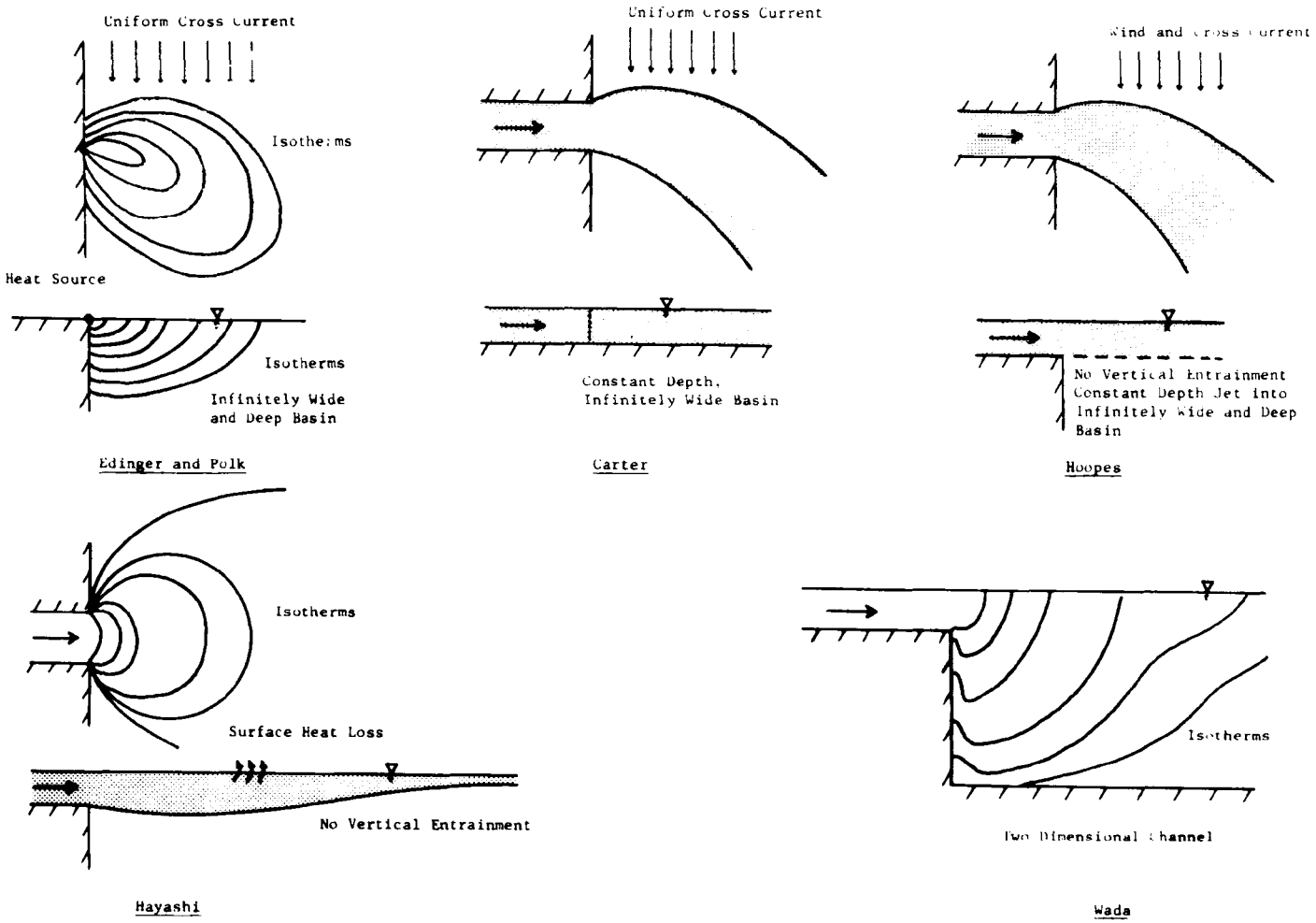

Figure 2-5. Schematics of Previous Theoretical Investigations

effects are not considered. The results are fitted to field data by adjusting the value of the vertical and horizontal diffusivities. No correlation between the fitted values of the diffusivities and values estimated a priori is found. This treatment is clearly valid only for the region dominated by ambient turbulence as discussed in Chapter 1. The difficulty in determining natural turbulent diffusivities is a severe limitation on the practical use of Edinger and Polk's theory.

Carter treats the case of a heated discharge from a channel into an infinitely long and wide basin whose depth is uniformly the same as that of the discharge channel and in which a uniform cross current is flowing at right angles to the discharge. The jet velocity and temperature are assumed to be uniform across the width and depth of the jet, varying only along the centerline coordinate. The jet is deflected by pressure drag and entrainment of lateral momentum as expressed in integral momentum equations. Laboratory experiments are performed in which the temperature field is measured. The entrainment into the jet is determined from the experimental data and is input to the theory to obtain predictions of the centerline trajectory which are compared with the data. The scatter of the data is large but the points are near the theoretical curves on the average. The neglect of buoyancy and surface heat loss seems justified for this physical situation although the spreading of the jet is not measured and may be dependent on buoyant forces. Extrapolation of Carter's results to a deep receiving basin are not possible since his measured entrainment curves would not be valid. (5)

Hoopes treats a physical problem very similar to Carter's. He assumes that the effect of buoyancy is to make the vertical entrainment zero and that the jet is vertically uniform and of constant depth even though the receiving basin is infinitely deep. Hoopes assumes Gaussian similarity functions for velocity and temperature and accounts for lateral entrainment by defining a lateral entrainment coefficient. Integrated continuity, momentum, and heat equations yield expressions for jet deflection, width, and centerline temperature and velocity. The theoretical model is compared with field measurements. Uncertainty in the values of the ambient cross flows makes comparison of the theoretical and actual jet trajectories difficult. Also most of the temperature data is taken far from the discharge where the temperature is nearly the ambient value. This study illustrates the extreme difficulty in using field data to check a theoretical model. (18)

Hayashi proposes a theory for a discharge from a channel of finite width into a large, stagnant receiving body of water. He assumes that the buoyant stability is so great that vertical entrainment is zero and that all of the convective terms in the governing equations are negligible. The equations are integrated over the jet depth using a similarity function to describe vertical temperature and velocity distributions. Analytical solutions for temperature and velocity are obtained by assuming that horizontal eddy diffusivities are not functions of space and taking into account heat loss from the water surface. Experiments done by Hayashi do not agree with the theory and show a large amount of scatter. The discrepancy between data and theory is a result

of initial mixing near the discharge point which the theory does not account for. As discussed in Chapter 1, initial mixing is important in most heated discharges. Also, the formation of stagnant cold water wedges in discharge channels of low densimetric Froude number, $\mathbb{F}$, prevents the local value of $\mathbb{F}$ at the discharge point from being less than unity. Thus Hayashi's theory, which is valid for $\mathbb{F} = 0$, will not apply to actual heated discharges. (15)

Wada considers a two-dimensional flow (vertical and longitudinal) of heated water and treats the full equations of motion in which turbulent terms are represented by eddy coefficients. The vertical eddy coefficients for heat and momentum have the form

$$e = e_o + e_1 \exp(-cR_i) \tag{2.29}$$

where e_o, e_1, and c are constants which are different for heat and momentum and R_i is the local Richardson number. (35)

The equations of motion are transformed into a vorticity equation and solved numerically. The results are physically reasonable, indicating an initial entrainment near the discharge and a stable two layer system farther from the discharge. Wada states that the theory is valid for discharges in which the ambient turbulence controls the diffusion processes, making e_o and e_1 relatively constant in space.

The details of Wada's numerical scheme are not given in his papers and a calculation for only one case is shown. It is doubtful that many field conditions correspond to Wada's problem. If the dis-

charge channel is wide, the jet may behave initially like a two-dimensional flow with little lateral variations in temperature and velocity, but the turbulent structure close to the discharge origin is jet-like and is not constant in space as Wada assumes.

Table 2-1 summarizes the studies from the point of view of the processes affecting the temperature distribution and the number of physical dimensions considered. Each of the authors presents a satisfactory theory based on the physical situation he assumes. None of the theories consider all of the factors discussed in Chapter 1 as being important for the prediction of temperatures in the vicinity of a heated discharge.

Investigator	Direction of Temperature Variation			Factors Affecting Temperature Distribution						
	x	y	z	Initial Mixing	Buoyancy	Discharge Channel Geometry	Bottom Slope	Surface Heat Loss	Ambient Cross Flow	Ambient Turbulence
Edinger (8)	yes	yes	yes	no	no	no	no	no	yes	yes
Carter (5)	yes	yes	no	yes	no	yes	no	no	yes	no
Hoopes (18)	yes	yes	no	yes	no	yes	no	no	yes	no
Hayashi (15)	yes	yes	yes	no	yes	yes	no	yes	no	no
Wada (35)	yes	no	yes	yes	yes	yes	yes	no	no	yes
This Study	yes	yes	yes	yes	yes	yes	yes	yes	yes	no

Table 2-1. Summary of Previous Theoretical Investigations

III. Theoretical Considerations

3.1 Statement of the Problem

The preceding chapter reviews earlier theoretical investigations of heated surface discharges. Each is severely limited: only Hayashi considers surface heat loss. There is no attempt to include buoyant convective motions and none of the theories reproduce the initial core region in a turbulent jet. There is a need for a three-dimensional theoretical development which considers all these factors.

This study treats a horizontal discharge of heated water at the surface of a large body of ambient water. Figure 3-1 shows the relevant geometrical characteristics of the discharge and the definition of a Cartesian coordinate system. A theory for predicting the three-dimensional velocity and temperature distribution within the discharge jet is developed in the following sections. The initial temperature difference between discharge and ambient water, the discharge velocity, the channel geometry, surface heat transfer, the ambient cross flow, and the bottom slope will determine the temperature and velocities in the jet.

The theory is limited to the region of flow where jet turbulence dominates ambient turbulence. The ambient cross flow is not necessarily uniform but far from the jet the free surface is uniformly at $z = 0$ and the temperature is T_a.

The basic hydrodynamic and thermodynamic equations governing the flow are first transformed into usable form for the case of a non-buoyant discharge into deep, stagnant ambient water. The effects of an

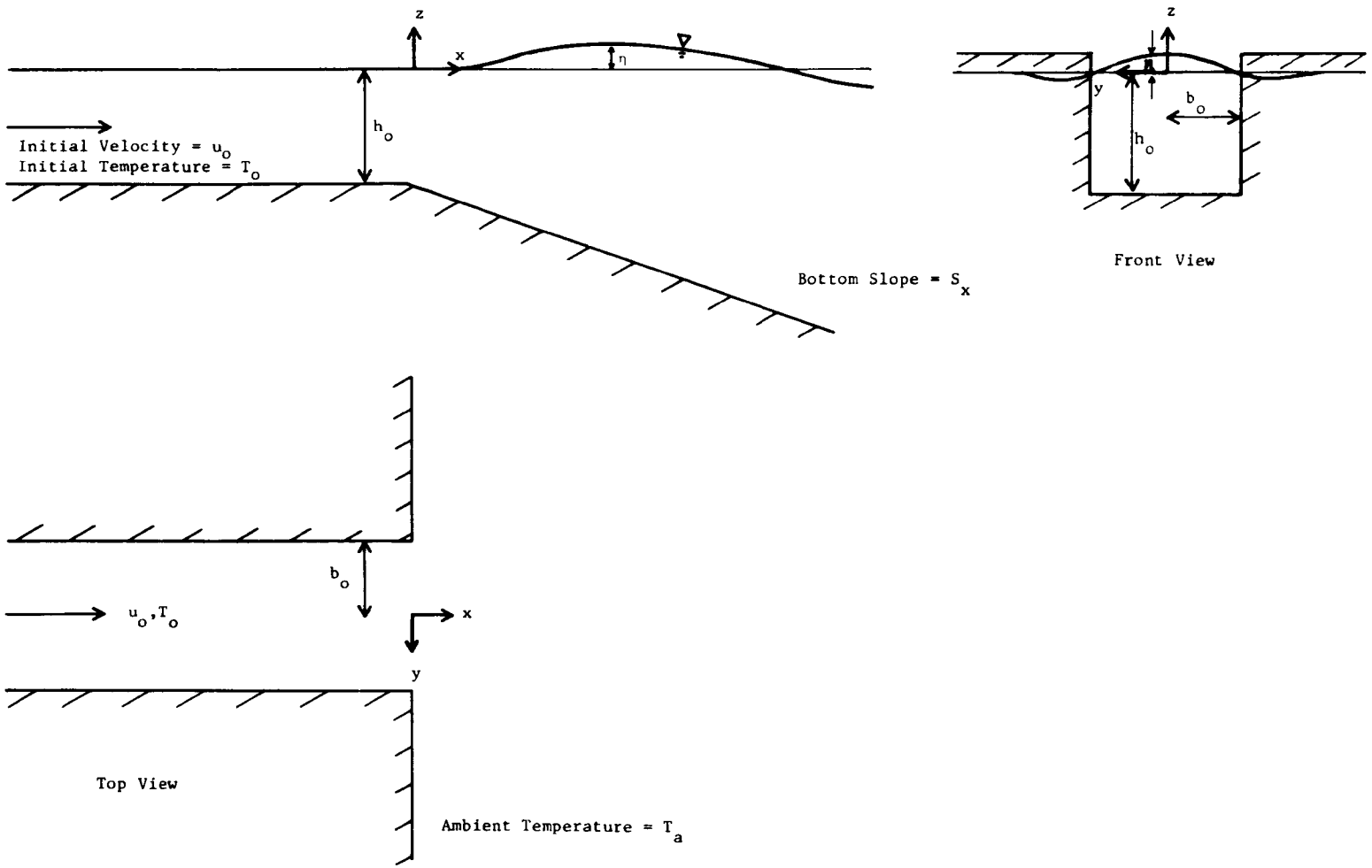

Figure 3-1. Characteristics of the Discharge Channel

initial temperature difference are then included in the theoretical model. Finally, a buoyant jet discharged over a bottom slope or into a cross flow is considered.

3.2 The Governing Equations

3.2.1 Basic Equations

A fluid flow is characterized by its velocity, density, pressure, and temperature, all of which may be a function of space and time. These four variables are related by equations expressing conservation of mass, momentum, and heat energy and an equation of state which relates density, pressure, and temperature. In Cartesian coordinates the complete equations for water flow, incorporating the Boussinesq approximation, are:

$$\frac{\partial \rho}{\partial t} + \frac{\partial \rho u}{\partial x} + \frac{\partial \rho v}{\partial y} + \frac{\partial \rho w}{\partial z} = 0 \tag{3.1}$$

$$\frac{\partial u}{\partial t} + \frac{\partial u^2}{\partial x} + \frac{\partial uv}{\partial y} + \frac{\partial uw}{\partial z} = -\frac{1}{\rho}\frac{\partial p}{\partial x} + \nu\left[\frac{\partial^2 u}{\partial x^2} + \frac{\partial^2 u}{\partial y^2} + \frac{\partial^2 u}{\partial z^2}\right] \tag{3.2}$$

$$\frac{\partial v}{\partial t} + \frac{\partial uv}{\partial x} + \frac{\partial v^2}{\partial y} + \frac{\partial vw}{\partial z} = -\frac{1}{\rho}\frac{\partial p}{\partial y} + \nu\left[\frac{\partial^2 v}{\partial x^2} + \frac{\partial^2 v}{\partial y^2} + \frac{\partial^2 v}{\partial z^2}\right] \tag{3.3}$$

$$\frac{\partial w}{\partial t} + \frac{\partial uw}{\partial x} + \frac{\partial vw}{\partial y} + \frac{\partial w^2}{\partial z} = -\frac{1}{\rho}\frac{\partial p}{\partial z} - g + \nu\left[\frac{\partial^2 w}{\partial x^2} + \frac{\partial^2 w}{\partial y^2} + \frac{\partial^2 w}{\partial z^2}\right] \tag{3.4}$$

$$\frac{\partial T}{\partial t} + \frac{\partial uT}{\partial x} + \frac{\partial vT}{\partial y} + \frac{\partial wT}{\partial z} = k\left[\frac{\partial^2 T}{\partial x^2} + \frac{\partial^2 T}{\partial y^2} + \frac{\partial^2 T}{\partial z^2}\right] + \Phi \tag{3.5}$$

$$\frac{\partial \rho}{\partial T} + a = 0 \tag{3.6}$$

where u,v,w = velocity components in the x,y,z direction

ρ = density

p = pressure

T = temperature

ν = viscosity

g = gravitational acceleration

k = thermal conductivity

a = thermal expansion coefficient

Φ = viscous generation of heat

In conjunction with initial and boundary conditions the fluid flow is determined by these equations. There is no closed form solution to the governing equations. Approximations must be introduced which simplify the equations to the point where solutions may be obtained. The transformation of the governing equations will consist of dropping certain negligible terms, of assuming the form of certain variables, and of integrating the equations over a region in space.

3.2.2 Steady, Turbulent Flow Equations

In accordance with standard practice when dealing with turbulent flows the velocity, pressure, density, and temperature are separated into mean and fluctuating parts:

$$\begin{aligned} u &= \bar{u} + u' \\ v &= \bar{v} + v' \\ w &= \bar{w} + w' \\ \rho &= \bar{\rho} + \rho' \\ p &= \bar{p} + p' \\ T &= \bar{T} + T' \end{aligned} \qquad (3.7)$$

In general the mean values may be functions of time when considered over periods longer than the periods of the turbulent fluctuations. This study considers only steady mean flows.

The result of substituting Equations 3.7 into Equations 3.1 - 3.6 and taking a time average of each term is the well known set of turbulent mass, momentum, and heat equations.

$$\bar{\rho}\left[\frac{\partial \bar{u}}{\partial x}+\frac{\partial \bar{v}}{\partial y}+\frac{\partial \bar{w}}{\partial z}\right]+\bar{u}\frac{\partial \bar{\rho}}{\partial x}+\bar{v}\frac{\partial \bar{\rho}}{\partial y}+\bar{w}\frac{\partial \bar{\rho}}{\partial z}+\frac{\partial \overline{\rho' u'}}{\partial x}+\frac{\partial \overline{\rho' v'}}{\partial y}+\frac{\partial \overline{\rho' w'}}{\partial z}=0 \tag{3.8}$$

$$\frac{\partial \bar{u}^2}{\partial x}+\frac{\partial \bar{u}\bar{v}}{\partial y}+\frac{\partial \bar{u}\bar{w}}{\partial z}=-\overline{\frac{1}{\rho}\frac{\partial p}{\partial x}}+\nu\left[\frac{\partial^2 \bar{u}}{\partial x^2}+\frac{\partial^2 \bar{u}}{\partial y^2}+\frac{\partial^2 \bar{u}}{\partial z^2}\right]-\frac{\partial \overline{u'^2}}{\partial x}-\frac{\partial \overline{u'v'}}{\partial y}-\frac{\partial \overline{u'w'}}{\partial z} \tag{3.9}$$

$$\frac{\partial \bar{u}\bar{v}}{\partial x}+\frac{\partial \bar{v}^2}{\partial y}+\frac{\partial \bar{v}\bar{w}}{\partial z}=-\overline{\frac{1}{\rho}\frac{\partial p}{\partial y}}+\nu\left[\frac{\partial^2 \bar{v}}{\partial x^2}+\frac{\partial^2 \bar{v}}{\partial y^2}+\frac{\partial^2 \bar{v}}{\partial z^2}\right]-\frac{\partial \overline{u'v'}}{\partial x}-\frac{\partial \overline{v'^2}}{\partial y}-\frac{\partial \overline{v'w'}}{\partial z} \tag{3.10}$$

$$\frac{\partial \bar{u}\bar{w}}{\partial x}+\frac{\partial \bar{v}\bar{w}}{\partial y}+\frac{\partial \bar{w}^2}{\partial z}=-\overline{\frac{1}{\rho}\frac{\partial p}{\partial z}}-g+\nu\left[\frac{\partial^2 \bar{w}}{\partial x^2}+\frac{\partial^2 \bar{w}}{\partial y^2}+\frac{\partial^2 \bar{w}}{\partial z^2}\right]-\frac{\partial \overline{u'w'}}{\partial x}-\frac{\partial \overline{v'w'}}{\partial y}-\frac{\partial \overline{w'^2}}{\partial z} \tag{3.11}$$

$$\frac{\partial \bar{u}\bar{T}}{\partial x}+\frac{\partial \bar{v}\bar{T}}{\partial y}+\frac{\partial \bar{w}\bar{T}}{\partial z}=k\left[\frac{\partial^2 \bar{T}}{\partial x^2}+\frac{\partial^2 \bar{T}}{\partial y^2}+\frac{\partial^2 \bar{T}}{\partial z^2}\right]-\frac{\partial \overline{u'T'}}{\partial x}-\frac{\partial \overline{v'T'}}{\partial y}-\frac{\partial \overline{w'T'}}{\partial z}+\bar{\Phi} \tag{3.12}$$

$$\overline{\frac{\partial \rho}{\partial T}}+a=0 \tag{3.13}$$

Henceforth the mean variables are written without the bar. Fluctuating qualities are still designated by a prime.

3.2.3 Hydrostatic Pressure

The mean pressure is considered to be the sum of two parts:

$$p = p_h + p_d \tag{3.14}$$

where the hydrostatic pressure, p_h, satisfies the equation

$$0 = -\frac{1}{\rho}\frac{\partial p_h}{\partial z} - g \tag{3.15}$$

The remaining component, p_d, is a dynamic pressure resulting from fluid acceleration.

Equation 3.15 may be integrated:

$$p_h = -\int_{z_o}^{z} \rho g dz + p_o \tag{3.16}$$

where z_o is a point at which $p_h = p_o$. In this case the elevation of the water surface, η, is a point where $p_h = 0$. Thus

$$p_h = -\int_{\eta}^{z} \rho g dz \tag{3.17}$$

The density is separated into components:

$$\rho = \rho_a - \Delta\rho \tag{3.18}$$

where ρ_a is the density of the ambient water and is not a function of space. The deviation from the ambient density is $-\Delta\rho$ and in a heated

jet results from a temperature difference as defined by the equation of state. If T_a is the ambient temperature corresponding to ρ_a, then

$$\rho = \rho_a - \int_{T_a}^{T} a\,dT \tag{3.19}$$

and

$$\Delta\rho = \int_{T_a}^{T} a\,dT \tag{3.20}$$

If Equation 3.18 is substituted into the pressure Equation 3.17:

$$p_h = -\int_{\eta}^{z} \rho_a g\,dz + \int_{\eta}^{z} \Delta\rho g\,dz \tag{3.21}$$

The pressure terms in the momentum equations are then:

$$-\frac{1}{\rho}\frac{\partial p}{\partial x} = -g\frac{\partial \eta}{\partial x} - \frac{g}{\rho_a - \Delta\rho}\int_{\eta}^{z}\frac{\partial \Delta\rho}{\partial x}\,dz - \frac{1}{\rho_a - \Delta\rho}\frac{\partial p_d}{\partial x} \tag{3.22}$$

$$-\frac{1}{\rho}\frac{\partial p}{\partial y} = -g\frac{\partial \eta}{\partial y} - \frac{g}{\rho_a - \Delta\rho}\int_{\eta}^{z}\frac{\partial \Delta\rho}{\partial y}\,dz - \frac{1}{\rho_a - \Delta\rho}\frac{\partial p_d}{\partial y} \tag{3.23}$$

$$-\frac{1}{\rho}\frac{\partial p}{\partial z} = g - \frac{1}{\rho_a - \Delta\rho}\frac{\partial p_d}{\partial z} \tag{3.24}$$

3.2.4 Scale Variables

The dominant terms in each equation are identified by estimating the scale of each variable and the magnitude of spatial changes in each variable. For this purpose the following "characteristic" or "scale"

variables are defined:

x^*, y^*, z^* = scale of changes in the x,y,z directions

η^* = scale of changes in the water surface elevation

u^*, v^*, w^* = scale of the mean velocity components

p_h^* = scale of hydrostatic pressure changes

p_d^* = scale of dynamic pressure changes

ΔT^* = scale of mean temperature changes

$\Delta\rho^*$ = scale of mean density changes

u'^*, v'^*, w'^* = scale of the velocity fluctuations u',v',w'

$\Delta T'^*$ = scale of the temperature fluctuations

$\Delta\rho'^*$ = scale of the density fluctuations

Φ^* = scale of the viscous heat production

In discussing relative magnitudes it is useful to define a quantity δ such that the following sequence of terms:

$$\delta^2, \quad \delta, \quad 1, \quad \frac{1}{\delta}, \quad \frac{1}{\delta^2}$$

is increasing and each term is an order of magnitude different from adjacent terms. The symbols << and >> are stronger statements of relative magnitude.

3.2.5 Large Reynolds Numbers

The ratio of any of the momentum terms to the viscous terms is:

$$\frac{(u^*, v^*, w^*)(x^*, y^*, z^*)}{\nu} = \mathbb{R} \tag{3.25}$$

where the appropriate choice of length and velocity scale is made. This ratio is the Reynolds number, $\mathbb{R}$. A condition for fully developed turbulence is that the Reynolds number be very large i.e. $\mathbb{R} >> 1$. The viscous terms are then negligible with respect to the convective terms. Since k is the same order as ν, the molecular heat transfer terms are also negligible.

In the heat energy equation, the ratio of viscous heat production to heat convection is

$$\frac{\phi^*}{\text{Heat Convection}} = \frac{1}{\mathbb{R}} \frac{(u^{*2}, v^{*2} w^{*2})}{c_p \Delta T^*} \tag{3.26}$$

where c_p is the specific heat of water. The quantity $\frac{(u^{*2}, v^{*2}, w^{*2})}{c_p \Delta T}$ is at most of order 1 in the jet. The viscous production of heat is therefore neglected.

3.2.6 Small Density Differences

The deviations from the ambient temperature, T_a, under consideration are of the order 0 - 30°F. The coefficient of thermal expansion is considered a constant over such a range and Equation 3.20 becomes

$$\Delta\rho = a (T - T_a) = a\Delta T \tag{3.27}$$

For T_a from 40°F to 100°F the value of $\frac{a}{\rho}$ varies from 0 to .0002°F^{-1}. Thus the maximum value of $\frac{\Delta\rho}{\rho_a}$ is .006 for ΔT = 30°F and T_a = 100°F. It may be said that

$$\frac{\Delta\rho^*}{\rho_a} << 1 \tag{3.28}$$

The pressure Equations 3.22 - 3.24 are simplified by noting that

$$\frac{1}{\rho_a - \Delta\rho} \simeq \frac{1}{\rho_a} \tag{3.29}$$

Since $\Delta T'^*$ can be no greater than ΔT^*, it must be that $\Delta\rho'^*$ is less than or equal to $\Delta\rho^*$. The mass conservation equation is simplified by dropping all terms scaled by $\Delta\rho^*$ or $\Delta\rho'^*$ since these are negligible compared to terms scaled by ρ_a. The mass conservation then becomes the familiar continuity equation for incompressible fluids.

$$\frac{\partial u}{\partial x} + \frac{\partial v}{\partial y} + \frac{\partial w}{\partial z} = 0 \tag{3.30}$$

3.2.7 Basic Scale Relationships

The continuity Equation 3.30 implies that:

$$v^* \sim \frac{y^*}{x^*} u^* \quad \text{and} \quad w^* \sim \frac{z^*}{x^*} u^* \tag{3.31}$$

The scale for free surface changes, η^*, may be determined by considering the momentum equations at very large depths i.e. as $z \to -\infty$. The effect of the jet is negligible and there is no motion at such depths. Equations 3.22 and 3.23 become:

$$0 = - g \frac{\partial \eta}{\partial x} - \frac{g}{\rho_a} \int_{\eta}^{-\infty} \frac{\partial \Delta\rho}{\partial x} \, dx - \frac{1}{\rho_a} \frac{\partial p_d}{\partial x} \text{ at } z = -\infty \tag{3.32}$$

$$0 = - g \frac{\partial \eta}{\partial y} - \frac{g}{\rho_a} \int_{\eta}^{-\infty} \frac{\partial \Delta\rho}{\partial y} dz - \frac{1}{\rho_a} \frac{\partial p_d}{\partial y} \text{ at } z = -\infty \tag{3.33}$$

It must be that

$$\eta^* \sim \frac{\Delta\rho^*}{\rho_a} z^* + \frac{p_d^*}{\rho_a g} \tag{3.34}$$

In a fully turbulent shear flow the turbulence is locally isotropic. The scale of the fluctuating components, (u'*,v'*,w'*), are the same order of magnitude. Furthermore the mean velocity in the direction of the flow is an order of magnitude greater than the fluctuating velocities:

$$\frac{u'^*}{u^*} \sim \frac{v'^*}{u^*} \sim \frac{w'^*}{u^*} \sim \delta \tag{3.35}$$

3.3 Non-Buoyant Surface Jets

3.3.1 Governing Equations

This section considers the case of a discharge of water horizontally from a rectangular open channel into a large body of water at the same temperature as the discharge. There is no bottom slope and no ambient cross flow. With these conditions the equation of mass conservation 3.30 is exact and the heat and state equations are not needed since ρ and T are not variables.

The momentum equations with all negligible terms dropped are shown below. The scale of each term is divided by $\frac{u^{*2}}{x^*}$ for convenience in comparison of terms:

$$\frac{\partial u^2}{\partial x} + \frac{\partial uv}{\partial y} + \frac{\partial uw}{\partial z} = -g\frac{\partial \eta}{\partial x} - \frac{1}{\rho_a}\frac{\partial p_d}{\partial x} - \frac{\partial u'^2}{\partial x} - \frac{\partial u'v'}{\partial y} - \frac{\partial u'w'}{\partial z}$$

$$1 \qquad 1 \qquad 1 \qquad \frac{p_d^*}{\rho_a u^{*2}} \qquad \frac{p_d^*}{\rho_a u^{*2}} \qquad \delta \qquad \delta\frac{x^*}{y^*} \qquad \delta\frac{x^*}{z^*} \tag{3.36}$$

$$\frac{\partial uv}{\partial x} + \frac{\partial v^2}{\partial y} + \frac{\partial vw}{\partial z} = -g\frac{\partial \eta}{\partial y} - \frac{1}{\rho_a}\frac{\partial p_d}{\partial y} - \frac{\partial u'v'}{\partial x} - \frac{\partial v'^2}{\partial y} - \frac{\partial v'w'}{\partial z}$$

$$\frac{y^*}{x^*} \qquad \frac{y^*}{x^*} \qquad \frac{y^*}{x^*} \qquad \frac{p_d^*}{\rho_a u^{*2}}\frac{x^*}{y^*} \qquad \frac{p_d^*}{\rho_a u^{*2}}\frac{x^*}{y^*} \qquad \delta \qquad \delta\frac{x^*}{y^*} \qquad \delta\frac{x^*}{z^*} \tag{3.37}$$

$$\frac{\partial uw}{\partial x} + \frac{\partial vw}{\partial y} + \frac{\partial w^2}{\partial z} = \frac{1}{\rho_a}\frac{\partial p_d}{\partial z} - \frac{\partial u'w'}{\partial x} - \frac{\partial v'w'}{\partial y} - \frac{\partial w'^2}{\partial z}$$

$$\frac{z^*}{x^*} \qquad \frac{z^*}{x^*} \qquad \frac{z^*}{x^*} \qquad \frac{p_d^*}{\rho_a u^{*2}}\frac{x^*}{z^*} \qquad \delta \qquad \delta\frac{x^*}{y^*} \qquad \delta\frac{x^*}{z^*} \tag{3.38}$$

If the turbulent terms in the x equation are to be the same order as the convective terms it must be that:

$$\frac{y^*}{x^*} \sim \delta \quad \text{and} \quad \frac{z^*}{x^*} \sim \delta \tag{3.39}$$

The first turbulent term is then negligible in all the momentum equations.

In the y and z equations the turbulent terms are of order 1 if 3.39 is true. The pressure term must also be of order 1 since the convective terms are of order δ:

$$\frac{p_d^*}{\rho_a u^{*2}} \sim \delta \tag{3.40}$$

The pressure term in the x equation is then negligible. The approximate equations become:

$$\frac{\partial u}{\partial x} + \frac{\partial v}{\partial y} + \frac{\partial w}{\partial z} = 0 \tag{3.41}$$

$$\frac{\partial u^2}{\partial x} + \frac{\partial uv}{\partial y} + \frac{\partial uw}{\partial z} = - \frac{\partial u'v'}{\partial y} - \frac{\partial u'w'}{\partial z} \tag{3.42}$$

$$0 = - g \frac{\partial n}{\partial y} - \frac{1}{\rho_a} \frac{\partial p_d}{\partial y} - \frac{\partial v'^2}{\partial y} - \frac{\partial v'w'}{\partial z} \tag{3.43}$$

$$0 = - \frac{1}{\rho_a} \frac{\partial p_d}{\partial z} - \frac{\partial v'w'}{\partial y} - \frac{\partial w'^2}{\partial z} \tag{3.44}$$

3.3.2 Structure of the Jet

The set of equations is a well known result for turbulent shear flows. Further assumptions about the nature of the jet are taken from established experimental and theoretical results in Chapter 2.

The gross features of the jet are defined in Figure 3-2. The core region has a half-width s and depth r. The turbulent shear region expanding horizontally has width b; the vertical shear region is of depth h. Section A-A in Figure 3-2 shows four regions in the jet cross

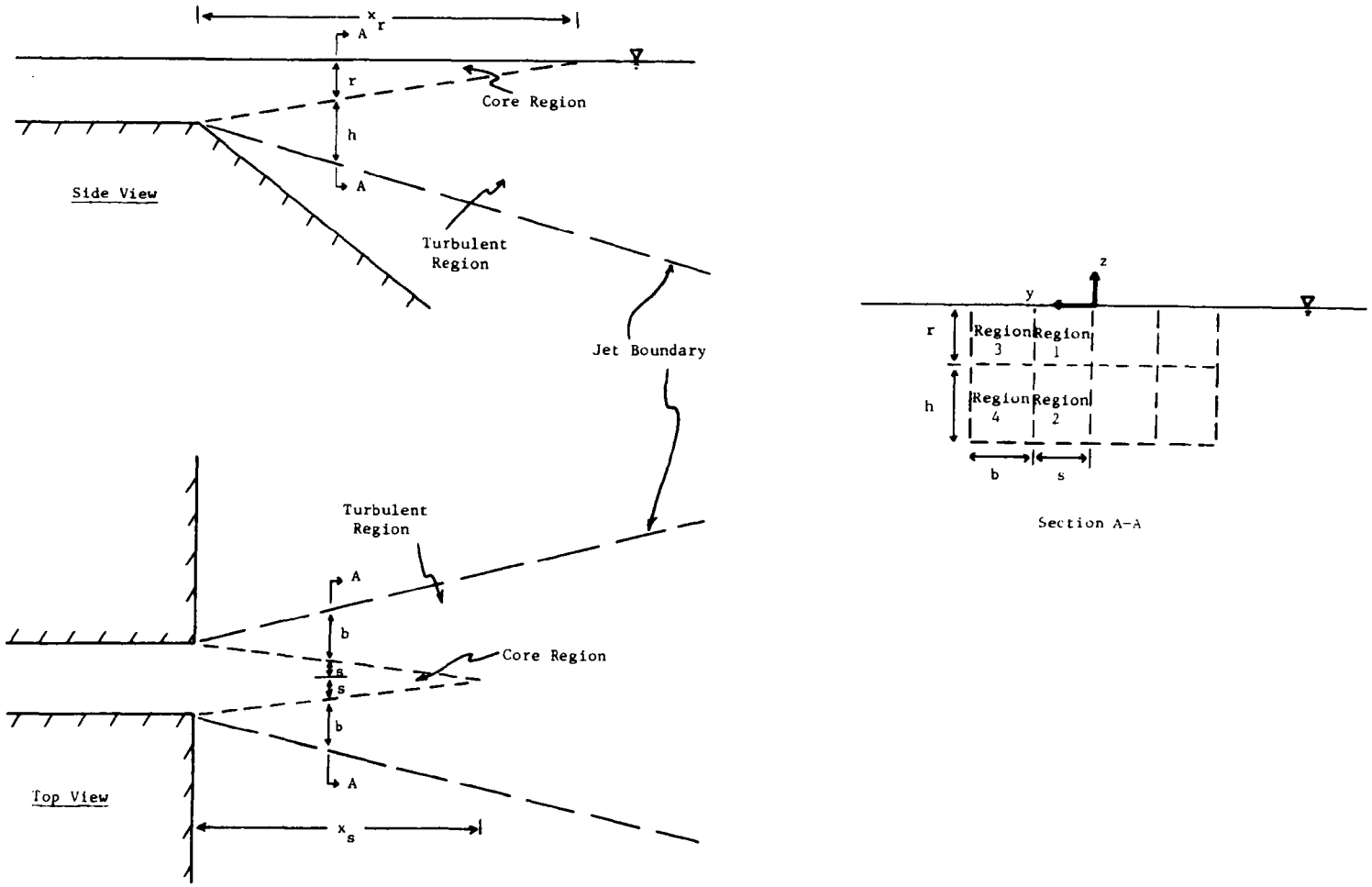

Figure 3-2. Geometrical Characteristics of the Jet

section: an unsheared core region (#1); a vertically sheared region (#2); a horizontally sheared region (#3); and a region sheared in both directions (#4). The jet is assumed to be symmetric about the plane $y = 0$. Thus only half the width of the jet will be considered in the theoretical development.

The core regions are eventually engulfed by the spreading turbulent zones. The distance at which r and s become zero are x_r and x_s respectively. If $x_r < x < x_s$ or $x_s < x < x_r$ the jet will have only two regions. For x greater than x_r or x_s a single region (#4) exists, sheared in both directions.

Figure 3-3 shows the assumed velocity distributions in the various regions of the jet:

$$u = u_c F_y(y) F_z(z) \tag{3.45}$$

where u_c is the centerline velocity at $y = 0, z = \eta$. F_y and F_z are given by:

$$\begin{aligned}
&F_y = 1.0 && 0 < y < s \\
&F_y = f(\zeta_y) && s < y < b && \zeta_y = \frac{y-s}{b} \\
&F_y = 0 && b < y
\end{aligned} \tag{3.46}$$

$$\begin{aligned}
&F_z = 1.0 && -r < z < \eta \\
&F_z = f(\zeta_z) && -h < z < -r && \zeta_z = \frac{-z-r}{h} \\
&F_z = 0 && z < -h
\end{aligned}$$

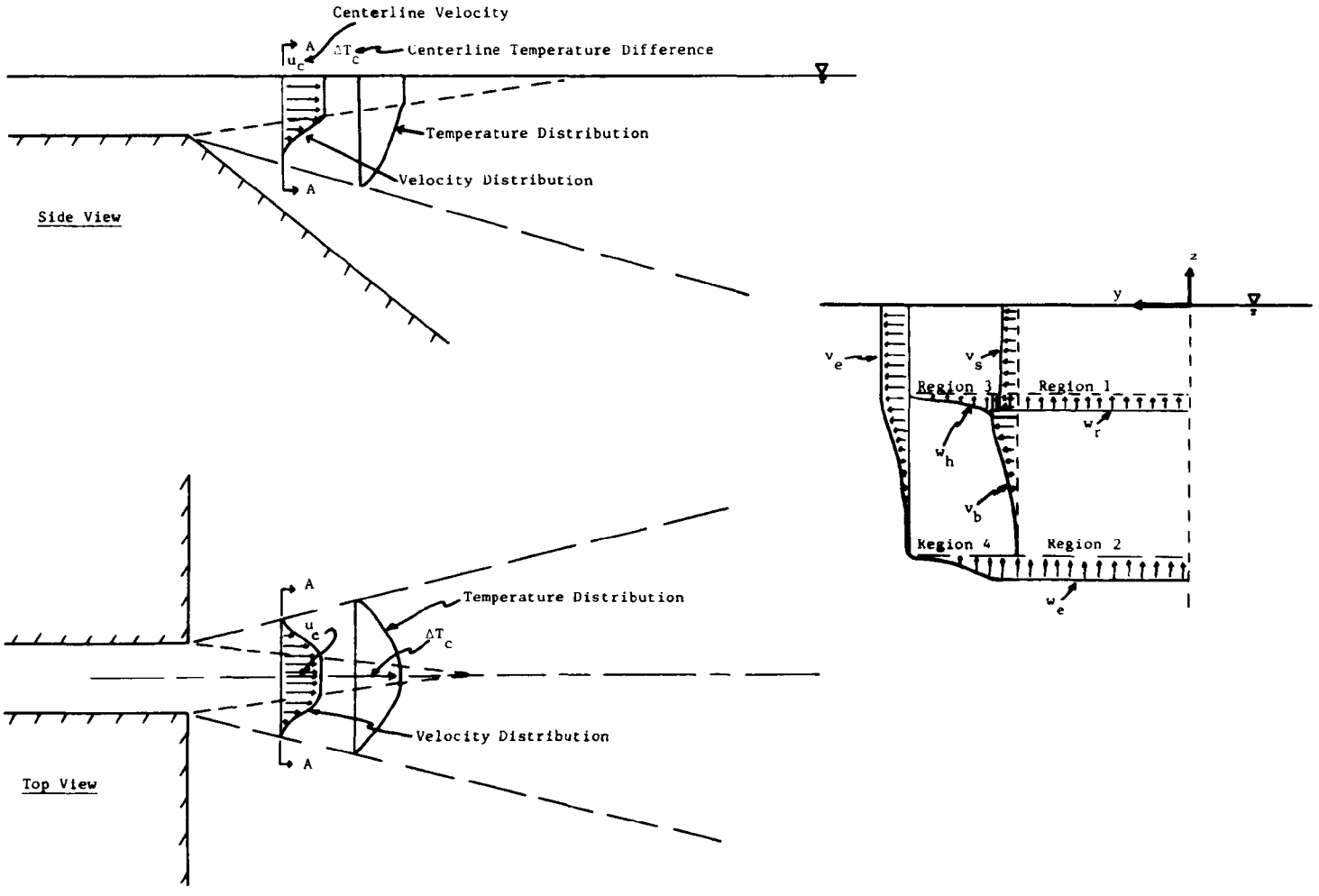

Figure 3-3. Velocity and Temperature Characteristics of the Jet

The form of the similarity function, f, is a basic assumption of this theory. A function introduced by Abramovich (1) for the main region of plane and axisymmetric jets is used

$$f = (1 - \zeta^{3/2})^2 \tag{3.47}$$

Abramovich uses a different function for the core region. The reason for using 3.47 throughout the jet in this theory is discussed in a later section.

3.3.3 Boundary Conditions

The conditions at x = 0 are assumed to be:

$$\begin{aligned} r &= h_o \\ s &= b_o \\ b &= h = 0 \\ u_c &= u_o \end{aligned} \tag{3.48}$$

These conditions imply that there is no significant turbulent boundary layer in the discharge channel.

The theoretical development treats each of the four jet regions. Thus boundary conditions must be specified on the boundaries between regions. In the following development use will be made of the kinematic boundary condition which states that particles of fluid on an impermeable flow boundary remain at the boundary.

$z = \eta$: The kinematic boundary condition holds on the free surface:

$$u \frac{d\eta}{dx} + v \frac{d\eta}{dy} = w \quad \text{at } z = \eta \tag{3.49}$$

There is no turbulent momentum transfer across the free surface

$$w'^2 = u'w' = v'w' = 0 \quad \text{at } z = \eta \tag{3.50}$$

<u>y = 0</u>: The jet is symmetrical about this plane. There is no net flux of mass or momentum across y = 0.

$$v = v'^2 = u'v' = v'w' = 0 \quad \text{at } y = 0 \tag{3.51}$$

<u>z = -r</u>: The boundary of the vertical shear region is not a rigid surface but there is no momentum transfer across this boundary:

$$w'^2 = u'w' = v'w' = 0 \quad \text{at } z = -r \tag{3.52}$$

It is assumed that the vertical velocity at z = -r is given by:

$$\begin{aligned} w &= w_r && 0 < y < s \\ w &= w_h f(\zeta_y) && s < y < b \quad \text{at } z = -r \\ w &= 0 && b < y \end{aligned} \tag{3.53}$$

where w_r and w_h are variables to be determined by the theory. If r = 0 the above conditions are not relevant and the free surface conditions hold at the upper boundary of the vertical shear region.

y = s: This boundary is analogous to z = -r. The conditions are:

$$u'v' = v'w' = v'^2 = 0$$

$$v = v_s \qquad -r < z < \eta \tag{3.54}$$

$$v = v_b f(\zeta_z) \qquad -h < z < -r \qquad \text{at } y = s$$

$$v = 0$$

where the new variables are v_s and v_b. If s = 0 the above conditions are replaced by those for y = 0.

z = -r-h: The outer boundary of the vertical shear region is assumed to be a surface with a normal velocity specified. This velocity is the entrainment velocity induced by the jet. The distribution of entrainment velocity is assumed to be:

$$\begin{aligned} w &= w_e && 0 < y < s \\ w &= w_e f(\zeta_y) && s < y < b \qquad z = -r-h \\ w &= 0 && b < y \end{aligned} \tag{3.55}$$

where w_e is to be determined. There is also no momentum transfer at this boundary

$$u'w' = w'^2 = w'v' = 0 \quad \text{at} \quad z = -r-h \tag{3.56}$$

$y = s + b$: This surface is analogous to $z = -r-h$. The conditions are:

$$v = v_e \qquad -r < z < \eta$$

$$v = v_e f(\zeta_z) \qquad -h < z < -r \qquad \text{at } y = s + b \tag{3.57}$$

$$v = 0 \qquad z < -h$$

$$v'^2 = u'v' = v'w' = 0$$

3.3.4 Integration of the Equations

To solve the equation set (3.41 - 3.49) it is necessary to integrate the equations over certain portions of the yz plane such that the contributions of the turbulent transfer terms, about which no assumption has been made, are zero.

If the y and z equations (3.43 and 3.44) are integrated over the entire yz plane of the half jet the result is:

$$0 = g(r+h)\,(\eta_{y=b} - \eta_{y=0}) - \int_{-(r+h)}^{\eta} \left.\frac{p_d}{\rho_a}\right|_{y=b} - \left.\frac{p_d}{\rho_a}\right|_{y=0} dz \tag{3.58}$$

$$0 = -\int_0^{s+b} \left.\frac{p_d}{\rho_a}\right|_{z=-\eta} - \left.\frac{p_d}{\rho_a}\right|_{z=-(r+h)} dy \tag{3.59}$$

Using Equation 3.40 it must be that

$$\frac{\eta^*}{z^*} \sim \frac{u^{*2}}{gz^*} \quad \delta \tag{2.60}$$

It is assumed that the discharge channel flow is subcritical so that the water level at x = 0 is controlled by the level of the ambient

fluid. This is true if the channel Froude number, $F_o = \frac{u_o}{\sqrt{gh_o}}$, is less than unity. It then must be that

$$\frac{n^*}{z^*} \leq \delta \tag{3.61}$$

and water surface elevations are negligible in comparison to the scale of vertical changes in the jet. Integration over the jet in the vertical direction may begin at $z = 0$ without significant error.

Equations 3.58 and 3.59 imply that the <u>total</u> pressure within the jet is constant from the interior to the boundary. This pressure may be estimated by Equation 3.40.

$$p_h^* + p_d^* \sim \delta \rho u^{*2} \tag{3.62}$$

Consider the flow of fluid outside the jet. Entrained fluid is transported from rest far from the jet, where the pressure difference induced by the jet is zero, to the boundary of the jet where it has velocity w_e or v_e. The flow outside the jet is nearly irrotational and Bernoulli's theorem may be applied along a streamline.

$$\begin{aligned} 0 &= \frac{1}{2}\rho v_e^2 + p_d \\ 0 &= \frac{1}{2}\rho w_e^2 + p_d \end{aligned} \tag{3.63}$$

or using 3.62

$$v_e \sim \delta u^*$$

$$w_e \sim \delta u^* \qquad (3.64)$$

The entrainment velocities are proportional to the local longitudinal velocity scale and are an order of magnitude less. This relationship is formalized by introducing entrainment coefficients:

$$v_e = \alpha_y u_c$$

$$w_e = \alpha_z u_c \qquad (3.65)$$

where α_y and α_z are variables to be determined by the theory.

The x momentum and the continuity equations are integrated over each region of the jet using (3.41 and 3.42) the similarity forms for velocities, the boundary conditions, and the entrainment definition:

Region # 1 - continuity

$$rs \frac{du_c}{dx} + rv_s - sw_r = 0$$

Region # 2 - continuity

$$I_1 s \frac{du_c h}{dx} + su_c \frac{dr}{dx} + v_b h I_1 + s [w_r - \alpha_z u_c] = 0 \qquad (3.66)$$

Region # 3 - continuity

$$I_1 r \frac{du_c b}{dx} + ru_c \frac{ds}{dx} - w_h b I_1 - r [v_s - \alpha_y u_c] = 0$$

Region # 4 - continuity

$$I_1^2 \frac{du_c hb}{dx} + u_c I_1 \left[b \frac{dr}{dx} + h \frac{ds}{dx} \right] + [w_h - \alpha_z u_c] I_1 b - (v_b - \alpha_y u_c) I_1 h = 0$$

Region # 1 - momentum

$$2rs \frac{du_c}{dx} + r v_s - s w_r = 0$$

Region # 2 - momentum

$$s I_2 \frac{du_c^2 h}{dx} + s u_c^2 \frac{dr}{dx} + u_c v_b h I_2 + u_c s w_r = 0$$

Region # 3 - momentum (3.66) cont'd

$$r I_2 \frac{du_c^2 b}{dx} + r u_c^2 \frac{ds}{dx} - u_c w_h b I_2 - u_c r v_s = 0$$

Region # 4 - momentum

$$I_2^2 \frac{du_c^2 hb}{dx} + u_c^2 I_2 \left[h \frac{ds}{dx} + b \frac{dr}{dx} \right] + u_c I_2 (w_h b - v_b h) = 0$$

where $I_1 = \int_0^1 f(\zeta)\, d\zeta \quad I_2 = \int_0^1 f^2(\zeta)\, d\zeta$

These eight equations are <u>not</u> sufficient to determine the eleven variables. The following experimentally observed relationships are assumed (1):

$$\frac{dr}{dx} = \frac{ds}{dx} \tag{3.67}$$

$$\frac{dh}{dx} = \frac{db}{dx} = \varepsilon \qquad (3.68)$$

Abramovich (1) notes that the value of ε is different in the core regions from that in the outer jet. He also uses a different similarity function for the core regions and matches the inner and outer regions by allowing h and b to change over a transition region. This difficulty is bypassed by allowing ε and f to be the same everywhere. The results for the outer region are the same as in Abramovich's work and the differencesin the core region are small. It is assumed that $\varepsilon = .22$ for all values of x.

3.3.5 The Solution for Non-Buoyant Jets

The solution of the Equations 3.66 - 3.68 is:

For all x,

$$v_s = v_b = w_r = w_h = 0$$

$$h = b = \varepsilon x$$

Initial Region $\quad x < \frac{h_o}{\varepsilon I_2}$, $\quad x < \frac{b_o}{\varepsilon I_2}$,

$$u_c = u_o$$

$$r = h_o - \varepsilon I_2 x$$

$$s = b_o - \varepsilon I_2 x$$

$$-\alpha_y = \alpha_z = \varepsilon(I_1 - I_2)$$

For $h_o < b_o$ $\qquad \frac{h_o}{\varepsilon I_2} < x < \frac{b_o}{\varepsilon I_2}$,

$$u_c = u_o\sqrt{\frac{h_o}{x\varepsilon I_2}}$$

$$r = 0$$

$$s = b_o - \varepsilon I_2 x$$

$$\alpha_y = -\varepsilon(I_1 - I_2)$$

$$\alpha_z = \frac{I_1 \varepsilon}{2}$$

For $b_o < h_o$ $\qquad \frac{b_o}{\varepsilon I_2} < x < \frac{h_o}{\varepsilon I_2}$,

$$u_c = u_o\sqrt{\frac{b_o}{x\varepsilon I_2}}$$

$$s = 0 \qquad (3.69)$$

$$r = h_o - \varepsilon I_2 x$$

$$\alpha_y = -\frac{I_1 \varepsilon}{2}$$

$$\alpha_z = \varepsilon(I_1 - I_2)$$

For $x > b_o/\varepsilon I_2$, $x > h_o/\varepsilon I_2$,

$$u_c = u_o\frac{\sqrt{h_o b_o}}{I_2 \varepsilon x}$$

$$r = s = 0$$

$$-\alpha_y = \alpha_z = \frac{I_1 \varepsilon}{2}$$

Defining the dimensionless variables:

$$\bar{u} = \frac{u_c}{u_o}$$

$$\bar{x} = \frac{x}{\sqrt{h_o b_o}}$$

$$\bar{h} = \frac{h}{\sqrt{h_o b_o}} \qquad (3.70)$$

$$\bar{b} = \frac{b}{\sqrt{h_o b_o}}$$

$$\bar{r} = \frac{r}{\sqrt{h_o b_o}}$$

$$\bar{s} = \frac{s}{\sqrt{h_o b_o}}$$

and the constants:

$$\bar{x}_r = \sqrt{\frac{h_o}{b_o}} \quad \frac{1}{\varepsilon I_2}$$

$$\bar{x}_s = \sqrt{\frac{b_o}{h_o}} \quad \frac{1}{\varepsilon I_2} \qquad (3.71)$$

$$A = \frac{h_o}{b_o}$$

the solution for velocity and jet dimensions is:

$$\bar{b} = \bar{h} = \varepsilon\bar{x} \qquad \bar{x} > 0$$

$$\left.\begin{aligned} \bar{u} &= 1.0 \\ \bar{r} &= \sqrt{A}\left(1 - \frac{\bar{x}}{\bar{x}_r}\right) \\ \bar{s} &= \frac{1}{\sqrt{A}}\left(1 - \frac{\bar{x}}{\bar{x}_s}\right) \end{aligned}\right\} \quad \bar{x} < \bar{x}_r \text{ and } \bar{x}_s$$

$$\left.\begin{aligned} \bar{u} &= \sqrt{\frac{\bar{x}_r}{\bar{x}}} \\ s &= 0 \\ r &= \sqrt{A}\left(1 - \frac{\bar{x}}{\bar{x}_r}\right) \end{aligned}\right\} \quad \bar{x}_s < \bar{x} < \bar{x}_r$$

$$\left.\begin{aligned} \bar{u} &= \sqrt{\frac{\bar{x}_s}{\bar{x}}} \\ r &= 0 \\ s &= \frac{1}{\sqrt{A}}\left(1 - \frac{\bar{x}}{\bar{x}_s}\right) \end{aligned}\right\} \quad \bar{x}_r < \bar{x} < \bar{x}_s \qquad (3.72)$$

$$\left.\begin{aligned} \bar{u} &= \sqrt{\frac{\bar{x}_r \bar{x}_s}{\bar{x}}} \\ \bar{r} &= \bar{s} = 0 \end{aligned}\right\} \quad \bar{x} > \bar{x}_s \text{ and } \bar{x}_r$$

For the assumed similarity function:

$$I_1 = .450$$

$$I_2 = .316 \tag{3.73}$$

and thus since $\varepsilon = .22$:

$$\bar{x}_r = 14.4\sqrt{A}$$

$$\bar{x}_s = \frac{14.4}{\sqrt{A}} \tag{3.74}$$

A plot of these solutions is shown in Figure 3-4. The data shown is from experiments by Yevdjevich (38) for turbulent air slot jets with values of A from 1.0 to 94.0. Scaling x by $\sqrt{h_o b_o}$ allows all of Yevdjevich's data to be plotted on a single line, where he presents separate curves for each value of h_o/b_o and scales x by b_o.

This section has considered a non-buoyant horizontal discharge. The solution is obtained by proposing similarity forms for velocity and temperature and by assuming linear jet spreading as discussed in Chapter 2. The definition and determination of entrainment coefficients are not necessary for the solution of the equations. However, in the following section, which treats buoyant discharges, the linear spread assumption is not valid and the entrainment coefficients determined for non-buoyant jets will be used to give information about entrainment

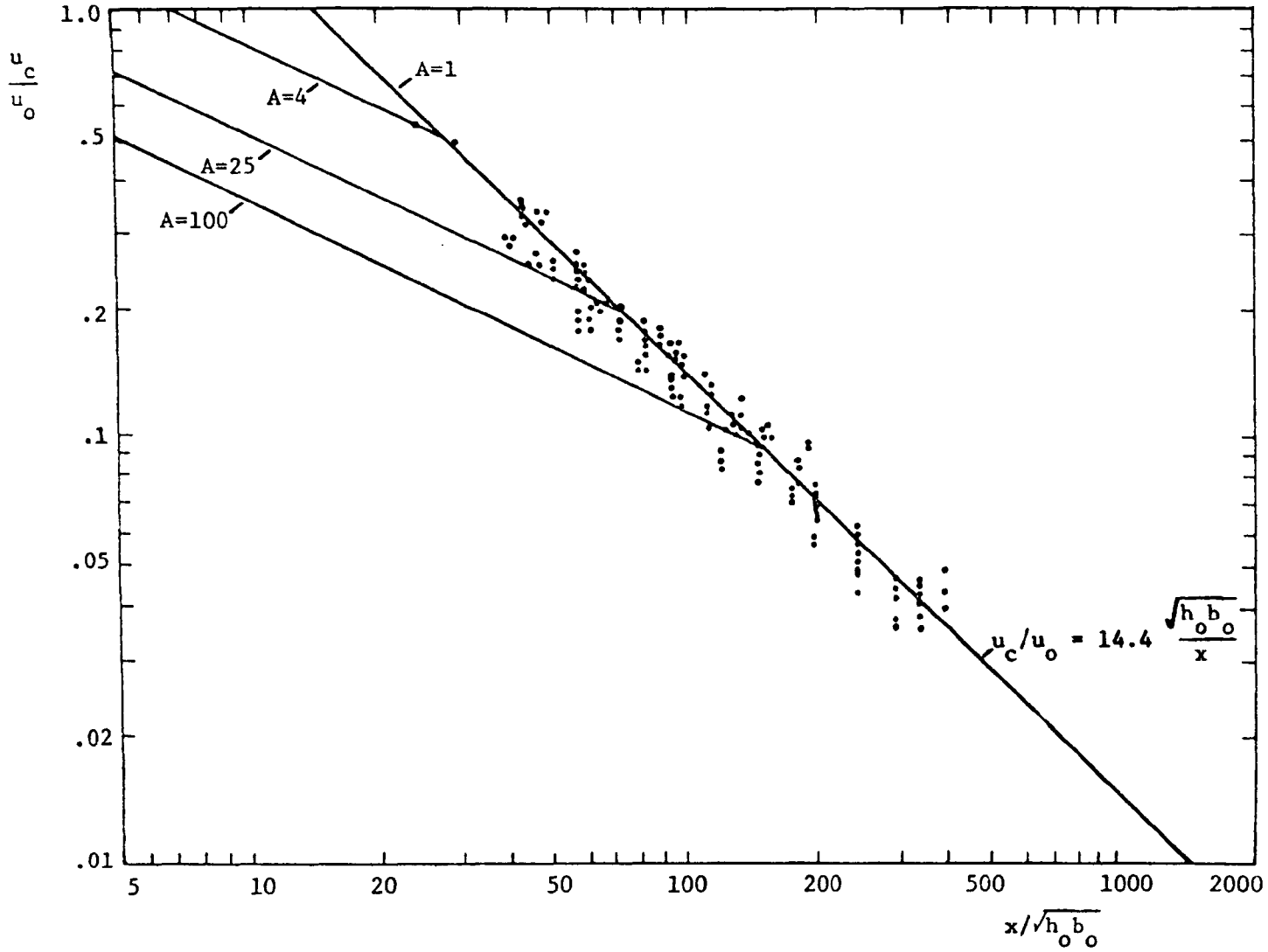

Figure 3-4. Non-Buoyant Jet Solutions: Data from Yevdjevich: $1 < A < 94$

in the buoyant case.

3.4 Buoyant Jets

3.4.1 Governing Equations

This section considers the horizontal surface discharge of water from a rectangular open channel into a large body of water. The temperature of the discharge is greater than that of the ambient water. There is no bottom slope and no ambient cross current, these effects will be included later. The heat energy and state equations are coupled with the mass and momentum conservation equations.

The scaled momentum and heat equations (3.9 - 3.12) are:

$$\frac{\partial u^2}{\partial x} + \frac{\partial uv}{\partial y} + \frac{\partial uw}{\partial z} = \underbrace{-g\frac{\partial \eta}{\partial x} - \frac{g}{\rho_a}\int_{\eta}^{-\infty}\frac{\partial \Delta\rho}{\partial x}\,dz - \frac{1}{\rho_a}\frac{\partial p_d}{\partial x}} - \frac{\partial u'^2}{\partial x} - \frac{\partial u'v'}{\partial y} - \frac{\partial u'w'}{\partial z} \tag{3.75}$$

$$1 \quad 1 \quad 1 \qquad \frac{p_d^*}{\rho_a u^{*2}} + \frac{\frac{\Delta\rho^*}{\rho_a} gz^*}{u^{*2}} \qquad \delta \quad \delta\frac{x^*}{y^*} \quad \delta\frac{x^*}{z^*}$$

$$\frac{\partial uv}{\partial x} + \frac{\partial v^2}{\partial y} + \frac{\partial vw}{\partial z} = \underbrace{-g\frac{\partial \eta}{\partial y} - \frac{g}{\rho_a}\int_{\eta}^{-\infty}\frac{\partial \Delta\rho}{\partial y}\,dz - \frac{1}{\rho_a}\frac{\partial p_d}{\partial y}} - \frac{\partial u'v'}{\partial x} - \frac{\partial v'^2}{\partial y} - \frac{\partial v'w'}{\partial z} \tag{3.76}$$

$$\frac{y^*}{x^*} \quad \frac{y^*}{x^*} \quad \frac{y^*}{x^*} \qquad \frac{p_d^*}{\rho_a u^{*2}} + \frac{\frac{\Delta\rho^*}{\rho_a} gz^*}{u^{*2}}\frac{x^*}{y^*} \qquad \delta \quad \delta\frac{x^*}{y^*} \quad \delta\frac{x^*}{z^*}$$

$$\frac{\partial uw}{\partial x} + \frac{\partial vw}{\partial y} + \frac{\partial w^2}{\partial z} = \frac{1}{\rho_a}\frac{\partial p_d}{\partial z} - \frac{\partial u'w'}{\partial x} - \frac{\partial v'w'}{\partial y} - \frac{\partial w'^2}{\partial z} \tag{3.77}$$

$$\frac{z^*}{x^*} \quad \frac{z^*}{x^*} \quad \frac{z^*}{x^*} \qquad \frac{p_d^*}{\rho_a u^{*2}}\frac{x^*}{z^*} \qquad \delta \quad \delta\frac{x^*}{y^*} \quad \delta\frac{x^*}{z^*}$$

$$\frac{\partial uT}{\partial x} + \frac{\partial vT}{\partial y} + \frac{\partial wT}{\partial z} = - \frac{\partial u'T'}{\partial x} - \frac{\partial v'T'}{\partial y} - \frac{\partial w'T'}{\partial z} \qquad (3.78)$$

$$1 \qquad 1 \qquad 1 \qquad \delta \qquad \delta \frac{x^*}{y^*} \qquad \delta \frac{x^*}{y^*}$$

If, in the x equation (3.75), the pressure term related to the density difference is to be significant, it must be that:

$$\frac{g \frac{\Delta\rho^*}{\rho_a}}{u^{*2}} \sim 1 \qquad (3.79)$$

The y equation (3.76) indicates that if $y^*/x^* \sim \delta$, there is no term of sufficient magnitude to balance the y pressure terms which would be of order $1/\delta$. The conclusion is that

$$y^*/x^* \sim 1 \qquad (3.80)$$

and as in the non-buoyant jet, for some turbulent term to be important in the x equation,

$$z^*/x^* \sim \delta \qquad (3.81)$$

The z equation (3.77) implies that:

$$\frac{P_d^*}{\rho u^{*2}} \sim \delta \qquad (3.82)$$

The equations may now be written without the negligible terms. The progression from the non-buoyant jet to the buoyant case is of interest. For this reason all the terms appearing in the non-buoyant equations are retained. In addition the free surface variation terms are eliminated by using Equations 3.22 and 3.23. The density difference is replaced by the temperature difference using Equation 3.27.

$$\frac{\partial u}{\partial x} + \frac{\partial v}{\partial y} + \frac{\partial w}{\partial z} = 0 \tag{3.83}$$

$$\frac{\partial u^2}{\partial x} + \frac{\partial uv}{\partial y} + \frac{\partial uw}{\partial z} = \frac{ag}{\rho_a}\int_z^{-\infty} \frac{\partial \Delta T}{\partial x}\, dz - \frac{\partial u'v'}{\partial y} - \frac{\partial u'w'}{\partial z} \tag{3.84}$$

$$\frac{\partial uv}{\partial x} + \frac{\partial v^2}{\partial y} + \frac{\partial uv}{\partial z} = \frac{ag}{\rho_a}\int_z^{-\infty} \frac{\partial \Delta T}{\partial y}\, dz - \frac{1}{\rho_a}\frac{\partial p_d}{\partial y} - \frac{\partial v'^2}{\partial y} - \frac{\partial v'w'}{\partial z} \tag{3.85}$$

$$0 = -\frac{\partial p_d}{\partial z} - \frac{\partial v'w'}{\partial y} - \frac{\partial w'^2}{\partial z} \tag{3.86}$$

$$\frac{\partial u\Delta T}{\partial x} + \frac{\partial v\Delta T}{\partial y} + \frac{\partial w\Delta T}{\partial z} = -\frac{\partial v'\Delta T'}{\partial y} - \frac{\partial w'\Delta T'}{\partial z} \tag{3.87}$$

3.4.2 Structure of the Jet

A comparison of the non-buoyant governing equations (3.41 - 3.44) and those derived for buoyant jets (3.83 - 3.87) indicates the effects of adding an initial temperature difference to the non-buoyant case:

1) Buoyant forces in the x direction tending to accelerate the jet.

2) Buoyant forces in the y direction which increase the lateral convection.

These effects are incorporated into the jet structure as defined for the non-buoyant jet. All the definitions of initial channel geometry, jet regions, velocity distributions, and velocity boundary conditions are assumed to be the same as those defined for the non-buoyant jet as in Sections 3.3.2 and 3.3.3.

The temperature is assumed to be distributed as follows:

$$\Delta T = \Delta T_c \, T_y(y) \, T_z(z) \tag{3.88}$$

where ΔT_c is the centerline temperature difference. The similarity function for temperature is related to the similarity function for velocity by Equation 2.13:

$$\begin{aligned} T_y &= 1.0 && 0 < y < s \\ T_y &= t(\zeta_y) && s < y < b \qquad \zeta_y = \frac{y-s}{b} \\ T_y &= 0 && b < y \end{aligned} \tag{3.89}$$

$$\begin{aligned} T_z &= 1.0 && -r < z < \eta \\ T_z &= t(\zeta_z) && -h < z < -r \qquad \zeta_z = \frac{-z-r}{h} \\ T_z &= 0 && z < -h \end{aligned}$$

where

$$t = \sqrt{f} = 1 - \zeta^{3/2} \tag{3.90}$$

The boundary conditions on the turbulent transfer of heat are as follows:

$$\begin{aligned} w'T' &= 0 \qquad & z &= -r + h \\ v'T' &= 0 \qquad & y &= 0 \text{ and } y = s + b \end{aligned} \tag{3.91}$$

i.e. no transfer of heat is allowed from the jet into the ambient fluid.

$$w'T' = K(T - T_a) \quad \text{at } z = \eta \tag{3.92}$$

where K is the surface heat transfer coefficient as defined in Equation 2.28. It is assumed that the ambient temperature T_a is nearly the equilibrium temperature T_e.

3.4.3 The y Momentum Equation

The y momentum equation (3.43) formulated for a non-buoyant discharge expresses a balance between turbulent momentum transfer and the dynamic pressure gradient. The integrated form of Equation (3.43) implies a relationship between the centerline jet velocity and the entrainment velocity which is formalized by defining a lateral entrainment coefficient, α_y, as in Equation 3.65. The y equation in the case of a buoyant discharge (3.85) contains lateral convective terms and a

pressure gradient resulting from a lateral temperature gradient. It is assumed that the non-buoyant balance between lateral turbulent entrainment and the dynamic pressure as expressed in Equation 3.34 holds for the buoyant jets and that the discussion in Section 3.3.4 is valid for horizontal entrainment:

$$v_e = \alpha_y u_c \tag{3.93}$$

where α_y is assumed to be the same for each jet region as determined for the non-buoyant jet (Equations 3.69).

Subtracting Equation (3.43) from Equation (3.85) yields a relationship between the lateral temperature gradient and the lateral convective terms

$$\frac{\partial uv}{\partial x} + \frac{\partial v^2}{\partial y} + \frac{\partial vw}{\partial z} = \frac{ag}{\rho_a} \int_z^{-\infty} \frac{\partial \Delta T}{\partial y}\, dz \tag{3.94}$$

This equation may be integrated over the entire yz plane of the half jet:

$$\frac{d}{dx} \int_o^{b+s} \int_{-h-r}^{o} uv\, dzdy = \frac{ag}{\rho_a} \int_o^{s+b} \int_{-(r+h)}^{o} \int_z^{-\infty} \frac{\partial \Delta T}{\partial y}\, d\zeta dz\, dy \tag{3.95}$$

where ζ is a dummy variable for z in the integration. In (3.94) a lateral velocity, v, appears for which there is no previously assumed distribution which will make the integration possible. This lateral

velocity is a consequence of lateral pressure gradients and causes the lateral jet spread to be greater than the non-buoyant linear spread, $\left[\frac{db}{dx}\right]_{NB}$. It is assumed that the lateral spreading velocity is related to the difference in the buoyant and non-buoyant spreading.

$$v \sim \left[\frac{db}{dx} - \left[\frac{db}{dx}\right]_{NB}\right] u \tag{3.96}$$

Since the spreading is induced by the lateral temperature difference in the jet, the distribution of v is assumed to be proportional to the temperature gradient in the y direction which is:

$$\frac{\partial \Delta T}{\partial y} = 0 \qquad 0 < y < s$$

$$\frac{\partial \Delta T}{\partial y} = \Delta T_c \, t(\zeta_z) \, \frac{dt(\zeta_y)}{d\zeta_y} \, \frac{1}{b} = -\frac{\Delta T_c}{b} \left(1 - \zeta_z^{3/2}\right) \frac{3}{2} \, \zeta_y^{1/2} \qquad s < y < b$$

$$\frac{\partial \Delta T}{\partial y} = 0 \qquad b < y$$

(3.97)

Using only the y dependent part of (3.97) the lateral spreading velocity is:

$$v = 0 \qquad 0 < y < s$$

$$v = \left[\frac{db}{dx} - \left[\frac{db}{dx}\right]_{NB}\right] u_c \left(1 - \zeta_z^{3/2}\right)^2 \left(1 - \zeta_y^{3/2}\right)^2 \zeta_y^{1/2} \qquad s < y < b$$

$$v = 0 \qquad b < y$$

(3.98)

3.4.4 Vertical Entrainment

In Section 3.3.5 the solution of the non-buoyant jet equations included vertical and horizontal entrainment coefficients, α_y and α_z. In the previous Section 3.4.3 it is assumed that for buoyant jets the lateral entrainment is not affected by the buoyancy and that the lateral entrainment coefficient, α_y, is the same as derived for the non-buoyant jet. As discussed in Chapter 2, vertical entrainment is reduced in the presence of a vertical density gradient. In this section a relationship expressing the reduction of entrainment as a function of the local Richardson number (2.17) or alternately the local densimetric Froude number (2.18) is formulated. It is assumed that the entrainment for zero density gradient is, α_z, the value derived for non-buoyant jets.

The theory by Phillips presented in Chapter 2 is used to relate the vertical entrainment to the local temperature gradient. Hinze indicates that a reasonable form for double correlation functions such as R in Equation 2.24 is:

$$R(\xi) \sim e^{-\xi^2 c^2} \tag{3.99}$$

Then it is true that:

$$G_o = \frac{\sqrt{\pi}}{2c} \tag{3.100}$$

and using (2.26) with $\alpha_o = \alpha_z$:

$$\frac{\alpha_{sz}}{\alpha_z} = e^{-N^2/4c^2} \tag{3.101}$$

where α_{sz} is the reduced vertical entrainment coefficient.

Hinze points out that for flow advected in the x direction with velocity u, the integral time scale G is $G = \lambda/u$ where λ is the integral space scale of the turbulence. Furthermore in free turbulent jets λ is proportional to the width of the turbulent region (34). It must then be true that for vertical turbulent motions:

$$G_o \sim \frac{1}{c} \sim h/u_c \tag{3.102}$$

since N^2 (see Equation 2.22) may be approximated by

$$N^2 = \frac{g}{\rho_a}\frac{\partial \rho}{\partial y} \simeq g\frac{\Delta\rho}{\rho_a}\frac{1}{h} \tag{3.103}$$

the entrainment relationship becomes:

$$\frac{\alpha_{sz}}{\alpha_z} = e^{-\beta\frac{\frac{\Delta\rho}{\rho_a}gh}{u_c^2}} = e^{-\beta/IF_L^2} \tag{3.104}$$

where IF_L is a local densimetric Froude number which corresponds very closely to that defined by Ellison and Turner. Their data, see Figure 2-2, indicates that $\beta \simeq 5.0$. Thus it is assumed that in the buoyant jet:

$$\alpha_{sz} = \alpha_z \exp\left[-5.0\frac{agh\,\Delta T_c}{\rho_a u_c^2}\right] \tag{3.105}$$

3.4.5 Integration of the Equations

The momentum and continuity equations are integrated separately over the four jet regions shown in Figure 3-2 as in the case of the non-buoyant jet. The heat equation is integrated over the entire jet. The free surface elevation is estimated as

$$\frac{\eta^*}{z^*} \sim \delta + \frac{\Delta\rho^*}{\rho_a} << 1 \qquad (3.106)$$

and may be neglected in the integration. The complete set of equations are given in Table 3-1.

The equations governing the non-buoyant jet are a system of non-linear first order differential equations. There is in general more than one solution curve, the correct choice being determined by the conditions at x = 0. Physically a jump from one solution to another is possible as long as momentum, mass, and heat are conserved without a gain in mechanical energy. The system of equations may also have singular points where some or all of the derivitives are infinite. This study will not treat the possibility of jumps in the jet solution since downstream conditions must be specified.

3.5 The Deflected Jet

3.5.1 The Governing Equations

This section treats a jet discharging into an ambient cross flow. Figure 3-5 defines a coordinate system ($\tilde{x}$, $\tilde{y}$, $\tilde{z}$) which is oriented along the centerline of the jet. The angle between the $\tilde{x}$ and y axis is θ, the jet being discharged with an initial angle θ_o. The

Region # 1 - continuity

$$rs\frac{du_c}{dx} + rv_s - sw_r = 0$$

Region # 2 - continuity

$$I_1 s\frac{du_c h}{dx} + su_c\frac{dr}{dx} + v_b h I_1 + s\,[w_r - \alpha_{sz} u_c] = 0$$

Region # 3 - continuity

$$I_1 r\frac{du_c b}{dx} + ru_c\frac{ds}{dx} - w_h b I_1 - r\,[v_s - \alpha_y u_c] = 0$$

Region # 4 - continuity

$$I_1^2\frac{du_c hb}{dx} + u_c I_1\left[b\frac{dr}{dx} + h\frac{ds}{dx}\right] + [w_h - \alpha_{sz} u_c] I_1 b - (v_b - \alpha_y u_c) I_1 h = 0$$

Region # 1 - momentum

$$u_c\left[2rs\frac{du_c}{dx} + r\,v_s - s\,w_r\right] + \frac{ags}{\rho_a}\left[\frac{d}{dx}\Delta T_c\frac{r^2}{2} + I_3 r\frac{d}{dx}\Delta T_c h\right] = 0$$

Region # 2 - momentum

$$s\,I_2\frac{du_c^2 h}{dx} + s\,u_c^2\frac{dr}{dx} + u_c v_b h I_2 + u_c s w_r + \frac{ags}{\rho_a}\left[I_4\frac{d\Delta T_c h^2}{dx} + I_3\Delta T_c h\frac{dr}{dx}\right] = 0$$

Region # 3 - momentum

$$r\,I_2\frac{du_c^2 b}{dx} + r\,u_c^2\frac{ds}{dx} - u_c w_h b I_2 - u_c r v_s + \frac{ag}{\rho_a}\left[\frac{I_3}{2}\frac{d\Delta T_c b r^2}{dx} + I_3^2 r\frac{d\Delta T_c bh}{dx}\right.$$

Table 3-1. Integrated Equations for Buoyant Jets

$$+ \Delta T_c \left(\frac{r^2}{2} + I_3 hr \right) \frac{ds}{dx} \Big] = 0$$

Region # 4 - momentum

$$I_2^2 \frac{du_c^2 hb}{dx} + u_c^2 I_2 \left[h \frac{ds}{dx} + b \frac{dr}{dx} \right] + u_c I_2 \left(w_h b - v_b h \right) + \frac{ag}{\rho_a} \Big[I_3 I_4 \frac{d\Delta T_c h^2 b}{dx}$$

$$+ I_4 \Delta T_c h^2 \frac{ds}{dx} + I_3^2 \Delta T_c hb \frac{dr}{dx} \Big] = 0$$

y-momentum

$$\frac{d}{dx} \left[\frac{db}{dx} - \frac{db}{dx}_{NB} \right] \left[u_c^2 b I_6 \left(r + h I_2 \right) \right] - \frac{ag}{\rho_a} \Delta T_c \left[\frac{r^2}{2} + I_3 rh + I_4 h^2 \right] = 0$$

heat:

$$\frac{d}{dx} \left[u_c \Delta T_c (r + h I_7) (s + b I_7) \right] + K \Delta T_c (s + b I_3) = 0$$

where

$$I_1 = \int_o^1 f(\zeta) \, d\zeta = \int_o^1 (1 - \zeta^{3/2})^2 \, d\zeta = .4500$$

$$I_2 = \int_o^1 f^2(\zeta) d\zeta = \int_o^1 (1 - \zeta^{3/2})^4 \, d\zeta = .3160$$

$$I_3 = \int_o^1 t(\zeta) d\zeta = \int_o^1 (1 - \zeta^{3/2}) d\zeta = .6000$$

Table 3-1. Integrated Equations for Buoyant Jets (cont'd)

$$I_4 = \int_0^1 \int_\zeta^1 t(\zeta)\, d\zeta d\zeta = \int_0^1 \int_\zeta^1 (1 - \zeta^{3/2}) d\zeta d\zeta = .2143$$

$$I_5 = \int_0^1 F(\zeta)\, \zeta^{1/2}\, d\zeta = \int_0^1 (1 - \zeta^{3/2})^2\, \zeta^{1/2}\, d\zeta = .2222$$

$$I_6 = \int_0^1 f^2(\zeta)\, \zeta^{1/2} d\zeta = \int_0^1 (1 - \zeta^{3/2})^4\, \zeta^{1/2}\, d\zeta = .1333$$

$$I_7 = \int_0^1 f(\zeta)t(\zeta)\, d\zeta = \int_0^1 (1 - \zeta^{3/2})^3\, d\zeta = .3680$$

$\left(\frac{db}{dx}\right)_{NB}$ = nonbuoyant spreading rate calculated from the above equation set with $\Delta T = 0$.

$$\alpha_y = \begin{cases} -(I_1 - I_2)\varepsilon & s > 0 \\ -\dfrac{I_1 \varepsilon}{2} & s = 0 \end{cases}$$

$$\alpha_z = \begin{cases} (I_1 - I_2)\varepsilon & r > 0 \\ \dfrac{I_1 \varepsilon}{2} & r = 0 \end{cases} \qquad \alpha_{sz} = \alpha_z \exp\left[-5.0 \frac{ag\Delta T_c h}{\rho_a u_c^2}\right]$$

ε = spreading rate of a free turbulent region = .22

Table 3-1. Integrated Equations for Buoyant Jets (cont'd)

$$
\left.
\begin{aligned}
r &= h_o \\
s &= b_o \\
h &= b = 0 \\
\frac{db}{dx} &= \varepsilon \\
u &= u_o \\
\Delta T &= \Delta T_o
\end{aligned}
\right\} \quad x = 0
$$

Table 3-1. Integrated Equations for Buoyant Jets (cont'd)

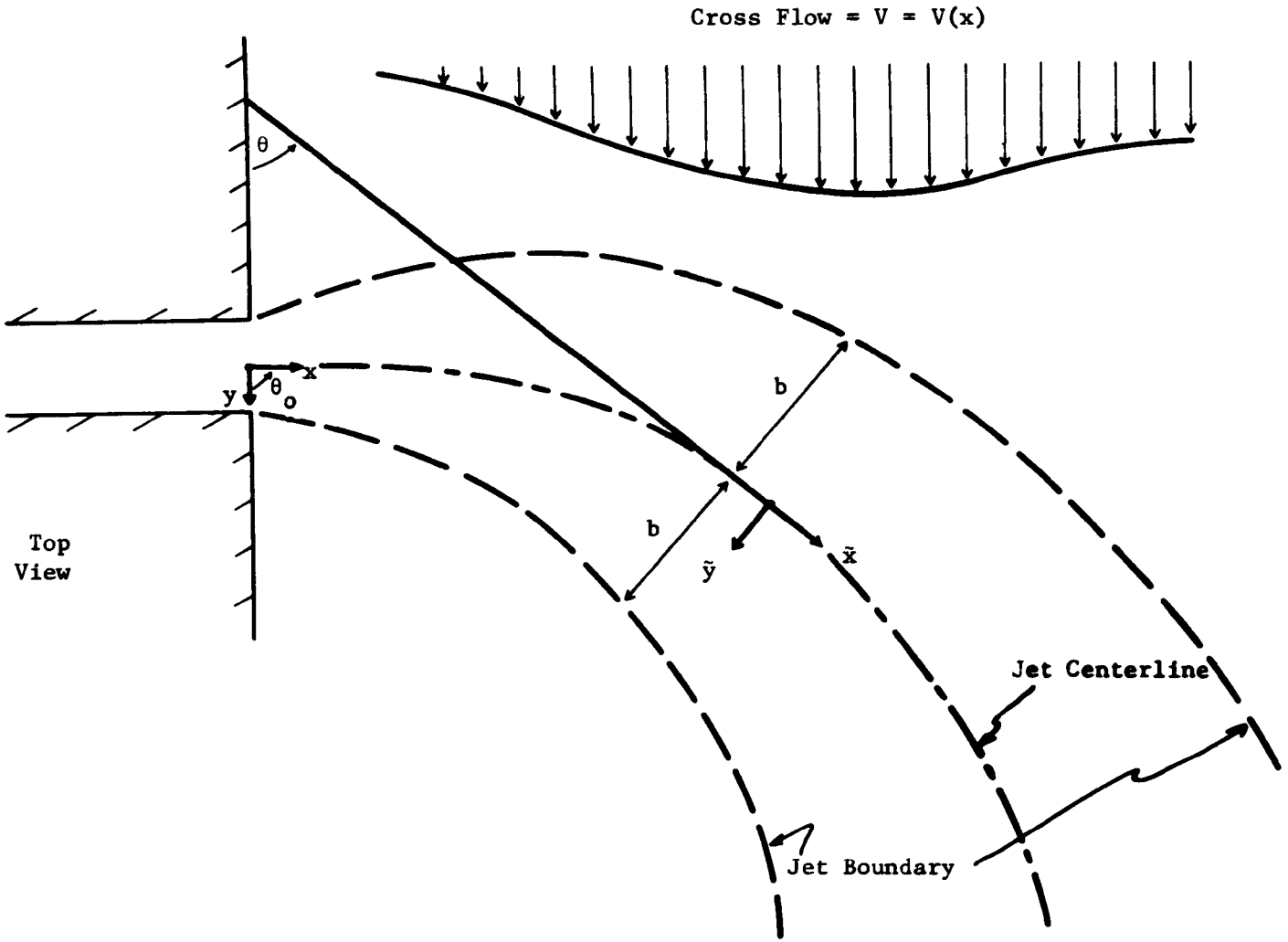

Figure 3-5. Characteristics of a Deflected Jet

cross flow velocity, V, may be a function of x but not y.

It is assumed that the deflection of the jet is sufficiently gradual that locally a cylindrical coordinate system may be defined in which $rd\theta = d\tilde{x}$, $dr = -dy$, and $r = -\left(\frac{\partial\theta}{\partial\tilde{x}}\right)^{-1}$

The governing equations for buoyant jets, (3.92 - 3.96) then contain extra terms which account for the jet curvature:

$$\frac{\partial\tilde{u}}{\partial\tilde{x}} + \frac{\partial\tilde{v}}{\partial\tilde{y}} + \frac{\partial\tilde{w}}{\partial\tilde{z}} + \tilde{v}\frac{\partial\theta}{\partial\tilde{x}} = 0 \tag{3.107}$$

$$\frac{\partial\tilde{u}^2}{\partial\tilde{x}} + \frac{\partial\tilde{u}\tilde{v}}{\partial\tilde{y}} + \frac{\partial\tilde{u}\tilde{w}}{\partial\tilde{z}} + 2\tilde{u}\tilde{v}\frac{\partial\theta}{\partial\tilde{x}} = \frac{ag}{\rho_a}\int_{\tilde{z}}^{-\infty}\frac{\partial\Delta T}{\partial\tilde{x}}\,d\tilde{z} - \frac{\partial\tilde{u}'\tilde{v}'}{\partial\tilde{y}} - \frac{\partial\tilde{u}'\tilde{w}'}{\partial\tilde{z}} - 2\tilde{u}'\tilde{v}'\frac{\partial\theta}{\partial\tilde{x}} \tag{3.108}$$

$$\frac{\partial\tilde{u}\tilde{v}}{\partial\tilde{x}} + \frac{\partial\tilde{v}^2}{\partial\tilde{y}} + \frac{\partial\tilde{v}\tilde{w}}{\partial\tilde{z}} - \tilde{u}^2\frac{\partial\theta}{\partial\tilde{x}} + \tilde{v}^2\frac{\partial\theta}{\partial\tilde{x}} = \frac{ag}{\rho_a}\int_{\tilde{z}}^{-\infty}\frac{\partial\Delta T}{\partial\tilde{y}}\,d\tilde{z} - \frac{1}{\rho_a}\frac{\partial p_d}{\partial\tilde{y}} - \frac{\partial\tilde{v}'^2}{\partial\tilde{y}}$$

$$- \frac{\partial\tilde{v}'\tilde{w}'}{\partial\tilde{z}} + \tilde{u}'^2\frac{\partial\theta}{\partial\tilde{x}} - \tilde{v}'^2\frac{\partial\theta}{\partial\tilde{x}} \tag{3.109}$$

$$0 = -\frac{\partial p_d}{\partial\tilde{z}} - \frac{\partial\tilde{v}'\tilde{w}'}{\partial\tilde{y}} - \frac{\partial\tilde{w}'^2}{\partial\tilde{z}} \tag{3.110}$$

$$\frac{\partial\tilde{u}\Delta T}{\partial\tilde{x}} + \frac{\partial\tilde{v}\Delta T}{\partial\tilde{y}} + \frac{\partial\tilde{w}\Delta T}{\partial\tilde{z}} = -\frac{\partial\tilde{v}'\Delta T'}{\partial\tilde{y}} - \frac{\partial\tilde{w}'\Delta T}{\partial\tilde{z}} \tag{3.111}$$

In the following treatment the effect of the cross flow on the jet will be expressed in terms of integrations of the equations of

motion over the entire jet. These results will be incorporated into the structure of the theory for the undeflected buoyant jet. A major assumption of the following development is that the cross flow velocities are small compared with the jet centerline velocities i.e. defining a cross flow scale velocity v^*:

$$\frac{v^*}{u^*} \sim \delta \tag{3.112}$$

If the $\tilde{x}$ and $\tilde{y}$ equations (3.108 and 3.109) are integrated over the entire jet (see Appendix II),

$$\frac{d}{d\tilde{x}} \int_{-(r+h)}^{o} \int_{-(s+b)}^{s+b} \tilde{u}^2 \, d\tilde{y}d\tilde{z} = \frac{\alpha g}{\rho_a} \int_{-(r+h)}^{o} \int_{-(s+b)}^{s+b} \int_{z}^{-\infty} \frac{d\Delta T}{d\tilde{x}} \, d\tilde{z}' \, d\tilde{y}d\tilde{z}$$

$$+ \; q_e \, V \cos\theta \tag{3.113}$$

$$\frac{d\theta}{d\tilde{x}} \int_{-(r+h)}^{o} \int_{-(s+b)}^{s+b} \tilde{u}^2 \, d\tilde{y}d\tilde{z} = - q_e \, V \sin\theta \tag{3.114}$$

where q_e is the <u>total</u> entrainment into the jet per unit distance along the $\tilde{x}$ axis. The derivation in Appendix II assumes 1) symmetry of the jet about the $\tilde{y} = 0$ plane and 2) a potential flow outside the jet which is equivalent to assuming that there is no pressure drag force on the jet.

Equations 3.113 and 3.114 are valid for the whole jet. The

effect of the cross flow is 1) to introduce an additional term in the $\tilde{x}$ momentum equation to account for entrainment of cross flow $\tilde{x}$ momentum and 2) a bending of the jet so as to balance the entrainment of cross flow $\tilde{y}$ momentum. The cross flow has the result of making the boundary conditions on velocity unsymmetrical around the jet boundary so that strictly speaking Equations 3.113 and 3.114 do not hold for any separate region of the jet. The jet will no longer be symmetrical and the analysis of the preceding sections on buoyant and non-buoyant jets cannot be applied.

It has been assumed, however, that for small cross flow velocities relative to the jet velocity the distortion of the jet is small. To apply the governing equations to the four separate jet regions the following is assumed also:

1) Equation 3.113 which holds for the entire jet is assumed to hold for each of the four jet regions separately, i.e. the effect of the cross flow on the integrated $\tilde{x}$ momentum equation (3.108) is to add a term which is the product of $V\cos\theta$ and the entrainment per unit length into the jet region being considered.
2) The similarity functions for velocity and temperature within the jet are all the same as for the undeflected jet except for u which is given by:

$$\tilde{u} = u_c F_y F_z + V \cos \theta \qquad (3.115)$$

where F_y and F_z are as defined in (3.46).

3) The boundary conditions are the same as for the undeflected jet except the conditions on the velocity at the jet boundary which are:

$$\tilde{w} = w_e - V \cos\theta \frac{dh}{d\tilde{x}} \qquad 0 < y < s \qquad \tilde{z} = -r-h$$

$$\tilde{w} = w_e f(\tilde{\zeta}_y) - V \cos\theta \frac{dh}{d\tilde{x}} \qquad s < y < b \qquad (3.116)$$

$$\tilde{v} = v_e + V \cos\theta \frac{db}{d\tilde{x}} \qquad -r < z < \eta \qquad \tilde{y} = s + b$$

$$\tilde{v} = v_e f(\tilde{\zeta}_z) + V \cos\theta \frac{db}{d\tilde{x}} \qquad -h < z < -r$$

where w_e and v_e are related to the centerline velocity, u_c, by the entrainment coefficients α_{sz} and α_y as defined for the undeflected jet.

4) Equation 3.114 which holds for the entire jet is assumed to hold for each half of the jet on either side of the surface $\tilde{y} = 0$. If the $\tilde{y}$ momentum equation (3.109) is then integrated over the half jet as in Section 3.4.3, and 3.114 is used, the result is a lateral spreading equation identical with (3.95) in the deflected coordinate system. The lateral spreading velocity is assumed to be distributed as in Section 3.4.3 taking into account the different distribution for $\tilde{u}$ i.e. for $s < y < b$

$$\tilde{v} = \left[\frac{db}{d\tilde{x}} - \left[\frac{db}{d\tilde{x}}\right]_{NB}\right] \zeta_y^{1/2} \left[u_c \left(1 - \tilde{\zeta}_z^{3/2}\right)^2 \left(1 - \tilde{\zeta}_y^{3/2}\right) + V \cos\theta\right] \tag{3.117}$$

and $\tilde{v} = 0$ elsewhere.

For deflected jets, the non-buoyant spreading rate, $\left[\frac{db}{d\tilde{x}}\right]_{NB}$, is no longer a constant but is defined by the assumption that the entrainment coefficients α_y and α_{sz} are the same in the deflected non-buoyant jet as in the non-deflected, non-buoyant jet. It is also assumed that $\frac{d}{d\tilde{x}} \left[\frac{db}{d\tilde{x}}\right]_{NB}$ is negligible i.e. that a non-buoyant, deflected jet boundary will not have a large curvature.

5) In the continuity Equation (3.107), the curvature term is negligible with respect to the other terms. Equation 3.114 implies that:

$$\frac{v^* \frac{d\theta}{d\tilde{x}}^*}{u^*/x^*} \sim \delta \frac{V^*}{u^*} \tag{3.118}$$

Thus this assumption is consistent with the basic premise (3.112).

With the above assumptions, the integrated equations governing a deflected, buoyant jet may be obtained with (3.114) determining the new variable θ. The coordinate system $\tilde{x}$, $\tilde{y}$, $\tilde{z}$ may also be related to the x,y,z system by geometrical considerations. The complete equation set is given in Table 3-2.

3.6 Bottom Slopes

The presence of a solid boundary complicates the derivation of

Region 1: continuity $rs \frac{d}{d\tilde{x}} [u_c + V\cos\theta] + rv_s - sw_r = 0$

Region 2: continuity $s \left[\frac{d}{d\tilde{x}} [h(u_c I_1 + V\cos\theta)] + (u_c + V\cos\theta) \frac{dr}{d\tilde{x}} + w_r - \alpha_{sz} u_c\right] + v_b h I_1 = 0$

Region 3: continuity $r \left[\frac{d}{d\tilde{x}} [b(u_c I_1 + V\cos\theta)] + (u_c + V\cos\theta) \frac{ds}{d\tilde{x}} - v_s + \alpha_y u_c\right] - w_r b I_1 = 0$

Region 4: continuity $\frac{d}{d\tilde{x}} \left[hb(u_c I_1^2 + V\cos\theta)\right] + (u_c I_1 + V\cos\theta) \left[b \frac{dr}{d\tilde{x}} + h \frac{ds}{d\tilde{x}}\right] + (w_h - \alpha_{sz} u_c) I_1 b$

$- (v_b - \alpha_y u_c) I_1 h = 0$

Region 1: $\tilde{x}$ momentum $(u_c + V\cos\theta)[2rs \frac{d}{d\tilde{x}} [u_c + V\cos\theta] + rv_s - sw_r] + \frac{ag}{\rho_a} s [\frac{d}{d\tilde{x}} (\Delta T_c \frac{r^2}{2}) + I_3 r \frac{d}{d\tilde{x}} (\Delta T_c h)]$

$= 0$

Region 2: $\tilde{x}$ momentum $s \left[\frac{d}{d\tilde{x}} [h (u_c^2 I_2 + 2V\cos\theta u_c I_1 + V^2\cos^2\theta)] + [u_c + V\cos\theta]^2 \frac{dr}{d\tilde{x}}\right.$

$\left. + w_r [u_c + V\cos\theta] - \alpha_{sz} u_c V\cos\theta + \frac{ag}{\rho_a} [I_4 \frac{d\Delta T_c h^2}{d\tilde{x}} + I_3 \Delta T_c h \frac{dr}{d\tilde{x}}]\right] + v_b h (u_c I_2 + V\cos\theta I_1) = 0$

Table 3-2. Integrated Equations for Deflected Buoyant Jets

Region 3: $\tilde{x}$ momentum

$$r\left[\frac{d}{d\tilde{x}}\left[b\left(u_c^2 I_2 + 2V\cos\theta u_c I_1 + V^2\cos^2\theta\right)\right] + \left[u_c + V\cos\theta\right]^2 \frac{ds}{d\tilde{x}} - v_s\left[u_c + V\cos\theta\right] + \alpha_y u_c V\cos\theta\right] - w_h b\left[u_c I_2 + V\cos\theta I_1\right] + \frac{ag}{\rho_a}\left[\frac{I_3}{2}\frac{d\Delta T_c b r^2}{d\tilde{x}} + I_3^2 r\frac{d\Delta T_c bh}{d\tilde{x}} + \Delta T_c\left(\frac{r^2}{2} + I_3 hr\right)\frac{ds}{d\tilde{x}}\right] = 0$$

Region 4: $\tilde{x}$ momentum

$$\frac{d}{d\tilde{x}}\left[hb(u_c^2 I_2^2 + 2V\cos\theta u_c I_1^2 + V^2\cos^2\theta)\right] + \left[u_c^2 I_2 + 2V\cos\theta u_c I_1 + V^2\cos^2\theta\right]\left[b\frac{dr}{d\tilde{x}} + h\frac{ds}{d\tilde{x}}\right] + \left[w_h b - v_b h\right]\left[u_c I_2 + V\cos\theta I_1\right] - u_c I_1\left[\alpha_{sz} b - \alpha_y h\right]V\cos\theta + \frac{ag}{\rho_a}\left[I_3 I_4\frac{d\Delta T_c h^2 b}{d\tilde{x}} + I_4\Delta T_c h^2\frac{ds}{d\tilde{x}} + I_3^2\Delta T_c hb\frac{dr}{d\tilde{x}}\right] = 0$$

Jet $\tilde{y}$ momentum

$$\frac{d}{d\tilde{x}}\left[\left[\frac{db}{d\tilde{x}} - \left[\frac{db}{d\tilde{x}}\right]_{NB}\right]\left[u_c^2 b I_6(r + hI_2) + 2V\cos\theta u_c b I_5(r + hI_1) + V^2\cos^2\theta b(r+h)\right] - \frac{ag}{\rho_a}\Delta T_c\left(\frac{r^2}{2} + I_3 rh + I_4 h^2\right) = 0$$

Table 3-2. Integrated Equations for Deflected Buoyant Jets (cont'd)

Jet heat	$\frac{d}{d\tilde{x}} \left[u_c \Delta T_c (s + bI_7)\ (r + hI_7) + V\cos\theta \Delta T_c\ (s + bI_3)\ (r + hI_3)\right]$
	$+ K\Delta T_c\ (s + bI_3) = 0$
Jet bending	$\left[u_c^2\ (s + bI_2)\ (r + hI_2) + 2V\cos\theta u_c\ (s + bI_1)\ (r + hI_1) +\right.$
	$\left. V^2\cos^2\theta (s+b)\ (r + h)\right] \frac{d\theta}{d\tilde{x}} - u_c V\sin\theta \left[-\alpha_{sz}(s + bI_1) + \alpha_y (r + hI_1)\right] = 0$
Jet x position	$\frac{dx}{d\tilde{x}} - \sin\theta = 0$
Jet y position	$\frac{dy}{d\tilde{x}} - \cos\theta = 0$
where:	$I_1, I_2, I_3, I_4, I_5, I_6, I_7$ are as defined in Table 3-1

Table 3-2. Integrated Equations for Deflected Buoyant Jets (cont'd)

$\frac{db}{d\tilde{x}}_{NB}$ = non-buoyant spreading rate calculated from above equations with $\Delta T = 0$

$$\alpha_y = \begin{cases} -(I_1 - I_2)\varepsilon & s > 0 \\ -\frac{I_1\varepsilon}{2} & s = 0 \end{cases}$$

$$\alpha_z = \begin{cases} (I_1 - I_2)\varepsilon & r > 0 \\ \frac{I_1\varepsilon}{2} & r = 0 \end{cases}$$

$$\alpha_{sz} = \alpha_z \exp\left[-5.0 \frac{ag\Delta T_c h}{\rho_a u_c^2}\right]$$

ε = spreading rate of a free turbulent region = .22

$r = h_o$

$s = b_o$

$x = y = h = b = 0$

$\frac{db}{d\tilde{x}} = \varepsilon$

$u = u_o$

$\Delta T = \Delta T_o$

$\theta = \theta_o$

$\tilde{x} = 0$

Table 3-2. Integrated Equations for Deflected Buoyant Jets (cont'd)

the governing equations since a number of the basic assumptions made for no slopes are no longer valid as discussed in Chapter 2. The jet will remain attached to the bottom until adverse pressure gradients or buoyancy effects cause separation, at which time vertical entrainment, until then inhibited, will begin. This study will not attempt a theory which predicts the point of separation due to adverse pressure gradients. It is assumed that the jet will not separate from the bottom, over the entire width of the jet, until the buoyant effects of lateral spreading cause the slope of the bottom of the jet to be less than the bottom slope i.e.

$$\frac{dh}{dx} + \frac{dr}{dx} < S_x \tag{3.119}$$

Before this point, vertical entrainment, w_e, is zero and the jet is attached to the bottom:

$$\frac{dh}{dx} + \frac{dr}{dx} = S_x \tag{3.120}$$

In addition, the presence of the bottom invalidates the expressions for pressure gradients since the pressure gradient at $z = -\infty$ is no longer known. It is assumed that until buoyant separation occurs that the buoyant terms have no effect on the jet.

The formulation of Equation 3.120 in the pre-separation zone, requires the relaxation of one of the other governing equations. It is assumed that frictional losses are negligible and that the x momentum equations are valid. Since the non-buoyant y-equations result in

$\frac{db}{dx} = \frac{dh}{dx}$ which is known to be true only for jets free from solid boundaries, the y-equation is dropped.

The calculation of a jet over a bottom slope proceeds by testing at each x step whether, if the bottom slope were not present, the inequality 3.119 would hold. If the jet is spreading less than the bottom slope, calculation proceeds as if the bottom were not there. This assumes that once separation occurs, the losses in the entrained flow between the jet and the bottom are small. If the jet is spreading more rapidly than the bottom allows, Equation 3.120 replaces the y-equation and the calculation proceeds with that set of equations. This formulation is valid with and without cross flows.

3.7 Solution Method

The solution of the governing equations is done using a fourth order Runge-Kutta integration technique supplied in the IBM Fortran Scientific Subroutine Package. The routine chooses a step size to meet a specified error bound for each step. The calling program keeps track of which region the calculation is in i.e. whether r or s are zero and supplies the appropriate equations. The actual IBM routine was modified slightly to prevent negative values of the physically positive variables. A listing of the program and an input format is given in Appendix I.

The results of the calculations are output in dimensionless form with u_o, ΔT_o and $\sqrt{h_o b_o}$ being the normalizing velocity, temperature and length respectively.

IV. Experimental Equipment and Procedure

4.1 Previous Experiments

As mentioned in Chapter 2, experimental studies of heated surface discharges have been done by Wiegel, Jen, Stefan, Tamai, and Hayashi. Some of the data from these experiments are compared with the theory of this study in the next chapter. An examination of the experimental techniques of the previous investigators is useful in designing improved experiments and in avoiding duplication of effort. Table 4-1 gives a summary of the characteristics of each previous experimental study:

1) Interest has clearly focused on low densimetric Froude number jets. Only Stefan considers a case where $\mathbb{F} < 1.0$ and a wedge of ambient water intrudes into the discharge channel. Good control of discharge flow and temperature is necessary if $\mathbb{F}$ is to be held constant during the course of an experiment. Wiegel's and Jen's experiments have a large variation in $\mathbb{F}$ for each case.
2) The magnitudes of the Reynolds numbers in Table 4-1 reflect the difficulty of achieving a large Reynolds number in a laboratory experiment, especially when low Froude numbers are required. Wiegel, Stefan and Hayashi report values of $\mathbb{R}$ close to or below 3000, the minimum value for fully developed turbulence in circular jets as discussed in Chapter 2.
3) The dimensions of the receiving basins are typical of

Investigator	$\mathbb{F}$	$\mathbb{R}$	Receiving Basin	Boundary Flow Control	Maximum $x/\sqrt{h_o b_o}$	Measurements
Jen (21)	18-180	8300-21000	26' x 15' x 1.5'	none	400 $.010' < h_o < .016'$ $.032' < b_o < .05'$	Thermocouples Scanned to Each x-then Moved
Wiegel (37)	20-30	700-9300	26' x 15' x 1.5'	none	400 Circular $.0164' < D < .0361'$	Thermocouples Scanned at Each x-then Moved
Tamai (32)	2.5-11.3	7100-21300	25' x 3.5' x 2'	none	100 Circular $.033' < D < .084'$	Fixed Thermistors Scanned
Hayashi (15)	1.4-16.1	3000-5600	36' x 17' x 1.5'	none	130 $2b_o = h_o = .154'$	Fixed Thermocouples Scanned
Stefan (31)	0.6-7.2	1200-9600	40' x 17' x 2'	Downstream Wier Overflow & Upstream Cold Water Make-up Flow	100 $b_o = .25'$ $.088' < h_o < .166'$	A Tethered Sphere Velocity Probe & a Thermistor Probe Scanned Vertically then Moved to a New Position

Table 4-1. Summary of Previous Experiments

university laboratory facilities except for Tamai who uses a narrow channel. It is likely that the side walls of Tamai's channel severely limit lateral mixing and spreading, thus distorting the jet behavior. For this reason, Tamai's data is not discussed in Chapter 5. None of the experiments considered cross currents in the receiving basin.

4) Only Stefan provides for a disposal of the heated discharge at the boundary of the basin. Such control is necessary if steady state conditions are to be achieved during an experimental run. Boundary flow control may also reduce eddying of the ambient water in the far corners of the receiving basins.

5) Low densimetric Froude number discharges require large channel dimensions if Reynolds numbers are to remain high. The available scaled distance, $x/\sqrt{h_o b_o}$, decreases as IF decreases. Many of Stefan's results are for $x/\sqrt{h_o b_o}$ less than 50. In such a limited distance the differences in jet behavior between separate runs are small and it is difficult to determine the effects of the controlling parameters.

6) As noted by Wiegel, buoyant surface jets have a tendency to meander in the horizontal plane about a mean centerline. A fast scanning multi-probe temperature measurement system

is best for obtaining an accurate three-dimensional determination of temperature. Measurements with a single movable probe such as Stefan uses must account for the unsteady nature of the flow.

7) The velocity of the discharge in the laboratory is usually less than 1 ft/sec and decreases rapidly away from the jet origin. A three-dimensional velocity determination requires a probe capable of measuring velocities less than .1 ft/sec. Only Stefan uses such a probe during the experimental runs.

8) None of the previous experiments involve control of the surface heat exchange from the water in the receiving basin. This requires a room in which temperature and humidity are regulated. This is usually difficult to achieve in a room large enough to hold the experimental basin necessary for jet studies.

In light of the above discussion of previous studies, the experiments in this investigation are designed with the following objectives:

1) Close control of discharge flow and temperature.

2) Reynolds numbers greater than 10,000.

3) Boundary flow control which allows operation of the experiment without a significant change in the steady state behavior.

4) Values of $x/\sqrt{h_o b_o}$ greater than 50.

5) An accurately positioned, fast scanning temperature measurement system.

6) The capability for generating cross flows in the receiving basin.

7) Addition of a sloping bottom in the receiving basin.

The measurement of velocity and the complete control of heat transfer are considered beyond the resources of this study. However, the laboratory is air conditioned so the ambient temperature remains reasonably constant.

4.2 Experimental Setup

Figure 4-1 shows the arrangement of the experimental equipment. The receiving basin is 46' x 28' x 1.5'. All the walls within the basin, including the discharge channel, are constructed of marine plywood. The adjustable sluice walls along the sides are held by c-clamps. The probe platform rests on four leveling jacks which may be reached from the sides of the basin. Point guages at each corner of the platform assure accurate control of the platform level. The sloping bottom is a lightweight aluminum frame over which industrial plastic sheeting is stretched. The water level in the basin is monitored by a fixed point guage.

The heated discharge is supplied from a steam heat exchanger capable of delivering up to 60 gallons per minute of water at a constant temperature up to 150°F. The flow is introduced into the discharge channel through a gravel filter to insure a uniform velocity distribution in the channel.

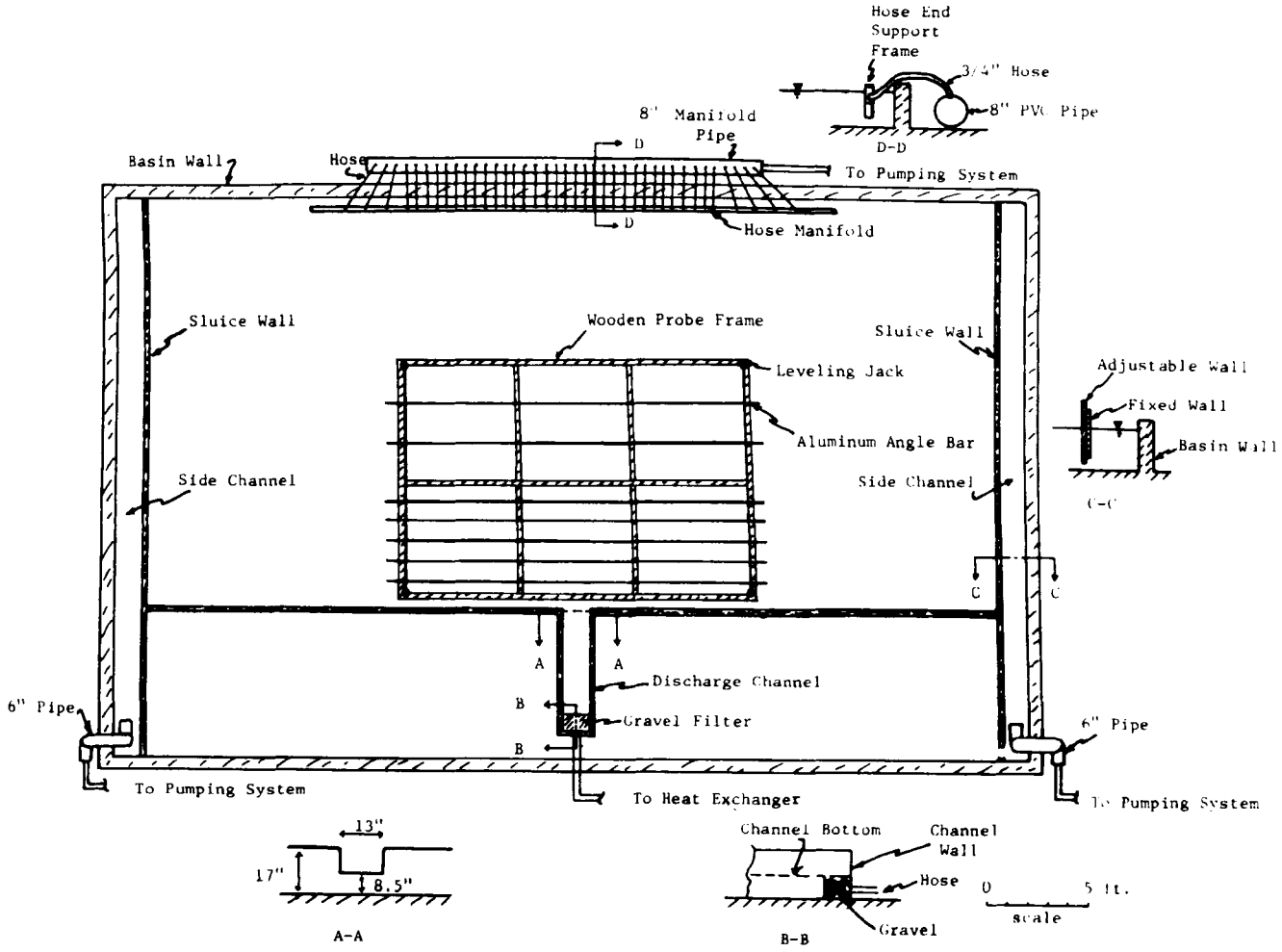

Figure 4-1. Experimental Set-Up

Boundary flow control is established at the sides and at the rear of the basin. Water may be pumped into or out of each side channel to create a cross flow in the receiving basin. At the rear of the basin there is a manifold consisting of 40 lengths of 3/4" hose with one end mounted on the basin and the other end tapped into a 30' x 8" PVC pipe outside the wall. The position and orientation of the hose ends in the basin are adjustable along a frame suspended parallel to the back wall.

A five horsepower centrifugal pump is used to provide two modes of boundary control. Water may be withdrawn from the rear of the basin through the hose manifold and returned to the side channels or a cross flow may be established in the basin by pumping from one side channel to the other. A drain line and a cold water inflow line are connected to the pumping system to permit replacement of heated water withdrawn from the basin by new colder water.

All flows are monitored by Brooks rotameter flowmeters except for the drain and cold water input flows which are measured with simple Venturi meters. Most of the pipe fittings and valves are schedule 80 PVC plastic. Water hose is used in place of pipe whenever possible.

The temperature measurement system consists of 67 Yellow Springs Instrument #401 thermistor probes, 59 of which are mounted on the basin platform (see Figure 4-2) and the remainder in the various inflow and outflow pipes. The probes are connected to a Digitec (United Systems) scanning and printing system capable of a scanning rate of 1 probe per second. The temperature in degrees Fahrenheit is printed on a paper

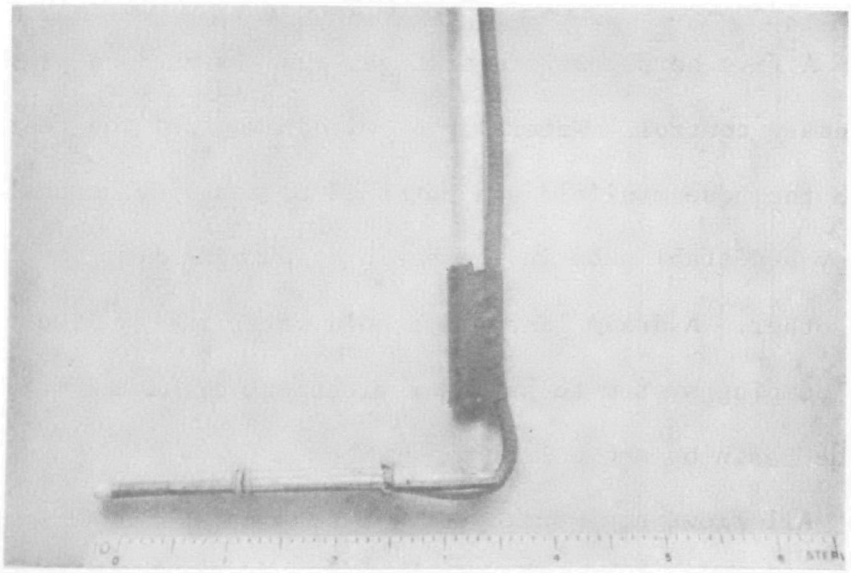

Figure 4-2. Mounted Thermistor Temperature Probes
(scale in inches)

tape. The probes have an accuracy of about $\pm$ .25°F with an interchangeability of $\pm$ .05°F. The response time constant of the probes is 7 seconds which filters out turbulent fluctuations. The probes are leveled using the water surface as a reference plane.

The laboratory building is air conditioned and the temperature is relatively constant. This has the advantage that surface heat loss rates do not vary greatly. The wet and dry bulb air temperatures are measured using two thermistor probes, one of which is covered by a water saturated gauze strip, mounted in an air flow provided by a small blower. The wet bulb and dry bulb temperatures are constant at about 66°F and 73°F from day to day.

4.3 Experimental Procedures

An entire experimental run is completed in about one hour. Surface temperatures are scanned initially to insure that no ambient temperature gradients are present. The basin boundary flows are then established. In the case of no cross flow, the back wall manifold is primed and an equal flow to each side wall of 50 gpm is established in all cases. The back manifold does not function well as a selective withdrawal device and cannot withdraw from a surface layer without suction of air. It is used solely as a means for maintaining the basin level and for preventing large eddies in the ambient fluid. The vertical position of the hose ends is maintained at about .5 ft. from the basin bottom, pointing toward the discharge. A very slow ambient current from the side walls to the back is set up which reduces eddying but does not distort the jet structure. The capability of the pumping

system to replace the manifold withdrawal with cold water is not used at all except to maintain the basin level by discharging into the drain line a flow equal to the channel discharge.

The channel flow is established by first turning on a bypass flow from the heat exchanger to a drain and adjusting the temperature of this flow to the desired value. The flow to the discharge channel is then gradually increased to the proper rate.

Table 4-2 gives a summary of the parameters of each run. The Reynolds number of all runs is near 10,000 and the density differences are all about .004, corresponding to a temperature difference of about 25°F. In Runs 1-10 only the densimetric Froude number and the channel geometry are varied with no bottom slope or cross flow. In Runs 11-19 the bottom slope is placed in the basin and varied from 1/100 to 1/25 for several values of F. The last runs, 20-25, investigate the case of an ambient cross flow, without bottom slope, over the entire width of the basin. To avoid difficulty in comparing the results of different cross flow runs, the same cross flow was maintained continuously during Runs 20-25. The distribution of cross flow velocity, measured by timing submerged floats, is shown in Figure 4-3.

4.4 Data Analysis

The data from each experiment consists of flow rates, temperatures in the jet, and temperatures of the various inflows and outflows from the basin. The ambient temperature is defined as the initial basin temperature. A variation in the surface temperature at the extremities of the basin is determined to be about 0.5°F per hour but the sub-sur-

	Physical Variables								Dimensionless Parameters				
Run No.	h_o (ft)	b_o (ft)	u_o $\frac{ft}{sec}$	T_a °F	ΔT_o °F	$\Delta\rho/\rho_a \times 10^3$	V_{max} $\frac{ft}{sec}$	S_x	$\mathbb{R}_o \times 10^4$	$\mathbb{F}_o$	h_o/b_o	$\frac{V_{max}}{u_o}$	$\frac{K}{u_o} \times 10^5$
1	.290	.380	.24	71.5	25.3	4.10	0	∞	1.5	1.00	.76	0	8.5
	(.417)		(.14)						(1.1)	(.58)	(1.10)		
2	.258	.315	.19	69.9	25.6	4.05	0	∞	1.1	1.03	.82	0	10.5
3	.164	.188	.32	72.1	24.3	3.95	0	∞	1.1	1.83	.87	0	6.2
4	.452	.104	.35	71.2	25.8	4.19	0	∞	1.2	1.42	4.30	0	5.8
5	.355	.063	.50	71.8	24.1	3.89	0	∞	1.1	2.35	5.70	0	4.0
6	.079	.229	.48	73.3	27.4	4.65	0	∞	1.1	4.40	.35	0	4.2
7	.088	.104	.58	72.3	26.1	4.31	0	∞	1.1	5.22	.84	0	3.5
8	.081	.063	.72	72.3	27.0	4.50	0	∞	1.0	6.53	1.30	0	2.8
9	.164	.042	.95	72.6	23.7	3.86	0	∞	1.3	6.60	3.95	0	2.1
10	.083	.042	1.06	71.8	27.6	4.60	0	∞	1.2	9.55	2.00	0	1.9
11	.246	.313	.20	73.7	23.6	3.91	0	.01	1.1	1.13	.78	0	10.0
12	.246	.313	.20	73.3	23.9	3.94	0	.02	1.1	1.13	.78	0	10.0
13	.246	.313	.20	72.8	24.3	3.99	0	.04	1.1	1.13	.78	0	10.0
14	.355	.063	.60	73.2	26.3	4.42	0	.01	1.3	2.70	5.70	0	3.3
15	.355	.063	.60	74.0	25.6	4.33	0	.02	1.3	2.70	5.70	0	3.3
16	.355	.063	.60	74.2	25.1	4.24	0	.04	1.3	2.70	5.70	0	3.3
17	.079	.043	1.25	70.4	28.0	4.55	0	.01	1.4	11.60	1.90	0	1.6
18	.079	.043	1.25	70.8	27.6	4.50	0	.02	1.4	11.60	1.90	0	1.6
19	.079	.043	1.25	71.2	27.2	4.45	0	.04	1.4	11.60	1.90	0	1.6
20	.164	.188	.33	70.9	32.2	5.45	.085	∞	1.1	1.16	.87	.26	6.2
21	.164	.188	.22	73.1	36.1	6.50	.085	∞	.8	1.20	.87	.39	9.0
22	.164	.188	.21	72.8	15.4	2.35	.085	∞	.7	1.88	.87	.40	9.5
23	.164	.042	.74	72.1	34.1	6.14	.085	∞	.9	4.10	3.95	.12	2.8
24	.164	.044	.98	71.5	31.2	5.29	.085	∞	1.3	5.85	3.95	.09	2.0
25	.164	.042	.74	72.6	15.5	2.35	.085	∞	.9	6.60	3.95	.12	2.8

Note: a) All cross flows as in Figure 4-3.
b) Surface heat loss coefficient, K, assumed to be 2×10^{-5} ft/sec in all cases (see Chapter 5).
c) For Run 1 numbers in parenthesis indicate values upstream of cold water wedge.
d) Reynolds number, $\mathbb{R}$, defined as $4u_o R_H/\nu$ where R_H = hydraulic radius = $b_o h_o/(h_o + b_o)$.

Table 4-2. Summary of Experimental Runs

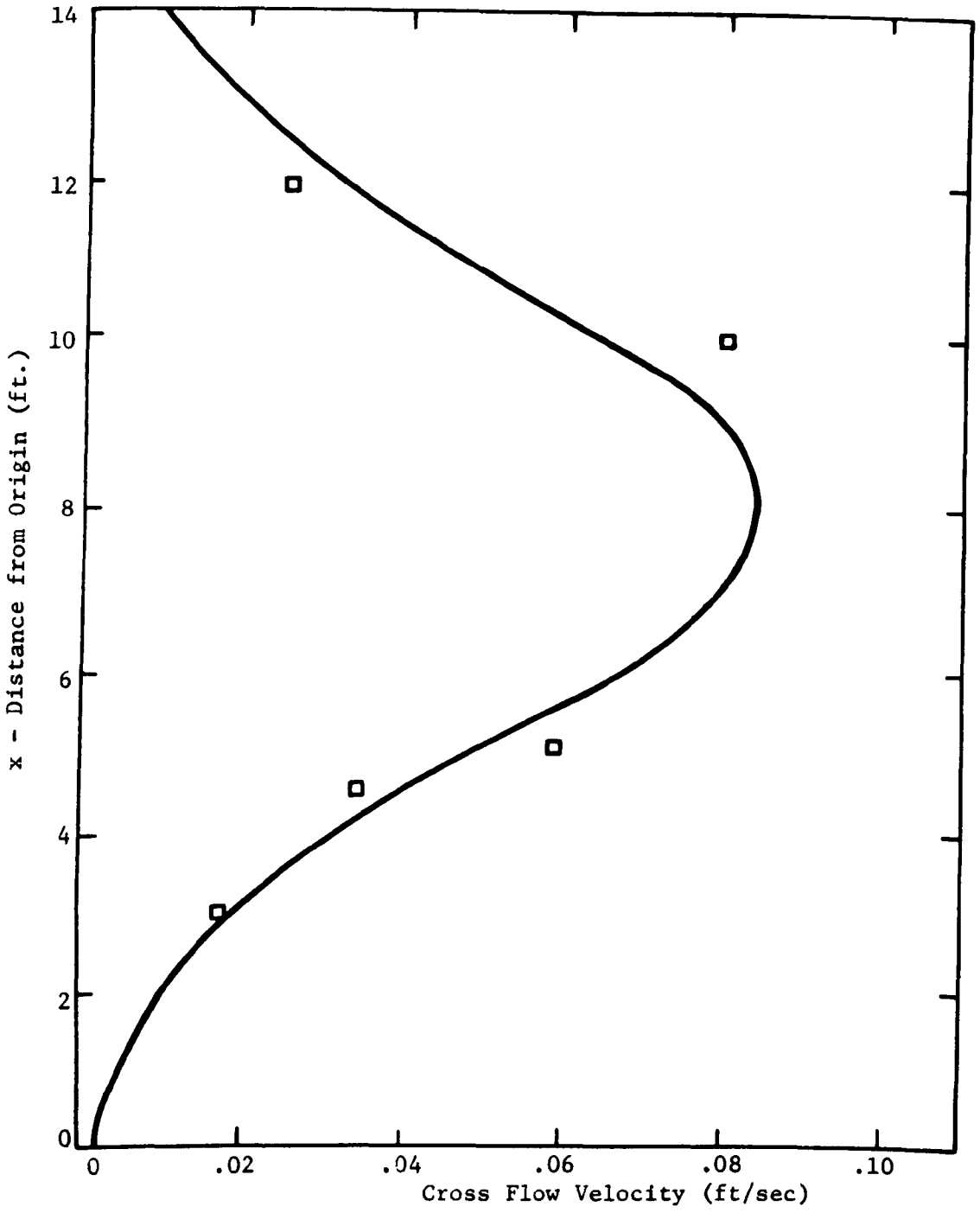

Figure 4-3. Cross Flow Velocity in Experimental Basin

□ Measured

——— Function used in Computer Program

face ambient temperature is constant over the time of the experiment. Figures 4-4 and 4-5 are a sample of the three-dimensional temperature distribution measured by the movable probes for Run No. 10 and Run No. 22. The data anlaysis resulted in centerline temperature rises and jet widths and depths as follows:

1) The lateral profiles of surface temperature at all x are plotted i.e. T vs. y at all x. Centerline temperature rises above the ambient, ΔT_c, are immediately available as in the position, y_c, of the centerline in the case of deflected jets.
2) The half width of the jet, $b_{1/2}$, is the distance between the centerline and the point where the surface temperature rise is half the centerline temperature rise. Actually the average of the left and right half widths is determined in the data analysis.
3) At each value of x centerline temperatures at each depth are determined and plotted i.e. ΔT_c vs. z at all x. The half depth, $h_{1/2}$, is the depth at which the centerline temperature rise is half the surface centerline temperature rise.

The temperature rises and distances obtained by these processes are normalized by the initial temperature rise, $T_o - T_a$, and the length, $\sqrt{h_o b_o}$, respectively.

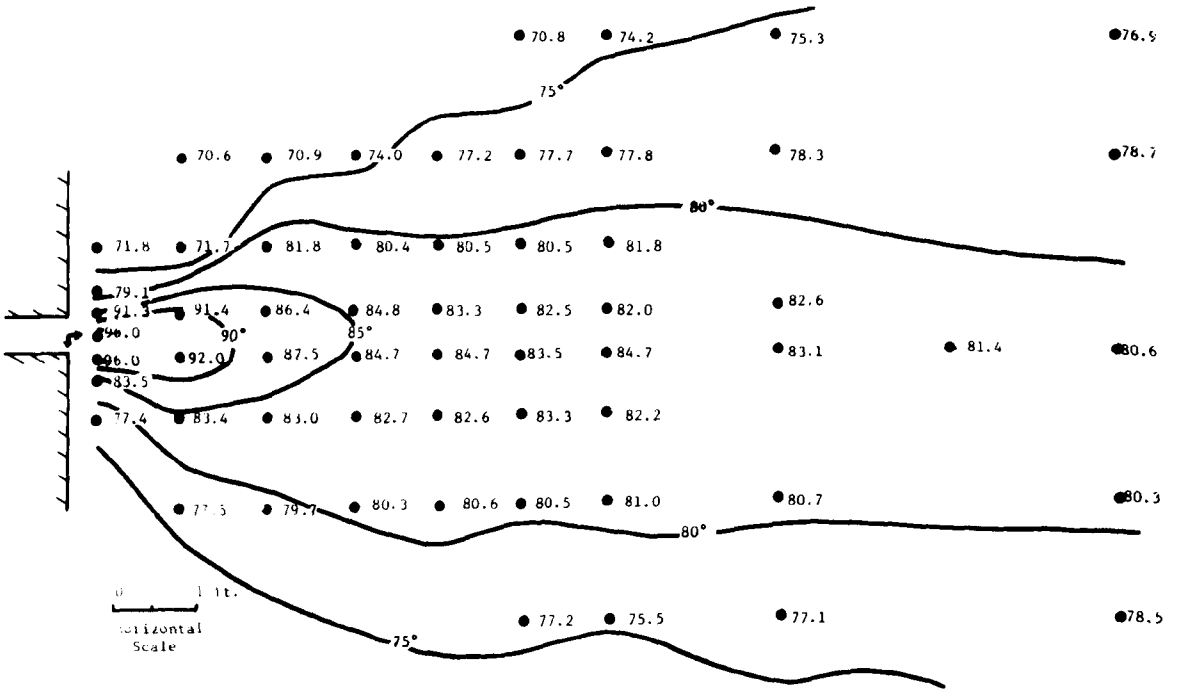

Surface Temperature Contours (z = 0)

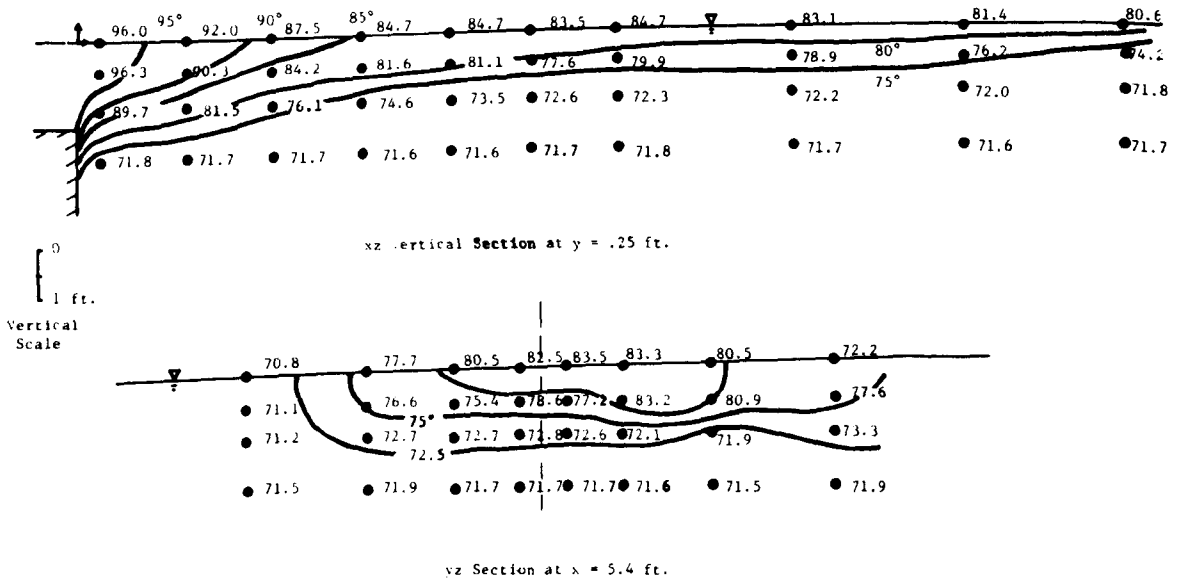

xz Vertical Section at y = .25 ft.

yz Section at x = 5.4 ft.

Figure 4-4. Temperature Distribution Measured for Run No. 3

Probe Position ●

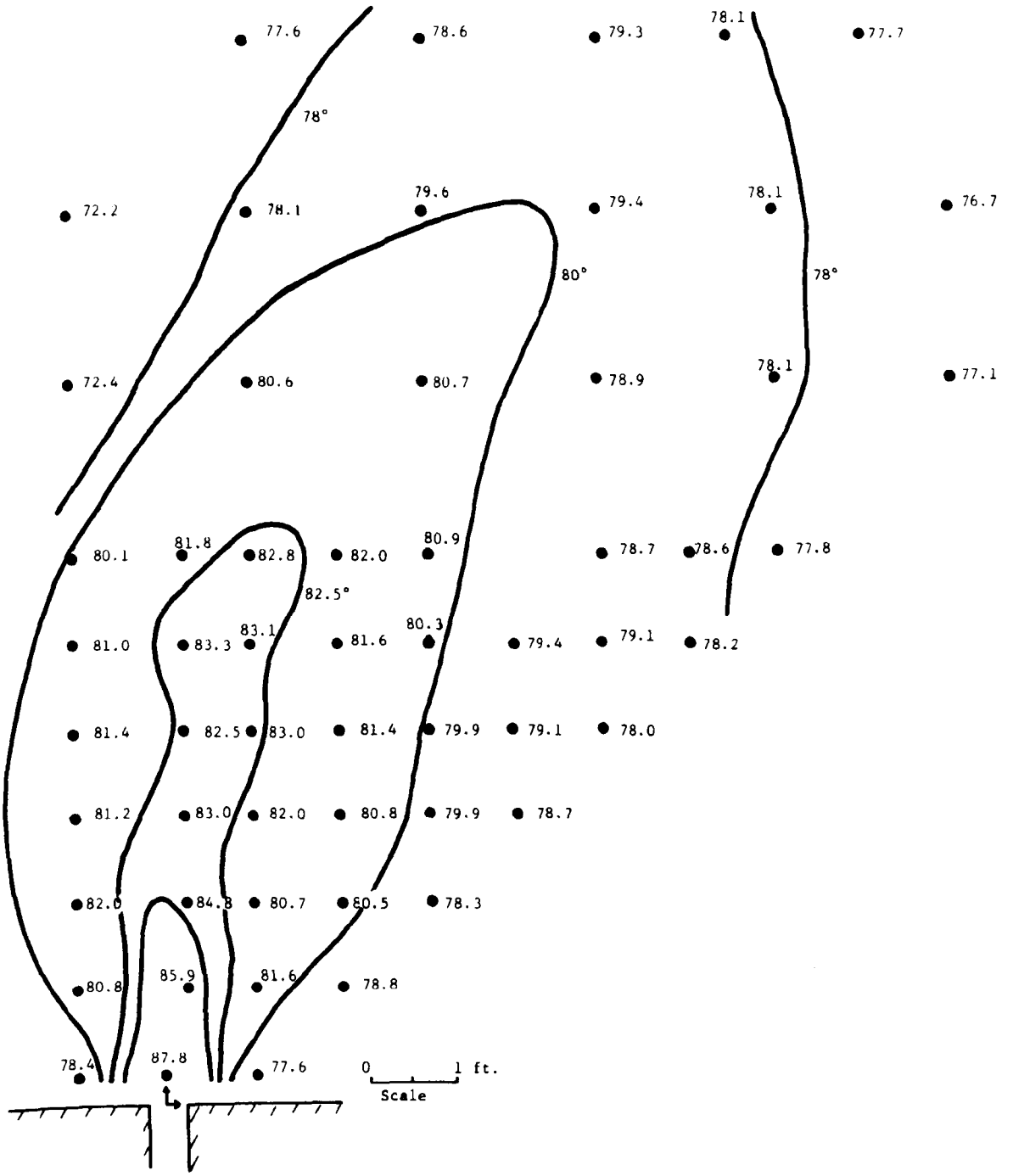

Figure 4-5. Surface (z = 0) Temperature Distribution Measured for Run 22 - With Cross Flow

Probe Position ●

V. Discussion of Results

5.1 The Controlling Parameters

This chapter is a comparison of the results of the laboratory experiments, in this study and others, with the calculations of the theoretical model developed in Chapter 3. The response of the characteristics of the heated discharge to the dimensionless parameters describing the discharge and the ambient conditions is examined.

The physical variables characterizing each discharge may be combined into the following dimensionless parameters (see Table 4-2):

$$F_o = \frac{u_o}{\sqrt{\frac{\Delta\rho_o}{\rho_a} g h_o}} = \frac{u_o}{\sqrt{\frac{ag\Delta T_o h_o}{\rho_a}}} = \text{densimetric Froude number}$$

$$A = h_o/b_o = \text{discharge channel aspect ratio}$$

$$\frac{K}{u_o} = \text{surface heat loss parameter}$$

$$S_x = \text{bottom slope}$$

$$\frac{V}{u_o} = \text{cross flow parameter}$$

The centerline velocity, centerline temperature and the shape of the jet are functions of the above parameters and of the distance from the origin:

$$\left[\frac{u_c}{u_o}, \frac{\Delta T_c}{\Delta T_o}, \frac{b}{\sqrt{h_o b_o}}, \frac{h}{\sqrt{h_o b_o}}, \frac{r}{\sqrt{h_o b_o}}, \frac{s}{\sqrt{h_o b_o}}\right] = \text{function}$$

$$\left[\mathbb{F}_o, A, \frac{K}{u_o}, S_x, \frac{V}{u_o}, \frac{x}{\sqrt{h_o b_o}}\right]$$

The internal velocities v_s, w_r, v_b and w_h are not determined explicitly by the theory nor are they measured in the experiments. The values of u and ΔT away from the centerline are calculated using the similarity functions f and t as in Equations 3.46 and 3.89.

Other interesting dependent variables which are also functions of x may be defined. In the buoyant jet the vertical entrainment is a function of a local densimetric Froude number:

$$\mathbb{F}_L = \frac{u_c}{\sqrt{\frac{ag\Delta T_c h}{\rho_a}}} = \text{local densimetric Froude number}$$

where u_c, ΔT_c, and h are local values at a given distance from the origin. The total flow in the jet may be determined by integrating the x velocity over the jet cross section. The ratio of the flow at a given x to the initial flow, $u_o h_o b_o$, is called the jet dilution:

$$D = \frac{\int_o^{s+b}\int_{-h-r}^{o} u\, dzdy}{u_o h_o b_o} = \frac{u_c(r + I_1 h)(s + I_1 b)}{u_o h_o b_o} = \text{dilution}$$

where the similarity function for u (Equation 3.45) is used in the integration. The effect of surface heat loss upon the heated discharge may be evaluated by calculating the excess heat flow in the jet where excess heat is defined as heat which raises the water temperature above ambient. A parameter, analogous to dilution, may be defined as the ratio of the local excess heat flow to the initial excess heat flow, $\rho c_p \Delta T_o u_o h_o b_o$:

$$H = \frac{\rho C_p \int_o^{s+b} \int_{-h-r}^{o} u \Delta T dz dy}{\rho C_p \Delta T_o u_o h_o b_o} = \frac{u_c \Delta T_c (r+I_7 h)(s+I_7 b)}{\Delta T_o u_o h_o b_o} = \frac{\text{excess heat in jet}}{\text{initial excess heat}}$$

5.2 An Example of a Theoretical Computation

Only b, h, and ΔT_c are determined in the experiments. Thus values of u_c, r, s, F_L, D and H cannot be compared with the theory. Figures 5-1 and 5-2 show the calculated results for Run No. 6 (see Table 4-2) which includes all the variables and which illustrates the following general structure of heated surface discharges.

1) A core region in which the centerline velocity and the centerline temperature rise decrease very slightly. The lateral spread of the jet is very large, requiring an initial rise of the jet bottom boundary to satisfy mass conservation. The dilution, D, and the local densimetric Froude number, F_L, do not vary greatly in this region. The magnitude of F_L is much larger than F_o because the initial depth of the turbulent region, h, is zero. There is no significant surface heat loss in the core region.

2) An entrainment region in which the centerline velocity and

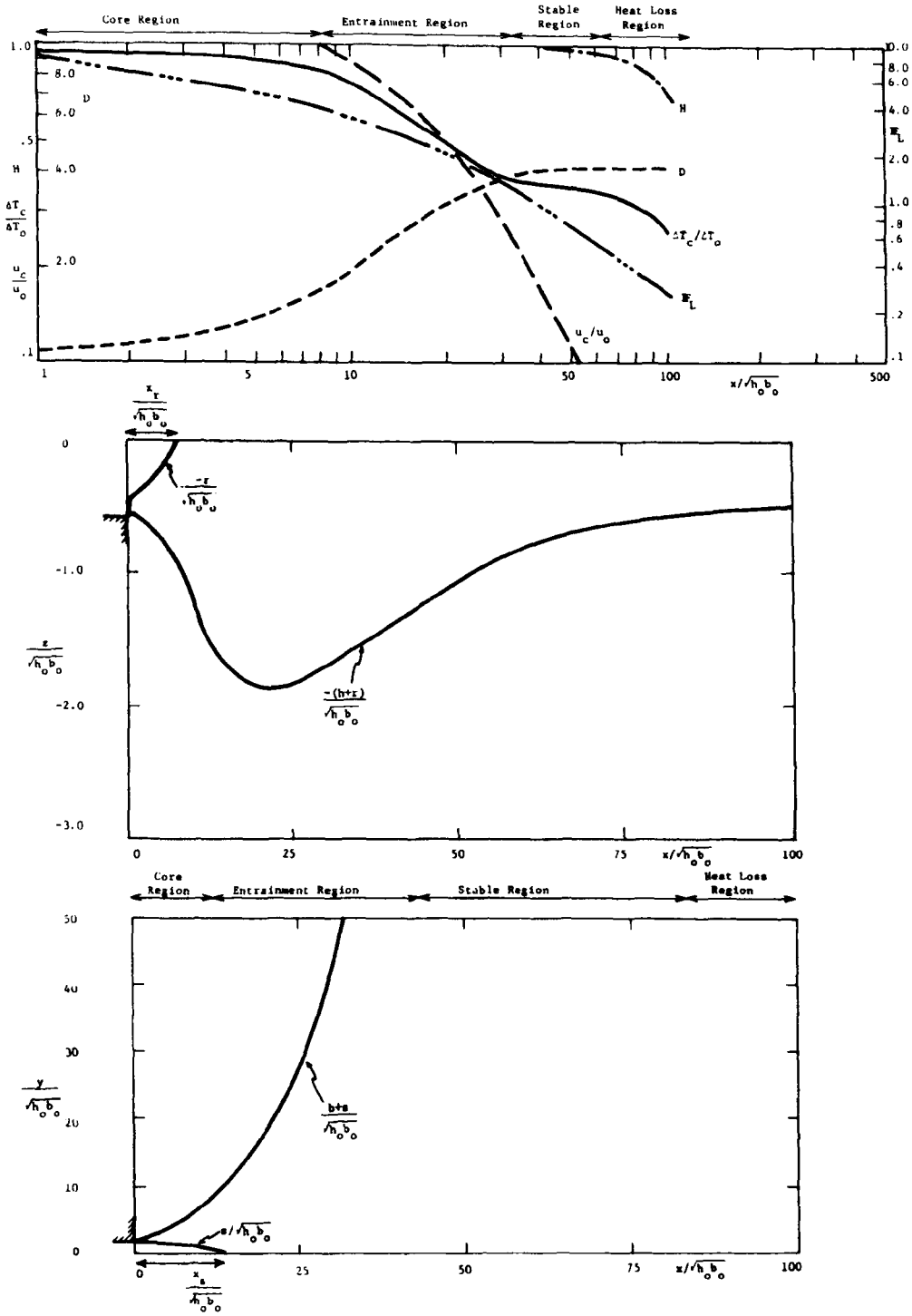

Figure 5-1. Theoretical Calculation of Jet Structure for Run 6.

$IF_o = 4.4$ $\quad K/u_o = 4.2 \times 10^{-5}$ $\quad V/u_o = 0$

$A = .35$ $\quad S_x = 0$

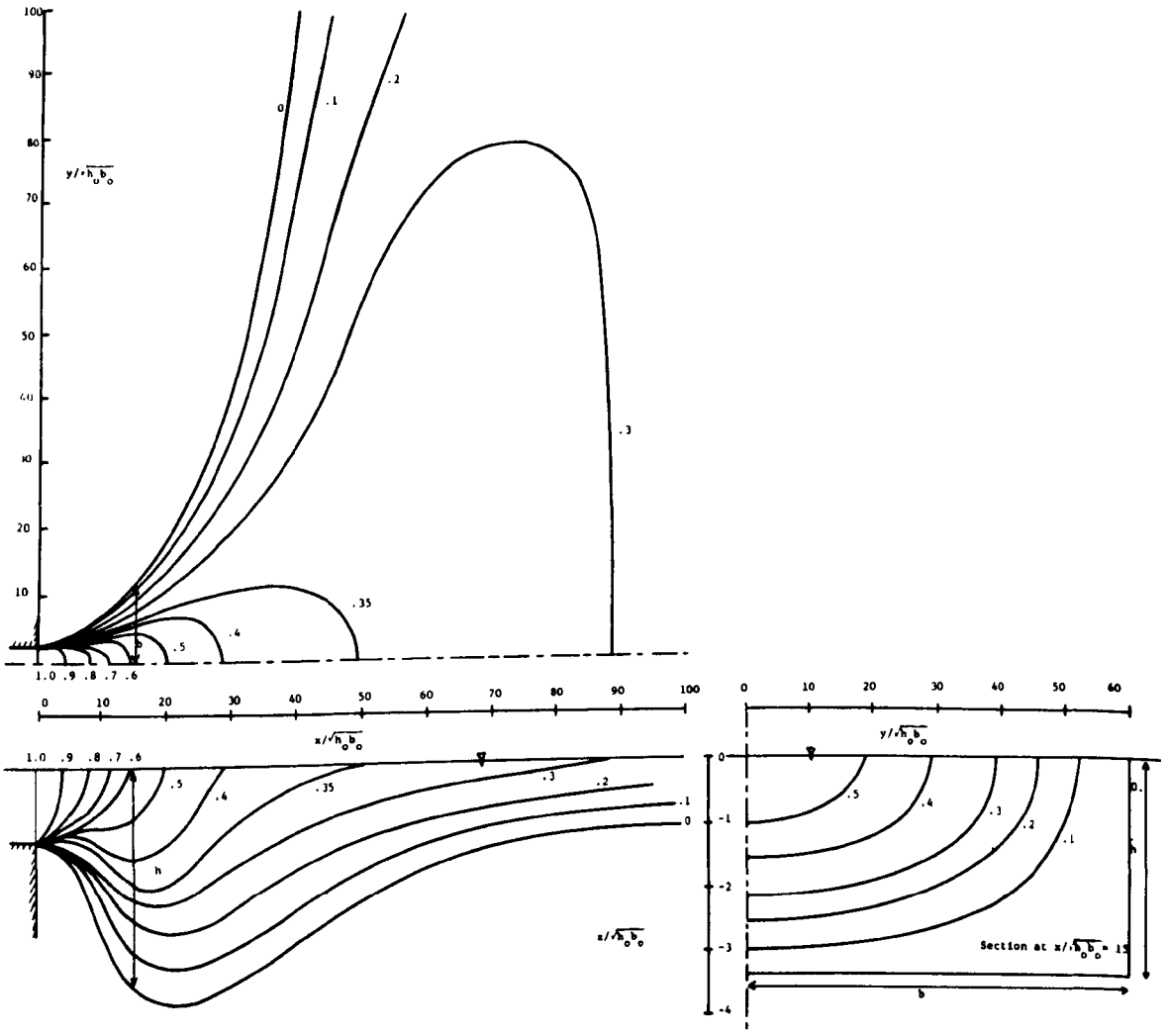

Figure 5-2. Calculated Isotherms of $\Delta T_c/\Delta T_o$ for Run 6.

$IF_o = 4.4$ $K/u_o = 4.2 \times 10^{-5}$ $V/u_o = 0.0$

$A = .35$ $S_x = 0$

temperature drop sharply, approximately as $1/x$, as in the non-buoyant jet. The jet spreads downward by turbulent processes at a rate of the order $dh/dx \simeq .22$. The lateral growth is dominated by gravitational spreading at a much greater rate than the vertical turbulent spread. Because of this large ratio of lateral to vertical spread, the jet reaches a maximum depth beyond which the bottom boundary rises to maintain mass conservation. Local densimetric Froude numbers in this region decrease rapidly and the dilution rises sharply as a result of entrainment. Surface heat loss is still negligible in this region i.e. $H = 1.0$.

3) A stable region in which vertical entrainment is inhibited by vertical stability as indicated by the local densimetric Froude number which is of order one or less. The jet depth continues to decrease because of lateral spreading. The small jet depths reduce the lateral entrainment, the dilution and centerline temperature remaining relatively constant in this region. The centerline velocity, however, drops sharply as a consequence of the large lateral spread. The surface temperature pattern, as shown in Figure 5-2, is dominated by the wide, constant temperature stable region.

4) A heat loss region marking the end of the stable region. The lateral spread is sufficiently large to allow significant surface heat transfer and the temperature begins to fall again. Once surface heat loss has begun to be important, the rate of temperature decrease is very rapid and in conjunction with the low centerline velocity the discharge may no longer be considered as a jet.

5) A far field region dominated by ambient convective and diffusive processes which are beyond the scope of this study. If ambient flow velocities are large, the far field region may begin before the stable region has formed. The excess discharge heat is ultimately lost to the atmosphere in the far field.

5.3 Comparison of Theory and Experiment

In the previous section the general behavior of heated discharges is discussed. Many of the characteristics of the discharges cannot be generalized and must be determined by examining each case. This section, in addition to comparing the data with the theory, examines the behavior of the jet as a function of the controlling parameters discussed in Section 5.1.

Chapter 4 includes a description of the determination of ΔT_c, $h_{1/2}$ and $b_{1/2}$ from the experimental data. It should be noted that the half width, $b_{1/2}$, and half depth, $h_{1/2}$, are defined in terms of the temperature distribution rather than by the velocity distribution as discussed in Chapter 2. The determination of the half width, $b_{1/2}$, is difficult because of a) distortion of the surface temperature distribution in the lateral portions of the jet by recirculation of heated water within the experimental basin and b) the small temperature differences in the jet far from the discharge point.

In the theoretical computations for all the laboratory cases, the surface heat loss coefficient is assumed to be 2×10^{-5} ft/sec. corresponding to a heat transfer rate of 110 BTU/ft^2-day-F°. This is in the low range of values predicted from standard formulas (3) and is

close to Hayashi's (15) estimate for laboratory environments, 1.8×10^{-5} ft/sec.

In Runs 1-10 the densimetric Froude number, F_o, and the aspect ratio, $A = h_o/b_o$, are varied. There is no bottom slope or cross flow. Figures 5-3 to 5-12 show the experimental data and the theoretical computations. For low values of F_o the jet spreading is too large to permit determination of the half width, $b_{1/2}$.

Runs 1 and 2 illustrate the case of $F_o = 1.0$ which is the lowest possible value of F_o. In Run No. 1 the channel densimetric Froude number is actually less than one and a cold water wedge is observed in the channel. As discussed in Chapter 2, the wedge will force the heated flow to obtain $F_o = 1.0$ at the discharge point. The value of u_o and h_o to be used in the theoretical calculation is determined by this condition. There is little difference between the temperature distribution for the wedge and non-wedge runs. In Run 2 the "toe" of the wedge is positioned at the channel expansion and the vertical structure of the jet is approximately the same as if the "toe" had intruded into the channel. For such low F_o discharges the entrainment region is very small, the temperature of the stable region is high, and the heat loss is promoted by large lateral spreading.

Runs 3 and 4 show the effect of the discharge channel aspect ratio, A, on low F_o discharges in which horizontal entrainment dominates vertical entrainment. Large aspect ratios provide larger available area for lateral entrainment and the temperature drops more quickly. Surface heat loss behaves in an opposite manner, being promoted by the

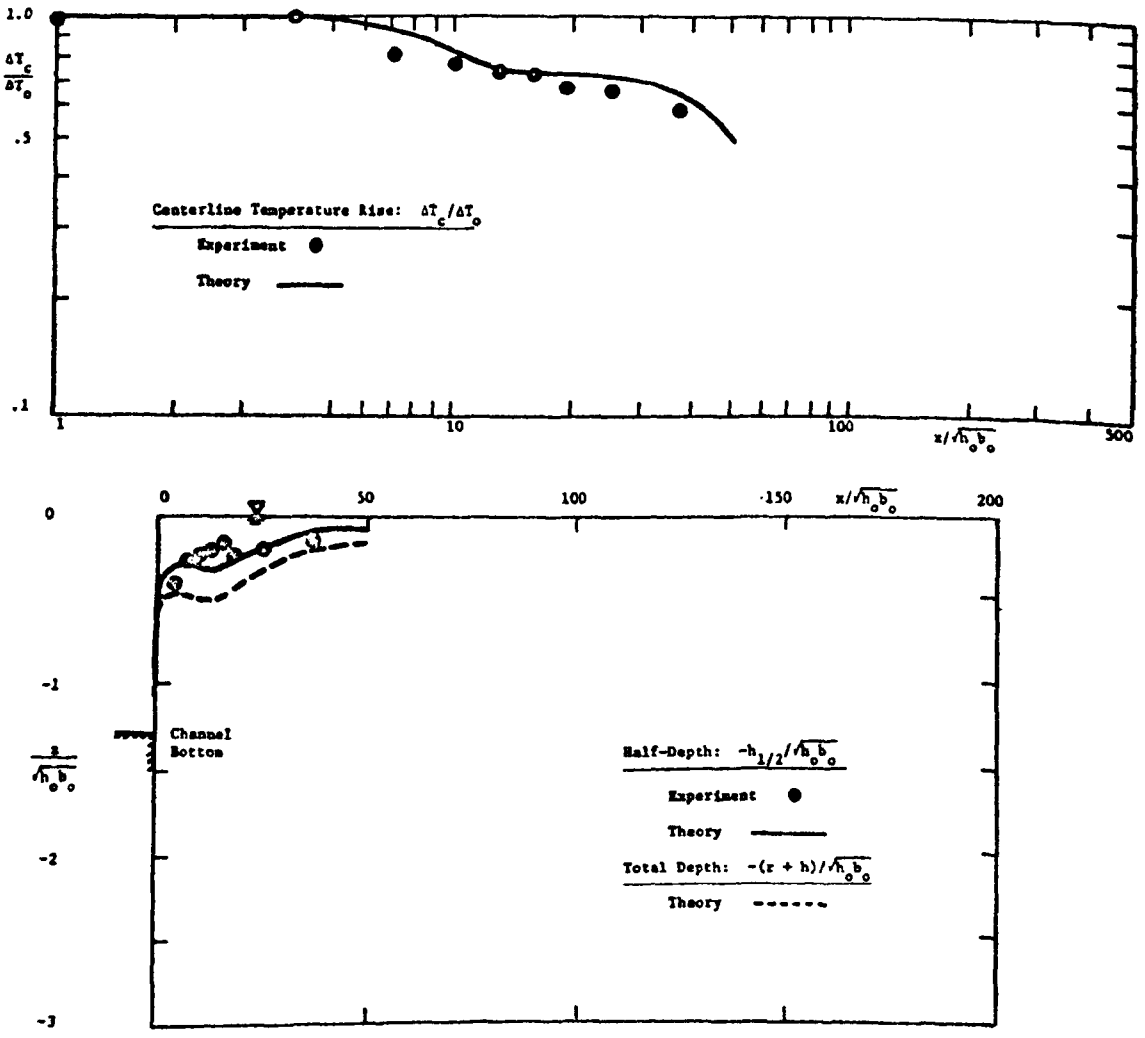

Figure 5-3. Theoretical Calculations and Experimental Data for Run 1.

$IF_o = 1.00$ (wedge present) $K/u_o = 8.5 \times 10^{-5}$ $V/u_o = 0$

$A = .76$ $S_x = \infty$

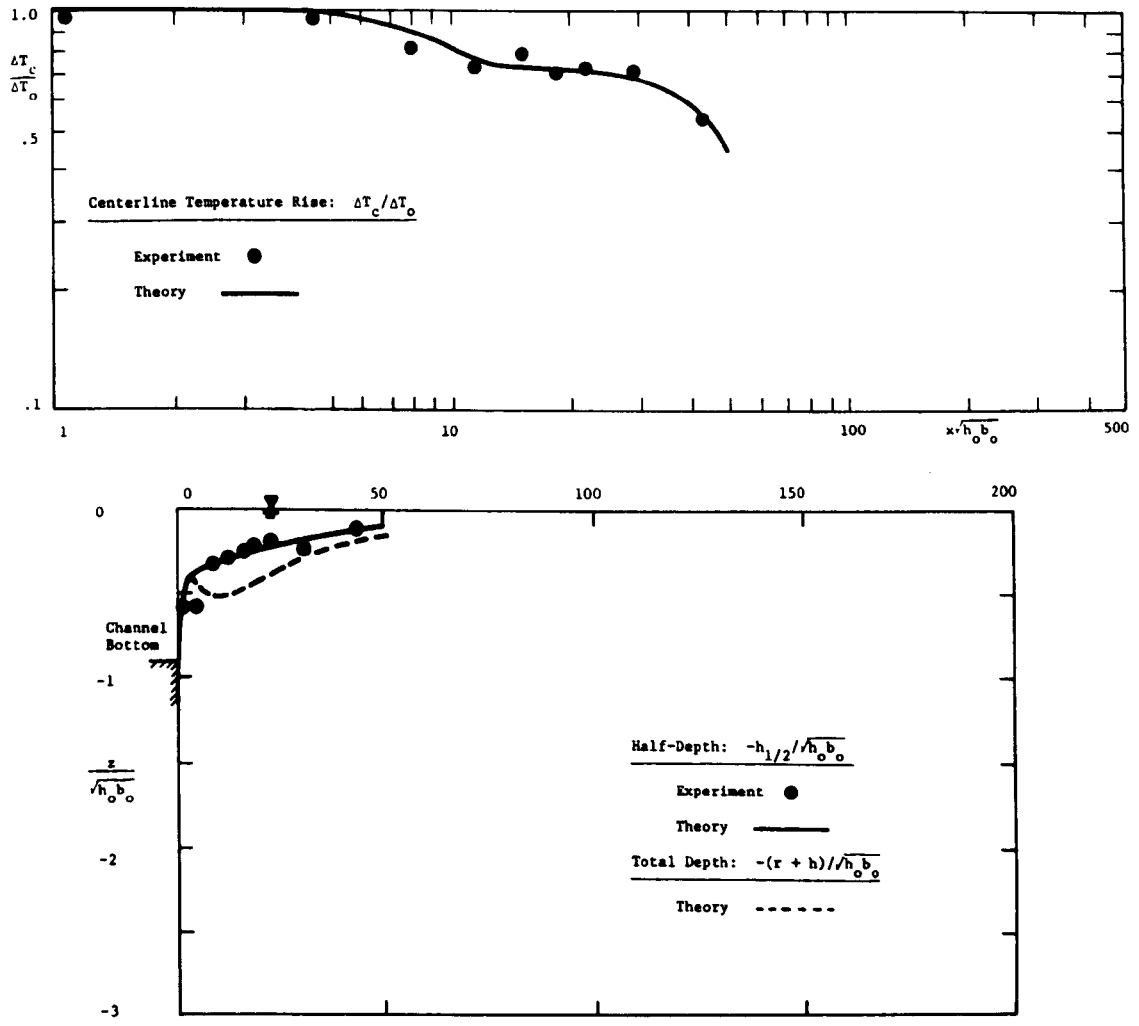

Figure 5-4. Theoretical Calculations and Experimental Data for Run 2.

$IF_o = 1.03$ $K/u_o = 10.5 \times 10^{-5}$ $V/u_o = 0$

$A = .82$ $S_x = \infty$

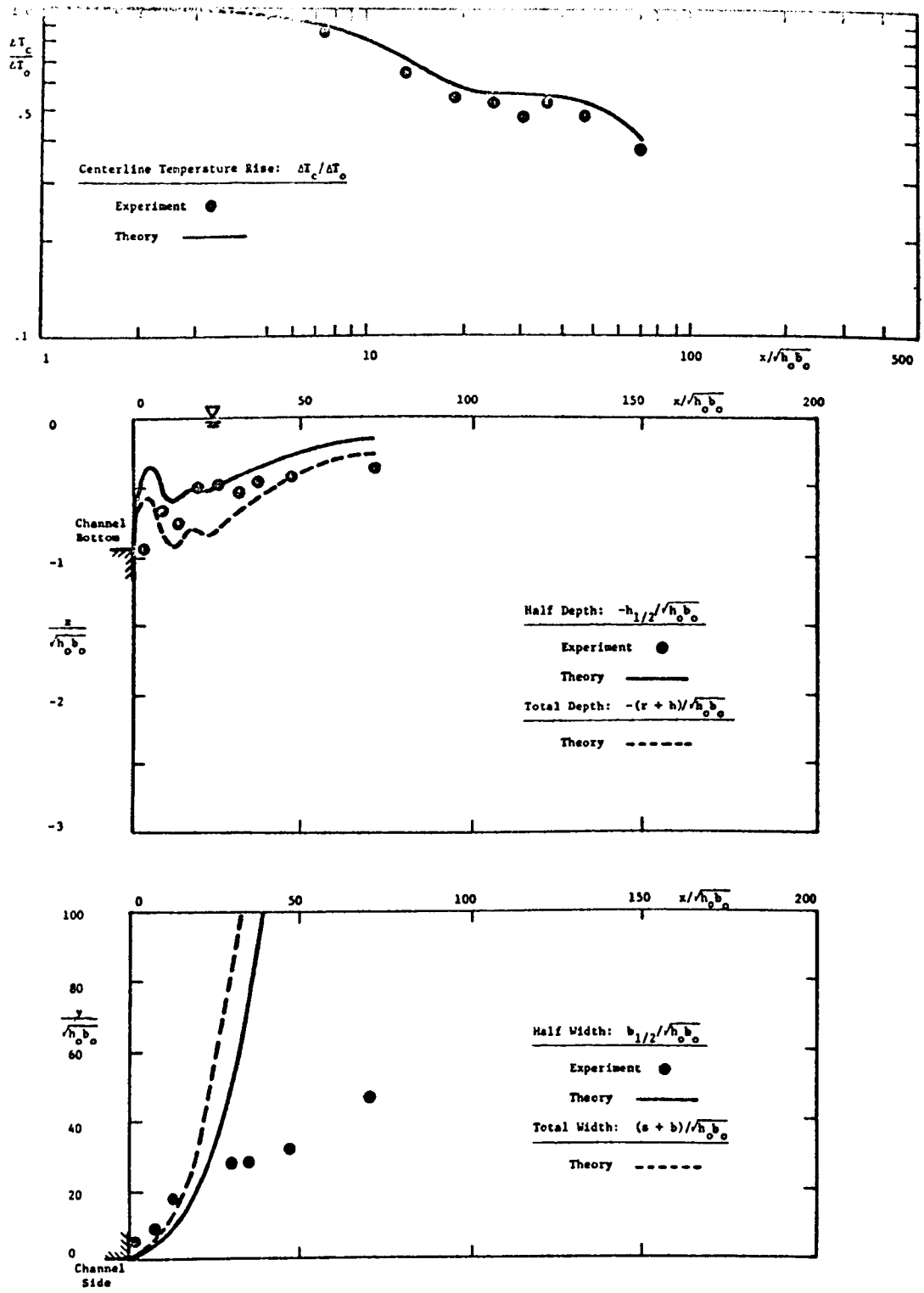

Figure 5-5. Theoretical Calculations and Experimental Data for Run 3.

$F_o = 1.83$ $K/u_o = 6.2 \times 10^{-5}$ $V/u_o = 0$

$A = .87$ $S_x = \infty$

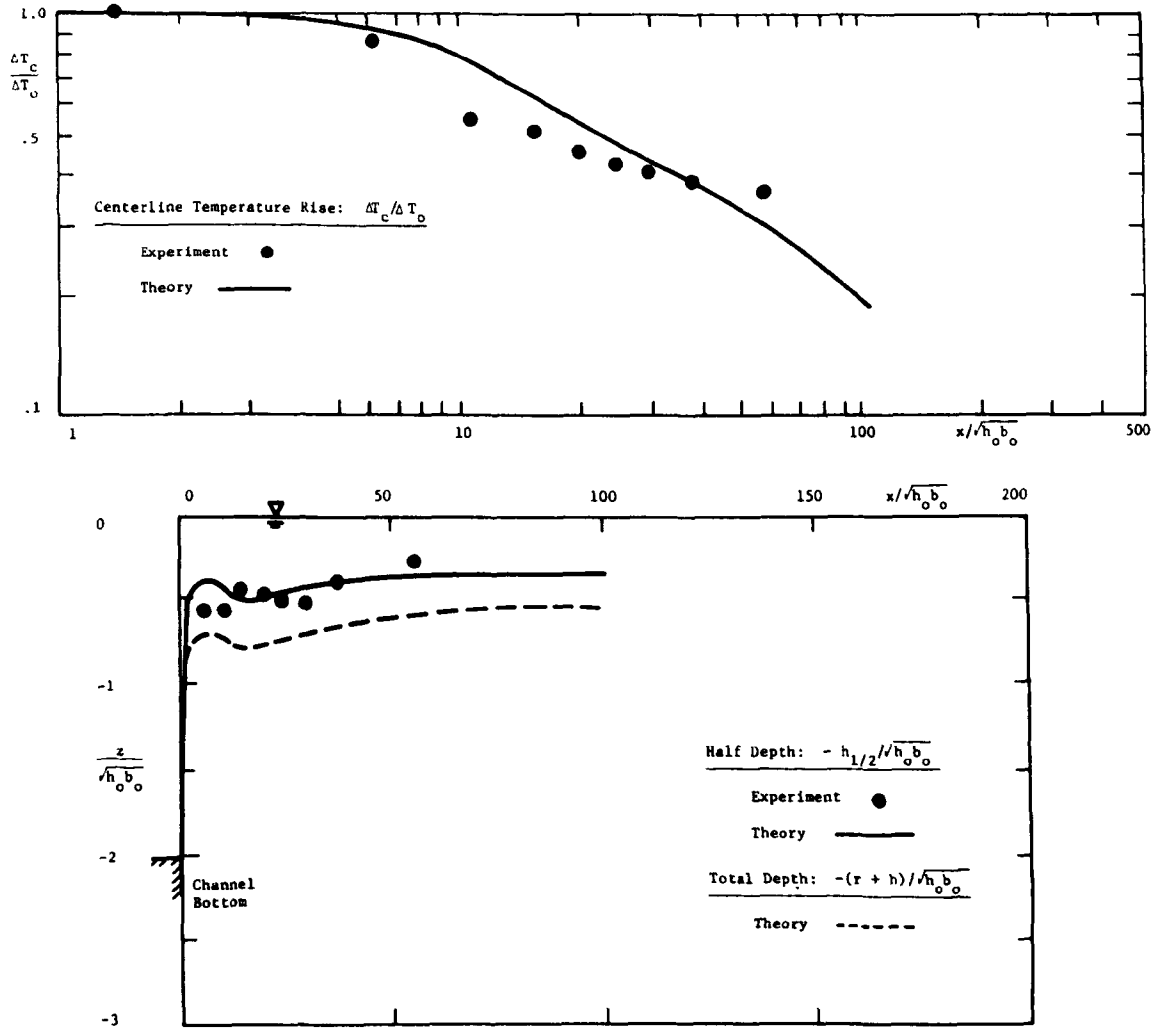

Figure 5-6. Theoretical Calculations and Experimental Data for Run 4.

$F_o = 1.42$ $K/u_o = 5.8 \times 10^{-5}$ $V/u_o = 0$

$A = 4.30$ $S_x = \infty$

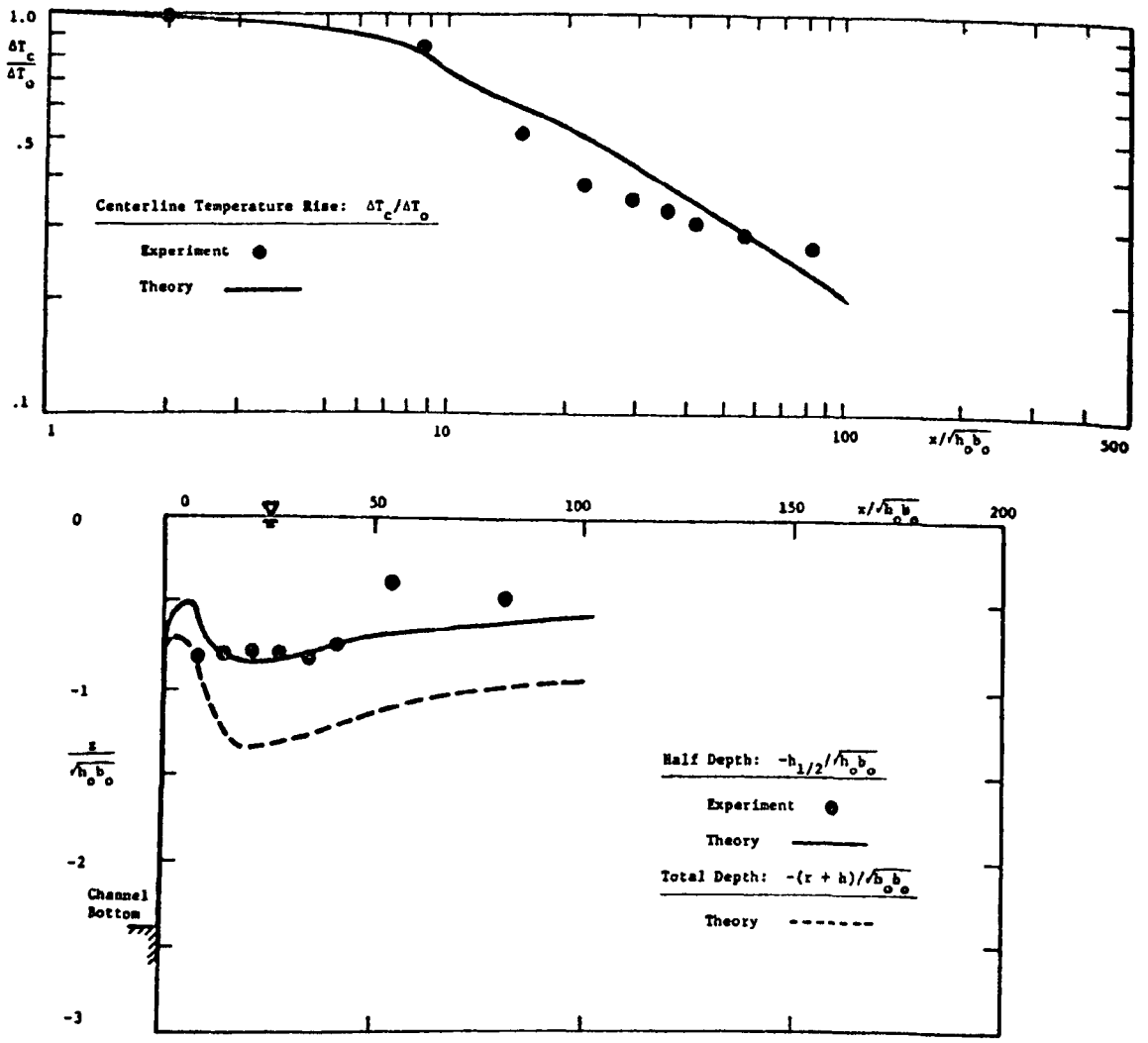

Figure 5-7. Theoretical Calculations and Experimental Data for Run 5.

$F_o = 2.35$ $\quad K/u_o = 4.0 \times 10^{-5}$ $\quad V/u_o = 0$

$A = 5.70$ $\quad S_x = \infty$

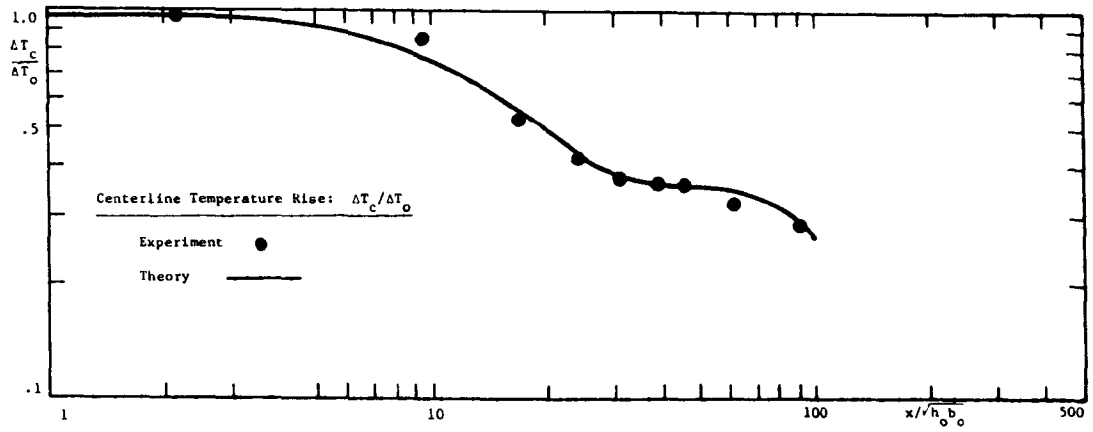

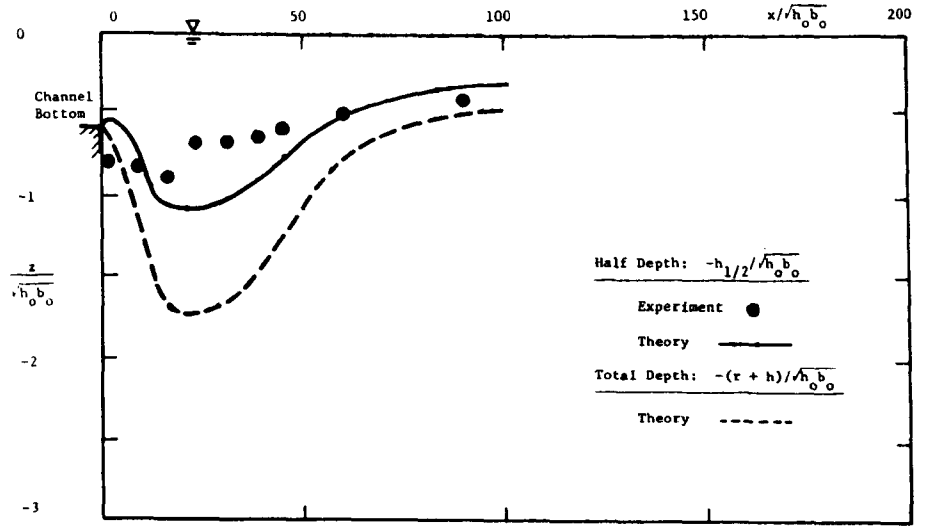

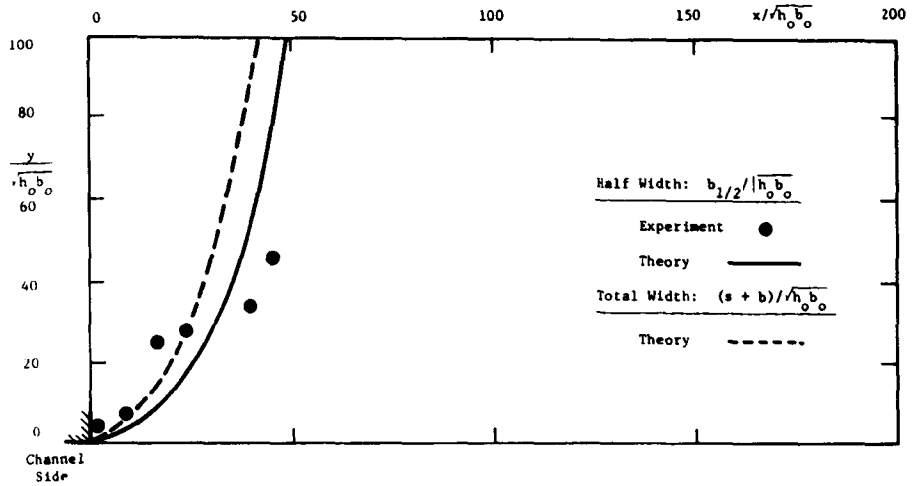

Figure 5-8. Theoretical Calculations and Experimental Data for Run 6.

$IF_o = 4.4$ $\quad K/u_o = 4.2 \times 10^{-5}$ $\quad V/u_o = 0$

$A = .35$ $\quad S_x = \infty$

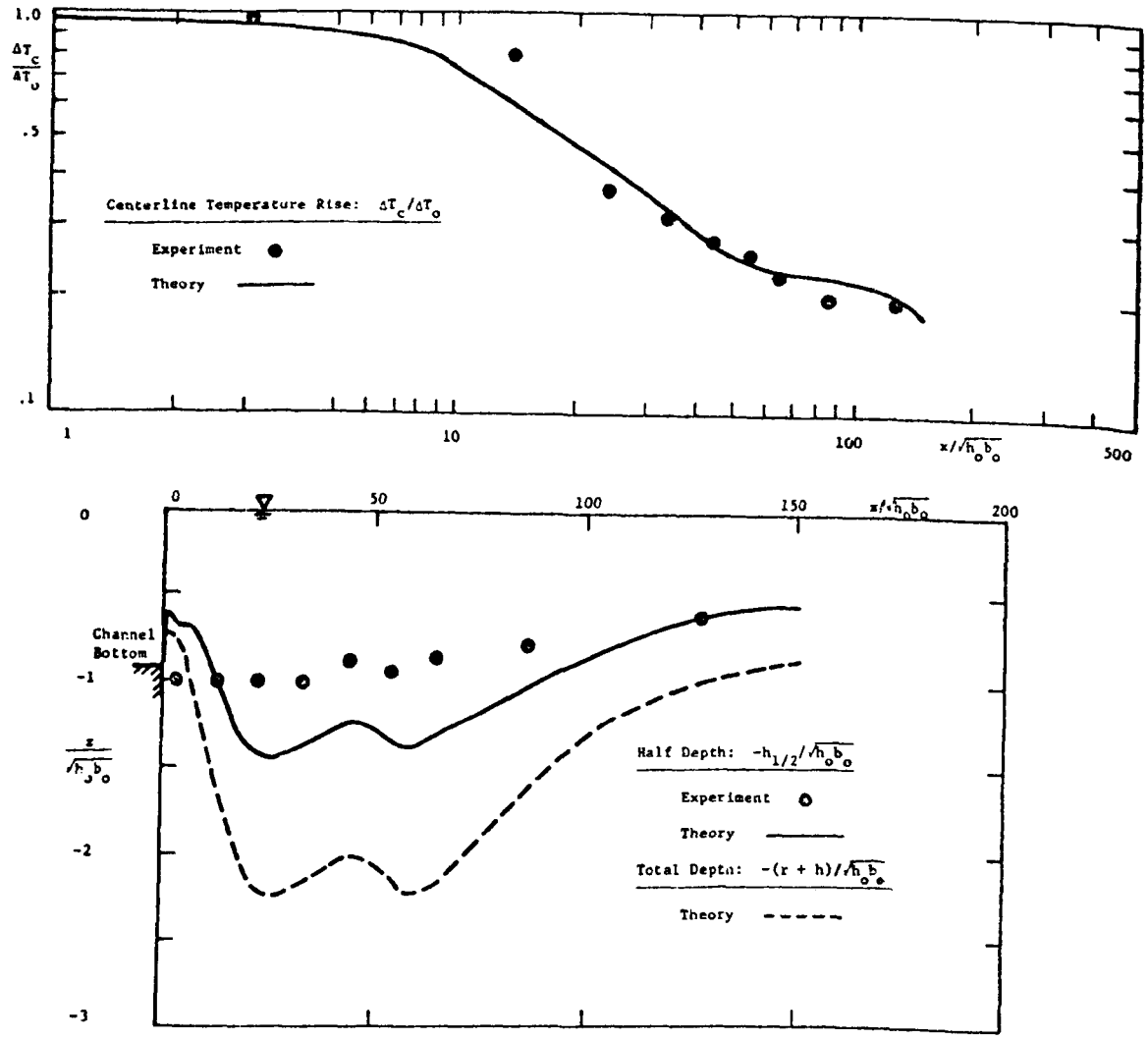

Figure 5-9. Theoretical Calculations and Experimental Data for Run 7.

F_o = 5.22 $K/u_o = 3.5 \times 10^{-5}$ $V/u_o = 0$

A = .84 $S_x = \infty$

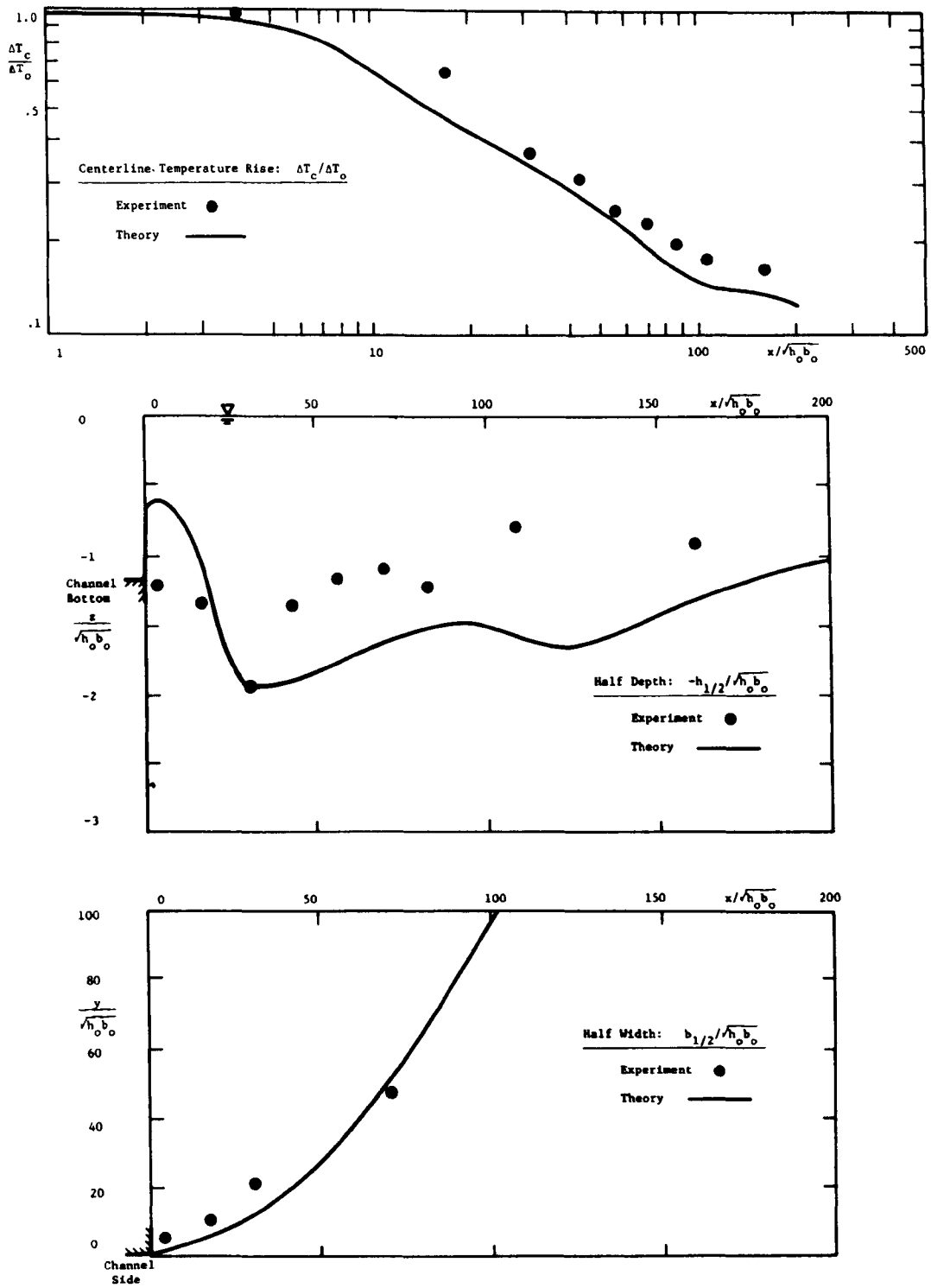

Figure 5-10. Theoretical Calculations and Experimental Data for Run 8.

$F_o = 6.53$ $K/u_o = 2.8 \times 10^{-5}$ $V/u_o = 0$

$A = 1.30$ $S_x = \infty$

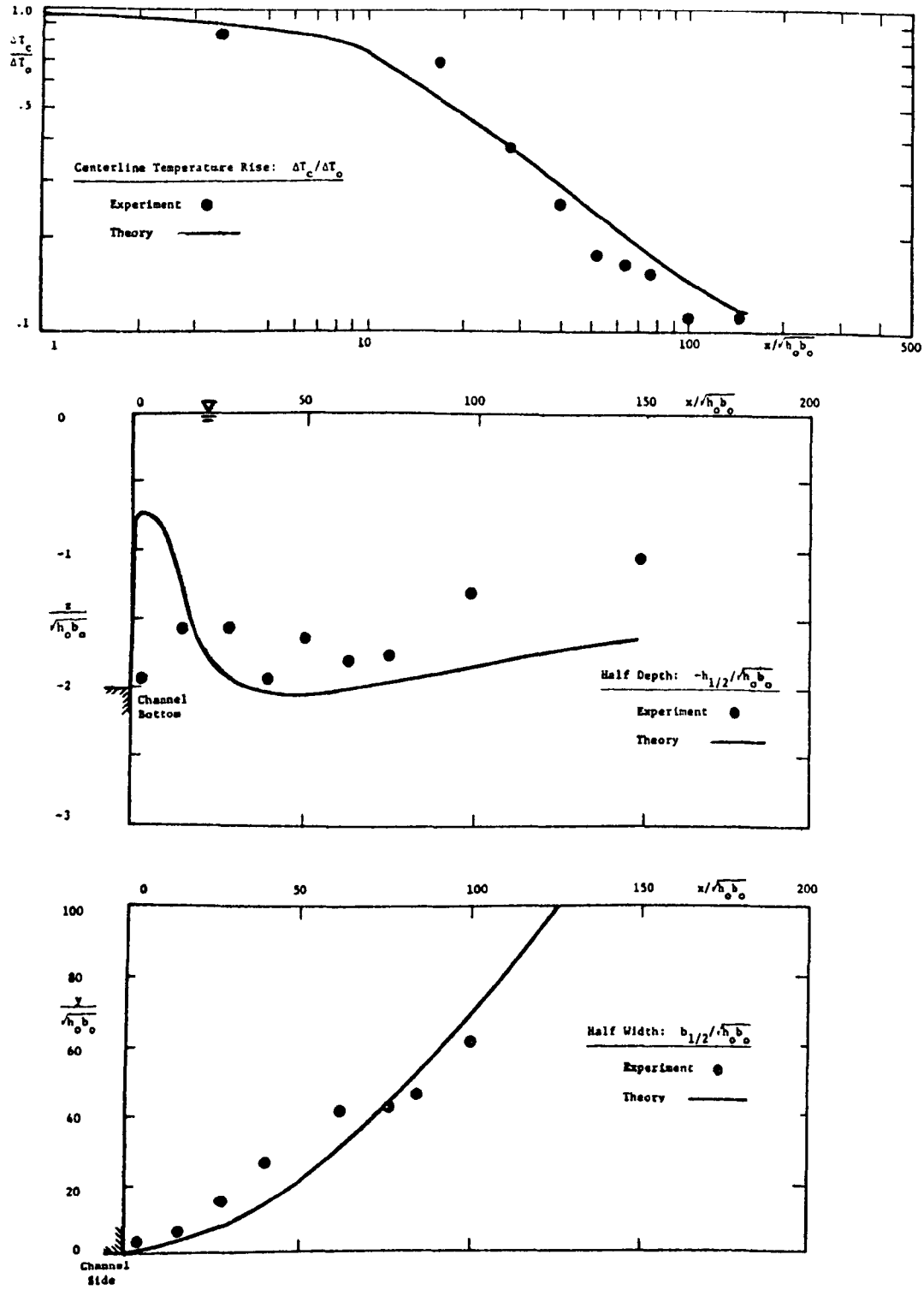

Figure 5-11. Theoretical Calculations and Experimental Data for Run 9.

$IF_o = 6.60$ $K/u_o = 2.1 \times 10^{-5}$ $V/u_o = 0$

$A = 3.95$ $S_x = \infty$

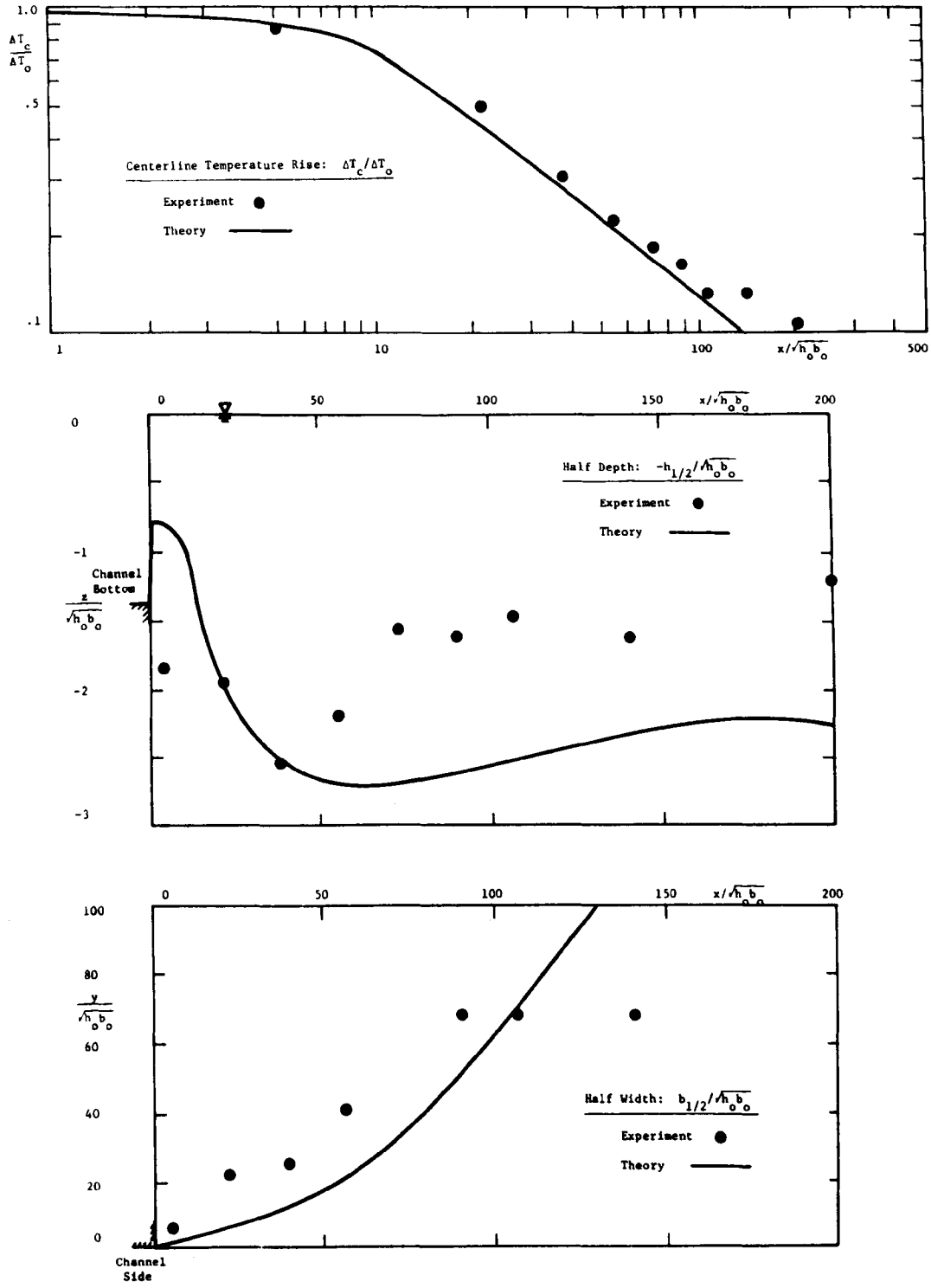

Figure 5-12. Theoretical Calculations and Experimental Data for Run 10.

$IF_o = 9.55$ $K/u_o = 1.9 \times 10^{-5}$ $V/u_o = 0$

$A = 2.00$ $S_x = \infty$

large horizontal surface areas in low aspect ratio discharges. The theory does not reproduce the centerline temperature drop for large aspect ratios as well as for smaller values.

The same principle is illustrated in Runs 5 and 6. An increase in aspect ratio may outweigh an increase in F_o as shown in Figures 5-7 and 5-8. In Runs 7-10 (Figures 5-9 to 5-12) the effect of aspect ratio and densimetric Froude number is diminished as F_o increases. The jet depths are much larger and heat loss is not as significant as in the discharges of lower F_o .

Runs 1-10 indicate that the theory agrees well with the data and is capable of predicting the structure of heated discharges as a function of F_o and A. The experimental error is greatest in the determination of $b_{1/2}$ and least for ΔT_c. Since the theory agrees best with the data for ΔT_c and worst for $b_{1/2}$ some of the discrepancy between the data and the theory, especially for the half widths, can be attributed to experimental error.

In the runs involving bottom slopes (Runs 11-19) (Figures 5-13 to 5-15) only surface temperatures are measured because of the difficulty of positioning probes near the solid bottom. The bottom slope has two counteracting effects upon the jet:

1) Vertical entrainment is inhibited by the presence of the solid boundary.
2) The vertical core region of depth r persists as long as the jet is attached to the bottom. This promotes lateral entrainment over the full depth of the jet.

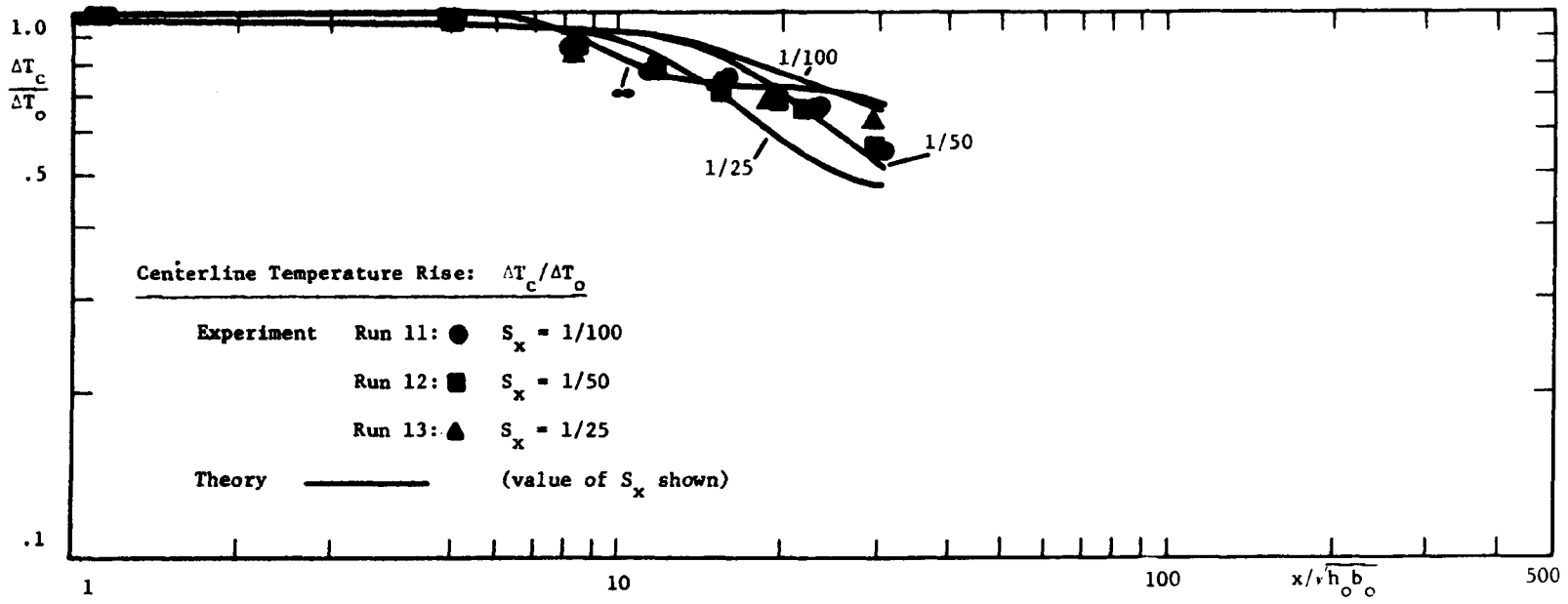

Figure 5-13. Theoretical Calculations and Experimental Data for Runs 11, 12 and 13.

F_o = 1.13 $K/u_o = 10.0 \times 10^{-5}$ Run 11: S_x = 1/100

A = .78 V/u_o = 0 Run 12: S_x = 1/50

Run 13: S_x = 1/25

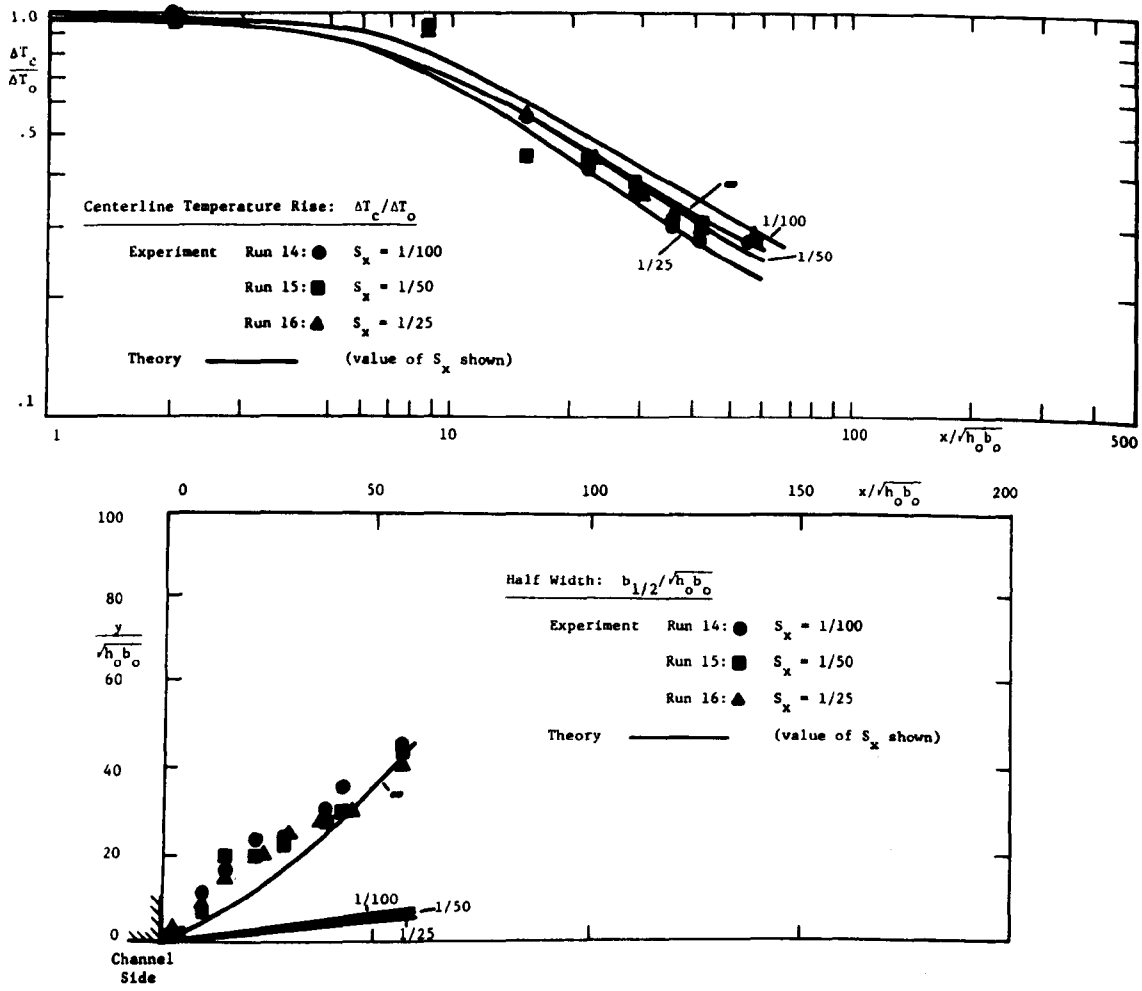

Figure 5-14. Theoretical Calculations and Experimental Data for Runs 14, 15 and 16.

IF_o = 2.7 $K/u_o = 3.3 \times 10^{-5}$ Run 14: S_x = 1/100

A = 5.7 V/u_o = 0 Run 15: S_x = 1/50

Run 16: S_x = 1/25

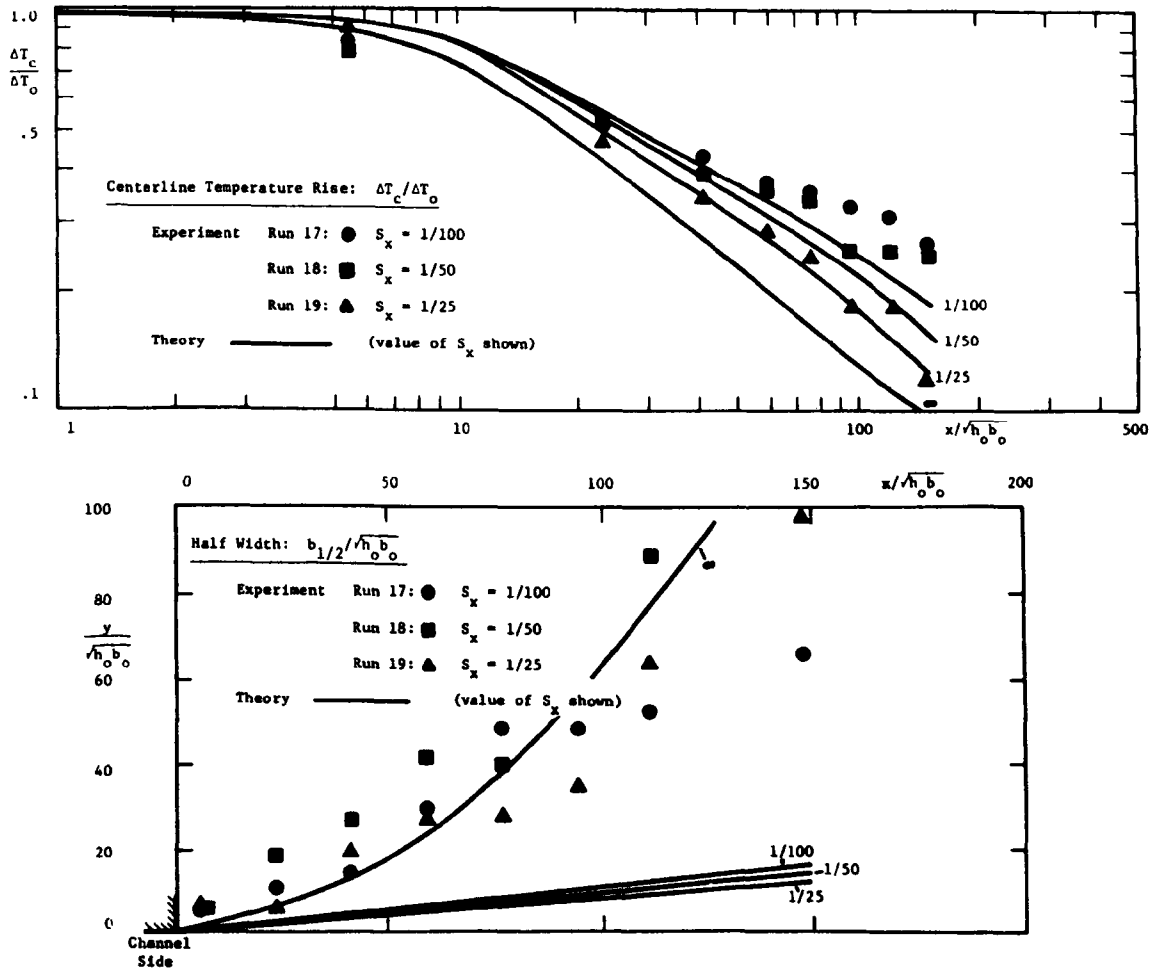

Figure 5-15: Theoretical Calculations and Experimental Data for Runs 17, 18 and 19.

F_o = 11.6 $K/u_o = 1.6 \times 10^{-5}$ Run 17: S_x = 1/100

A = 1.9 V/u_o = 0 Run 18: S_x = 1/50

Run 19: S_x = 1/25

The resultant effect of these two phenomena is dependent upon the values of F_o and A. Runs 11-13 indicate that for low F_o the jet detaches from the bottom almost immediately and that the centerline temperature rise is nearly the same for all the slopes considered and is near the value computed for no bottom slope. Runs 14-16 (Figure 5-14) show that for large aspect ratios and low F_o the bottom slope actually promotes higher entrainment than without a slope. As with Runs 11-13 the data shows no dependency upon the value of the bottom slope, indicating early separation of the jet from the bottom. In Runs 17-19 (Figure 5-15) the reduction of vertical entrainment increases as the slope decreases. This behavior is a consequence of the large densimetric Froude number and moderate aspect ratio for these cases. The jet remains attached to the bottom and the dilution is dependent upon the value of the slope.

The theory reproduces the trends in the data as discussed above. The low F_o computations (Runs 11-16) show more dependency on the value of S_x than do the data, indicating that the theory is not predicting separation of the jet sufficiently close to the jet origin. For the large F_o runs (17-19) the theory underestimates the effect of the slope on the reduction of entrainment. The theory fails to reproduce the lateral spreading of the jet which is seen to be close to the calculated curve for no slope rather than for the very small spread the theory predicts when a slope is present. The assumption put forth in Section 3.6 that the jet does not exhibit buoyant spreading is clearly not valid. The jet must be spreading laterally at the edges and remaining somewhat attached to the bottom near the centerline, distorting the jet beyond

the capability of the theory to describe it with simple similarity functions.

In Cases 20-25 a cross flow deflected the jet. Determination of the jet centerline position from the temperature data is very difficult since the total lateral temperature variation within the experimental measurement area and far from the discharge origin is only a few degrees. This is particularly true of the runs with low values of $I\!F_o$. The agreement of the experimental and calculated jet trajectories are scattered but good on the average (see Figures 5-16 to 5-21). The measured centerline temperature values are also close to the theoretical curves, being not much different than the no-cross flow cases with the same $I\!F_o$ and A. As expected from the formulation of the equations governing deflected jets, the jet deflection increases with $I\!F_o$, A, and $\frac{V}{u_o}$ since the only force turning the jet is entrainment of lateral momentum. The theoretical calculations are terminated when $u_c = V\cos\theta$ since the basic assumption of small cross flow velocities does not hold beyond that point. The theoretical calculations used an analytical expression for the cross flow velocity as a function of x (see Figure 4-3).

5.4 Comparison of Theory with Experimental Data by Other Investigators

As mentioned in Chapters 2 and 4 a number of other studies collected field and laboratory data for three-dimensional heated surface discharges. These results are compared with the theory in this section. Data from Stefan (31), Hoopes (18) and Tamai (32) are not used. Stefan's data points are too close to the jet origin in most cases to permit examination of trends in the data; Hoopes' field temperature measurements

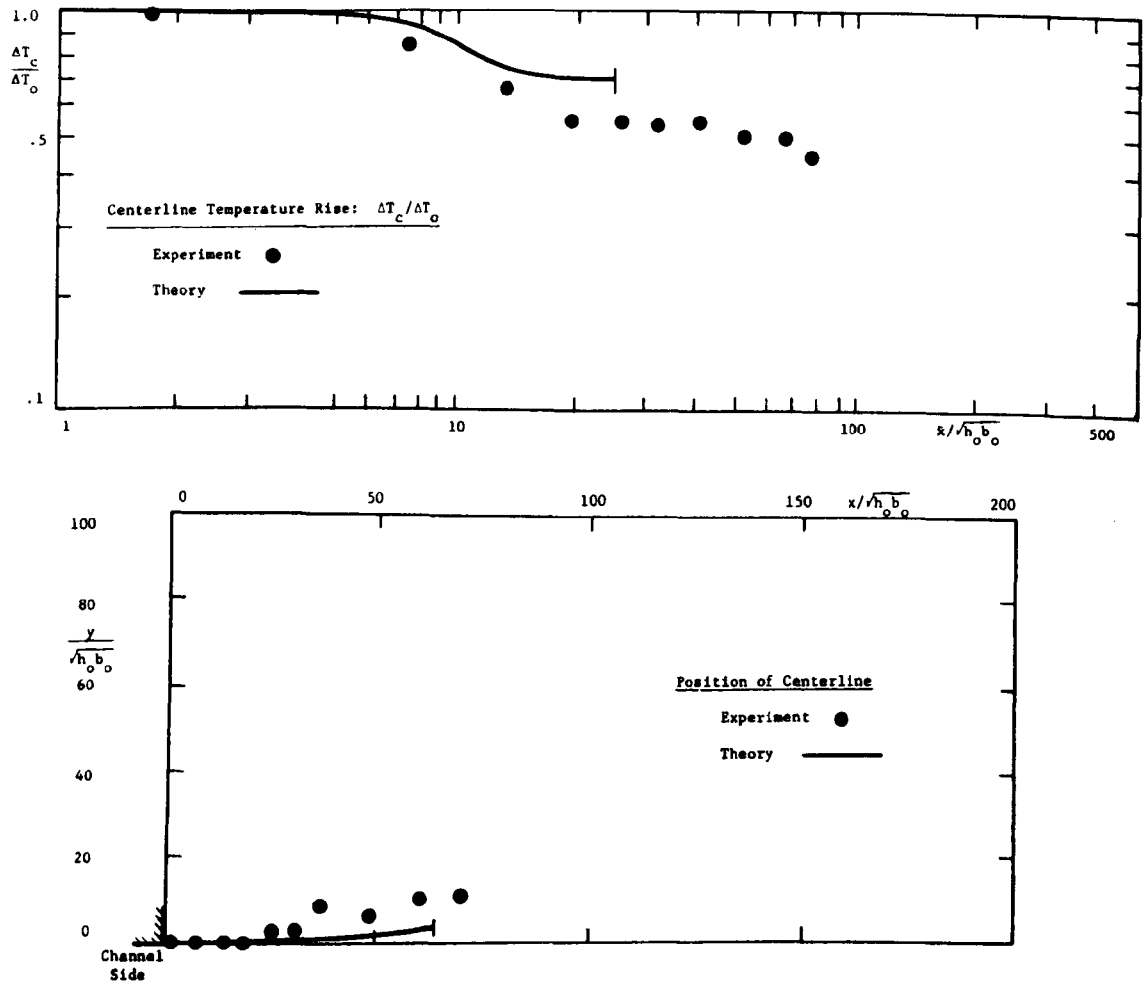

Figure 5-16. Theoretical Calculations and Experimental Data for Run 20.

$F_o = 1.16$ $\quad K/u_o = 6.2 \times 10^{-5}$ $\quad V_{max}/u_o = .26$

$S_x = .87$ $\quad S_x = \infty$

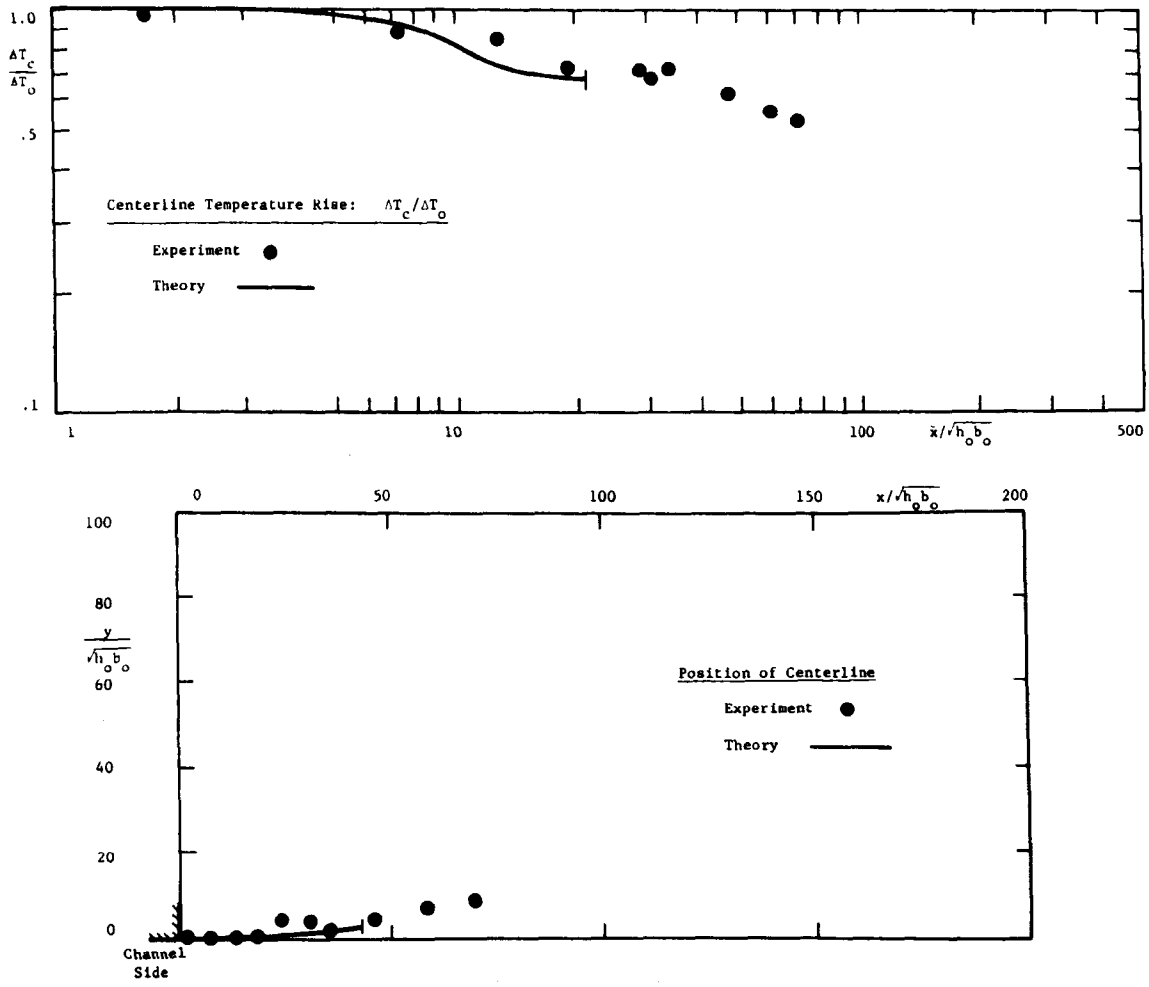

Figure 5-17. Theoretical Calculations and Experimental Data for Run 21.

$F_o = 1.20$ $K/u_o = 9.0 \times 10^{-5}$ $V_{max} = u_o = .39$

$A = .87$ $S_x = \infty$

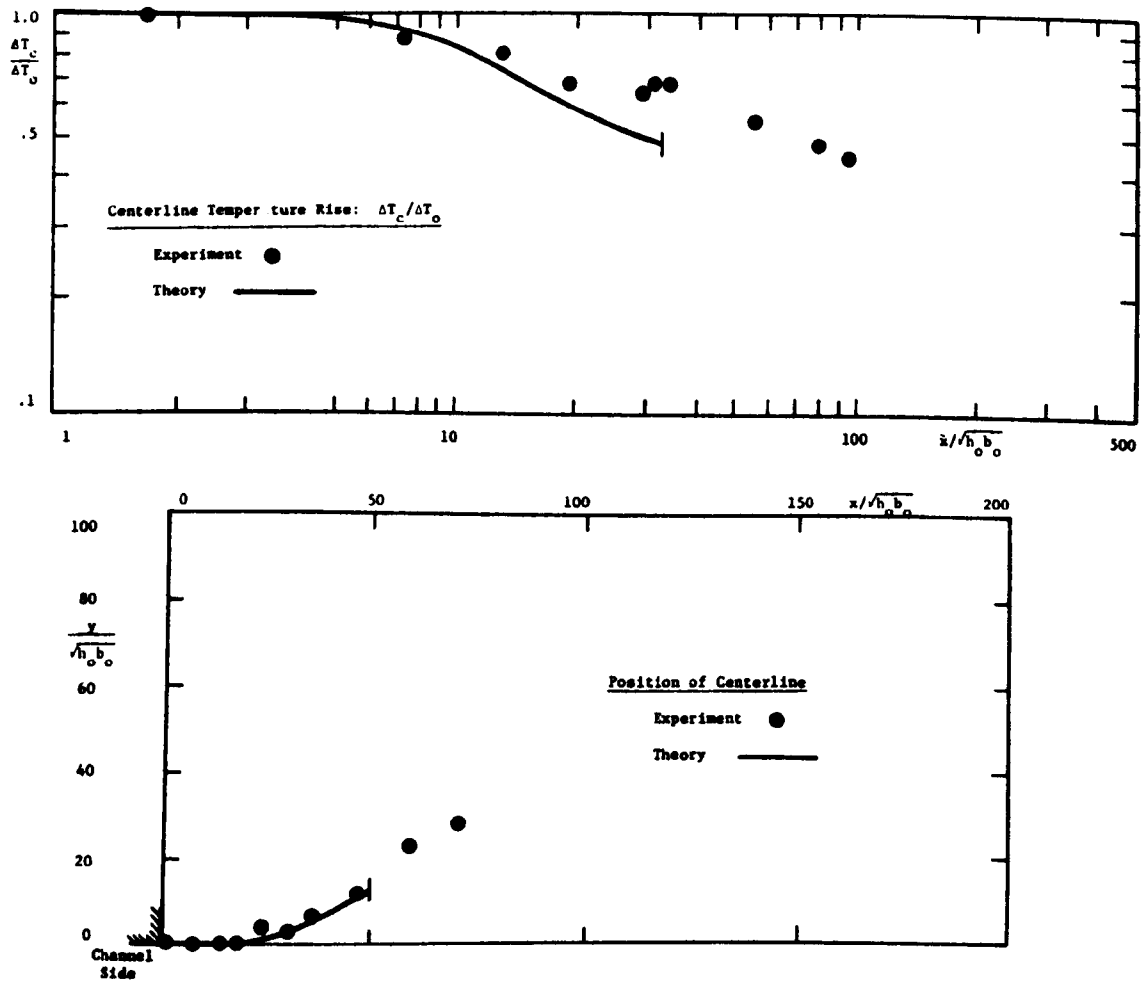

Figure 5-18. Theoretical Calculations and Experimental Data for Run 22.

$\mathbb{F}_o = 1.88$ $K/u_o = 9.5 \times 10^{-5}$ $V_{max}/u_o = .4$

$A = .87$ $S_x = \infty$

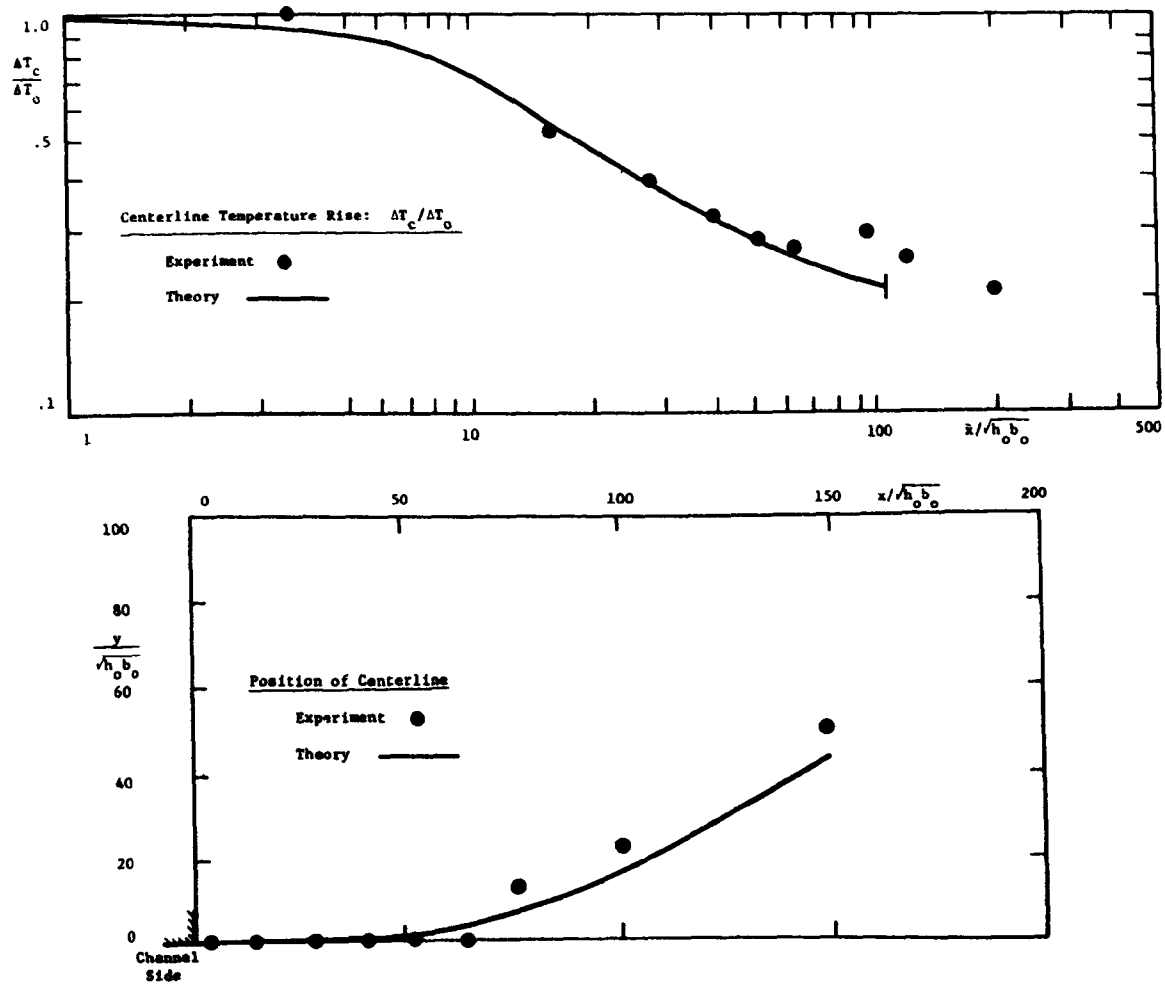

Figure 5-19. Theoretical Calculations and Experimental Data for Run 23.

$F_o = 4.10$ $K/u_o = 2.8 \times 10^{-5}$ $V_{max}/u_o = .12$

$A = 3.95$ $S_x = \infty$

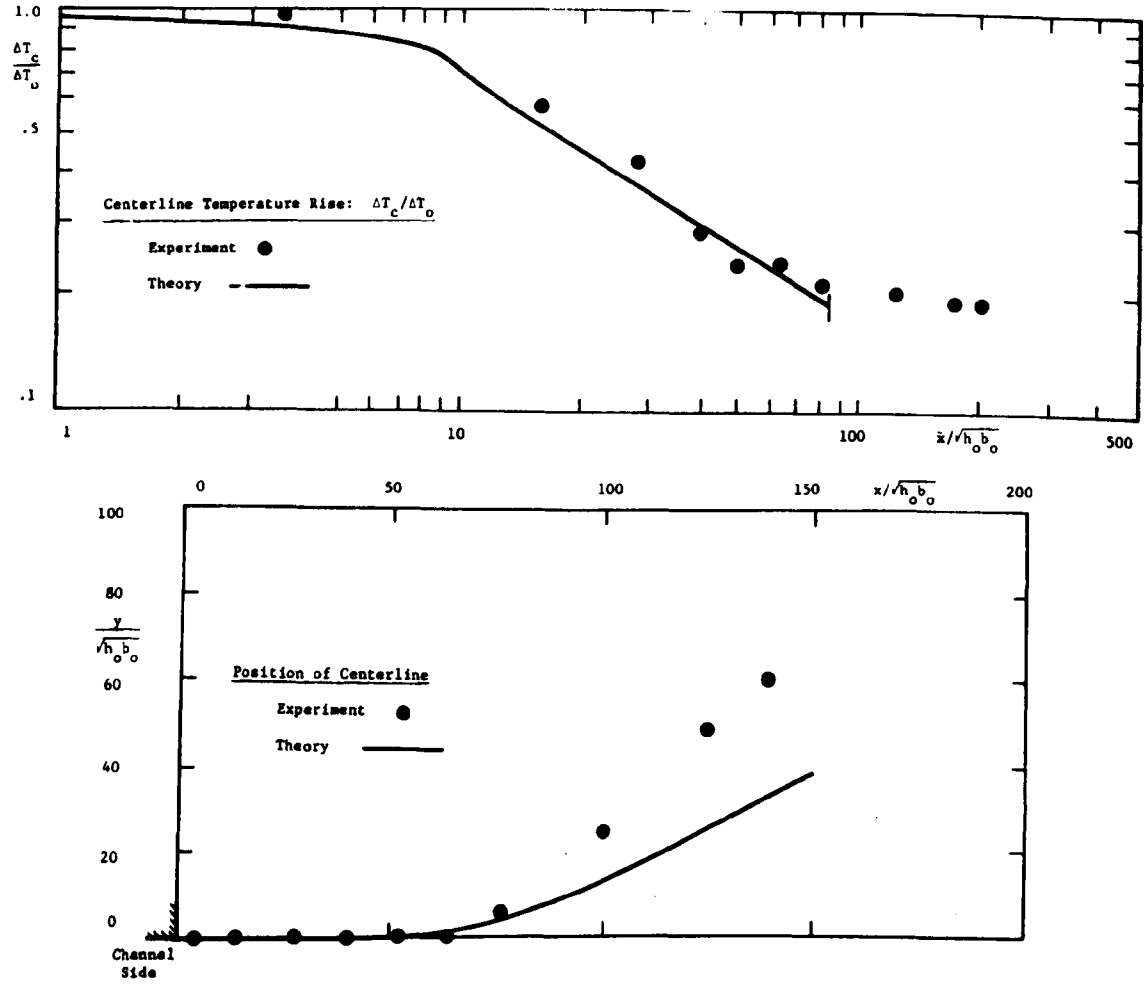

Figure 5-20. Theoretical Calculations and Experimental Data for Run 24.

$F_o = 5.85$ $K/u_o = 2.0 \times 10^{-5}$ $V_{max}/u_o = .09$

$A = 3.95$ $S_x = \infty$

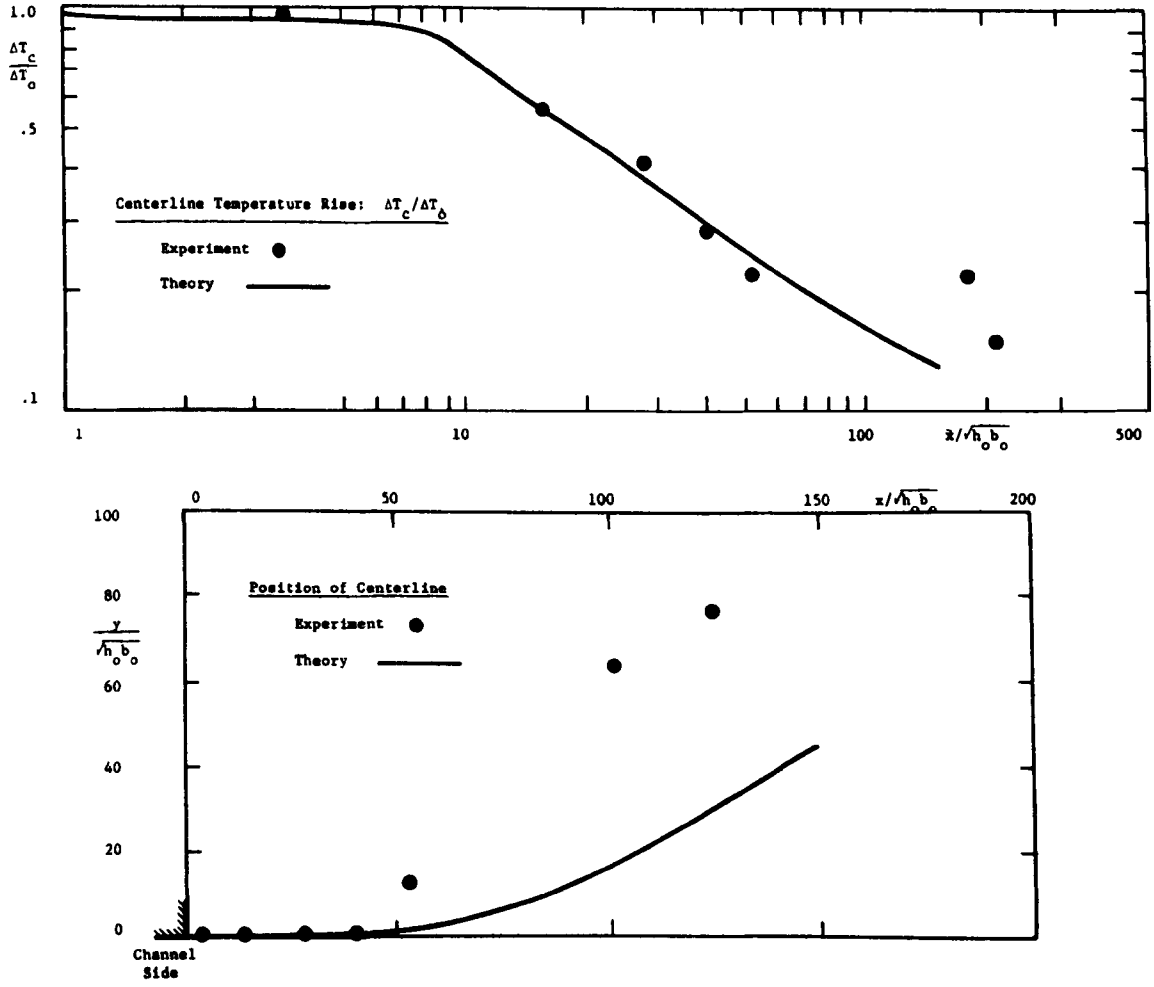

Figure 5-21. Theoretical Calculations and Experimental Data for Run 25.

$IF_o = 6.60$ $K/u_o = 2.8 \times 10^{-5}$ $V_{max}/u_o = .12$

$A = 3.95$ $S_x = \infty$

are too close to ambient values to be useful; and Tamai's data is severely affected by the fact that the experimental basin is no more than 40 times as wide as the discharge orifice. This inhibits the lateral entrainment which is so important in three-dimensional heated discharges.

Jen's (21) experiments are done with circular orifices and values of F_o from 18 to 180. He found that the centerline temperature drop, beyond the core region, is independent of F_o and given empirically by

$$\frac{\Delta T_c}{\Delta T_o} = \frac{14 R_o}{x} \tag{5.1}$$

where R_o is the initial jet radius. For $F_o = \infty$, the temperature rise beyond the core region predicted by the theory of this study is:

$$\frac{\Delta T_c}{\Delta T_o} = \frac{10.7\sqrt{h_o b_o}}{x} \tag{5.2}$$

which is valid for rectangular discharge channels. The experimental data for Jen indicates that the theoretical expressions for $F_o = \infty$ are approximately valid for $F_o > 15$. The quantity $\sqrt{h_o b_o}$ is the square root of half the discharge channel area. If it is assumed that for a fully submerged circular discharge pipe the proper scaling is also the square root of half the discharge area, then the quantity $\sqrt{h_o b_o}$ is replaced by $R_o \sqrt{\frac{\pi}{2}} = 1.25\ R_o$. Then the expression for the centerline temperature rise beyond the core region ($F_o = \infty$) and a fully submerged circular discharge pipe becomes, according to the theory of this study:

$$\frac{\Delta T_c}{\Delta T_o} = \frac{13.4\ R_o}{x} \qquad \text{(approximately valid for } F_o > 15\text{)} \qquad (5.3)$$

which is almost identical with Jen's empirical result (5.1). (see Figure 5-22) For circular discharges the aspect ratio should be taken as 2.0.

Wiegel (37) studied rectangular orifices with aspect ratios of 1/2 and 1/5 and F_o from 20 to 30. Figure 5-23 shows that his data, when normalized by $\sqrt{h_o b_o}$ falls close to the line given by Equation 5.2. Figure 5-23 also shows Wiegel's data for a discharge of F_o from 20 to 30, aspect ratio of 1/5, and bottom slopes from 1/200 to 1/50. The beginning of the entrainment region is delayed by the inhibition of vertical entrainment. Later dilution is seen to be a function of the slope value. The theory of this study satisfactorily reproduces the delay in initial entrainment but not the bahavior farther from the origin.

Hayashi (16) studied heated discharges from rectangular orifices into stagnant receiving water with no cross flow. His data and the corresponding theoretical calculations are shown in Figure 5-24. The data scatter is large and the agreement mostly qualitative. The results illustrate the property of heated discharges that a lower densimetric Froude number produces less dilution in the entrainment region but higher eventual heat loss far from the discharge point.

5.5 Summary of Jet Properties

The previous sections have considered the general structure of

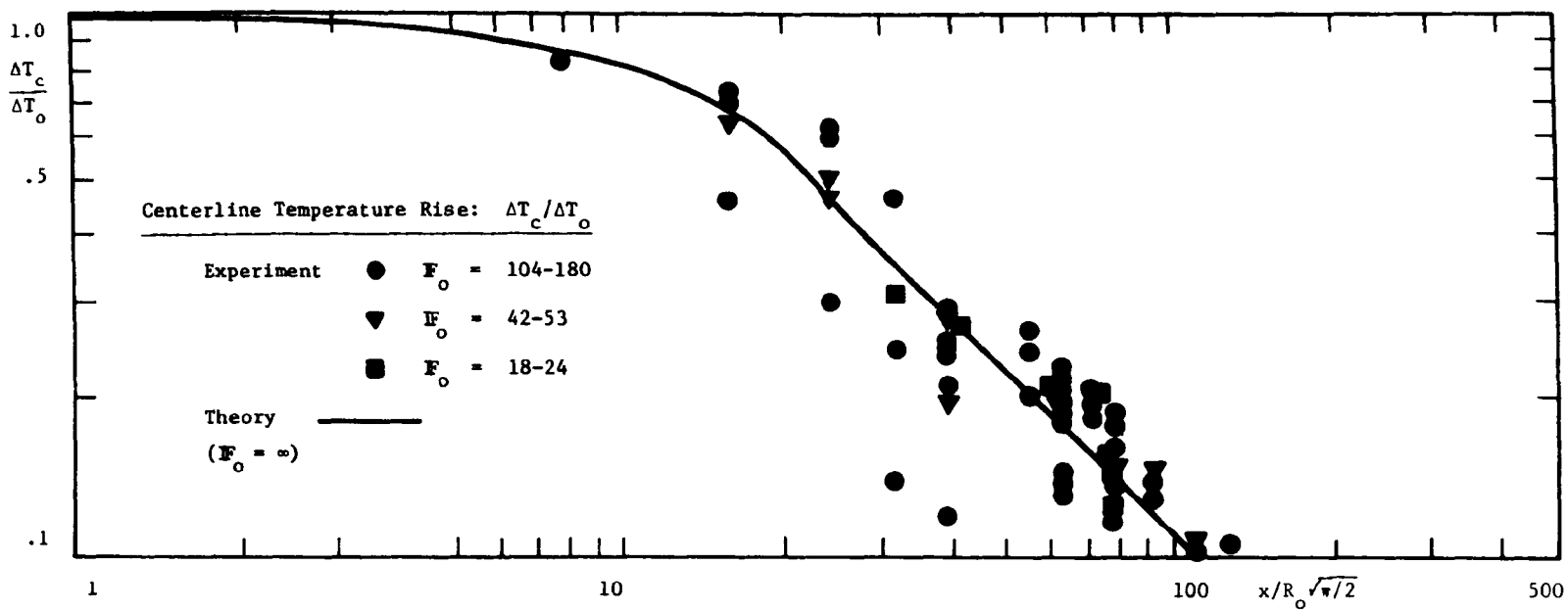

Figure 5-22. Theoretical Calculations and Experimental Data for Circular Orifices - Jen (21)

F_o = 18 - 180 $K/u_o = .5 \times 10^{-5}$ $V/u_o = 0$

A = 2.0 $S_x = \infty$

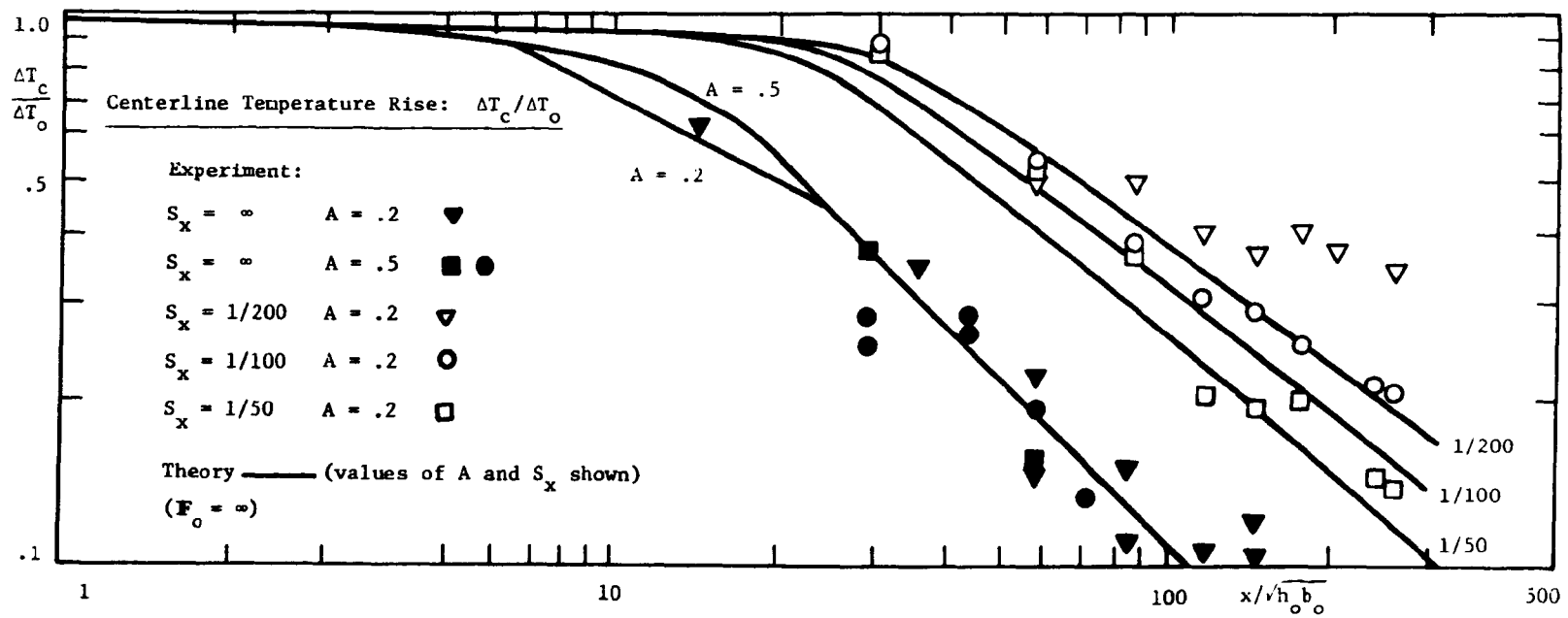

Figure 5-23. Theoretical Calculations and Experimental Data for Rectangular Orifices - Wiegel (36)

F_o = 20-30 $K/u_o = 1.0 \times 10^{-5}$ $V/u_o = 0$

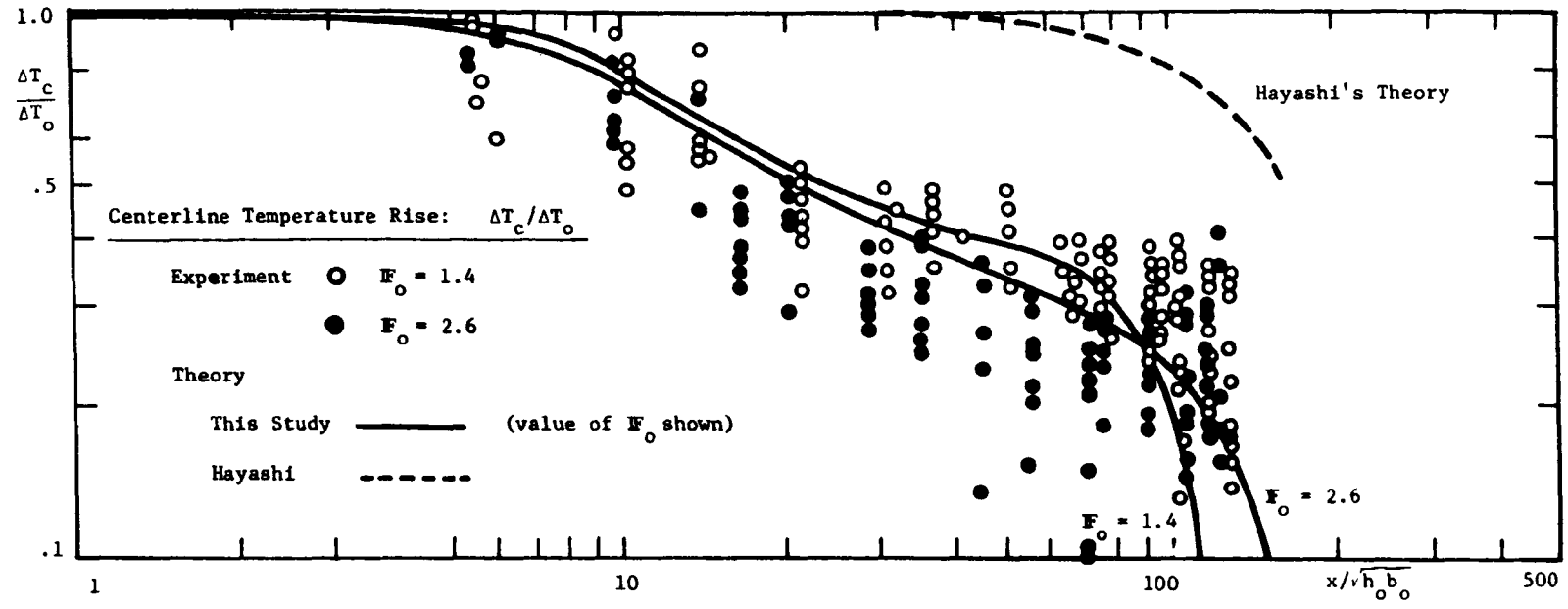

Figure 5-24. Theoretical Calculations and Experimental Data for Rectangular Orifices - Hayashi (16)

F_o = 1.4 and 2.6 $K/u_o = 10.0 \times 10^{-5}$ $V/u_o = 0$

A = 2.0 $S_x = \infty$

heated discharges, the dependence of the detailed structure of the discharge on the dimensionless parameters $\mathbb{F}_o$, A, K/u_o, S_x and V/u_o, and the ability of the theory of this study to reproduce experimental results. The theory successfully describes the jet behavior except for lateral spreading in the presence of a bottom slope. In this section the theoretical calculations are used to quantify some of the general statements in the previous sections.

The dilution and corresponding centerline temperature in the stable region are of interest since the stable region is a significant portion of the surface temperature distribution as previously discussed. The centerline temperature rise may be related to the dilution by assuming that no heat has been lost i.e. H = 1.0 and considering a position beyond the core region i.e. r = s = 0. The definitions of D and H may then be combined to yield:

$$\frac{\Delta T_c}{\Delta T_o} = \left[\frac{I_1}{I_7}\right]^2 \frac{1}{D} = \frac{1.5}{D} \qquad (5.4)$$

Figure 5-25 is a plot of the dilution in the stable region vs. $\mathbf{F}_o$ with values of A indicated. The points are the theoretical calculations for Runs 1-10 and for several of the previous investigations, all with no bottom slope or cross flow. Some tentative lines indicating the curves for constant A are drawn but many more calculations are needed to improve the reliability of the plot. Nevertheless it is clear that the ultimate stable dilution in a buoyant jet depends primarily upon $\mathbf{F}_o$ and to a lesser extent upon A.

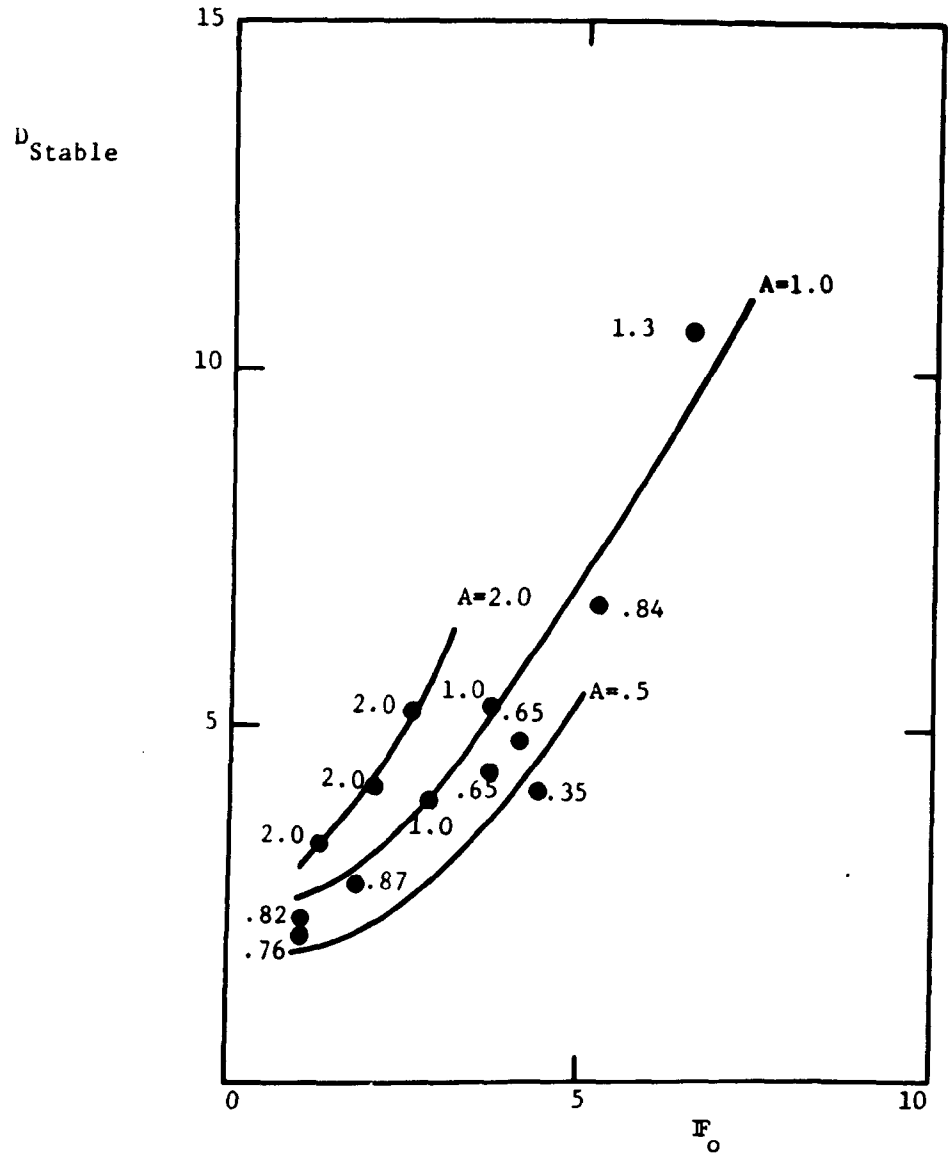

Figure 5-25. Dilution in the Stable Region of Buoyant Discharges (Points are calculated by the theoretical model - Values of A indicated)

The maximum depth of the discharge jet, $\frac{h_{max}}{\sqrt{h_o b_o}}$, is also of interest and may be determined from the theoretical calculations. Figure 5-26 indicates that the maximum vertical penetration of the jet is a function of $\mathbb{F}_o$ with a very small dependence upon A. The results are approximated by the following relationship:

$$\frac{h_{max}}{\sqrt{h_o b_o}} = .5\ \mathbb{F}_o \tag{5.5}$$

Other interesting features of the heated discharges treated in this study are the values of x at which the various jet regions begin. Unfortunately the boundaries of the jet regions are not well defined, transition zones being present between the regions. The lengths of the core regions, x_s and x_r, are not the same as for a non-buoyant jet, in which they are functions only of A, but are rather a function of both $\mathbb{F}_o$ and A in the buoyant discharge. In the absence of a great many calculations from which to make general plots, the detailed structure of each specific discharge is best determined by a separate theoretical calculation for each case.

In the previous section, little was said about the effect of the heat loss parameter, K/u_o, upon the jet behavior. For all but the lowest values of $\mathbb{F}_o$ and A, the theoretical calculations indicate that heat loss has no significant effect until after a stable region has formed and the jet has undergone considerable spreading. This is also indicated by the experimental data. Thus the value of K/u_o will affect only the rate

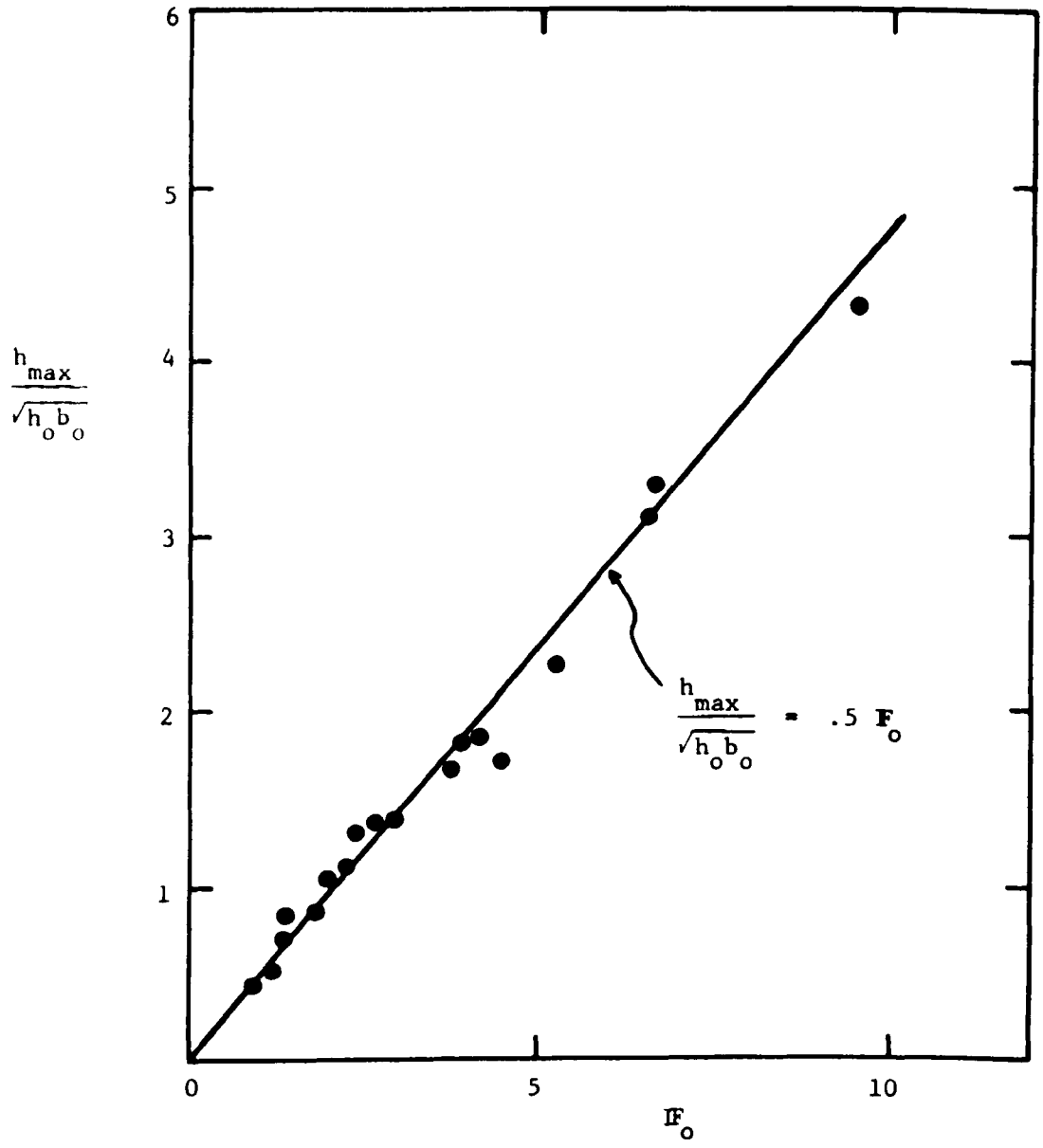

Figure 5-26. Maximum Jet Depth Vs. $\mathbb{F}_o$ as Calculated by Theory

at which the stable region loses heat. Since jet-like behavior ceases at this point, the value of K/u_o may be said to have no effect upon the region of the discharge considered in this study. Surface heat loss may, however, be important in the far field region as discussed in the following chapter.

VI. Applying the Theory

This chapter considers the use of the theoretical model for surface discharges of heated water in meeting the objectives outlined in Chapter 1 with respect to prototype temperature prediction and the design of scale models of heated discharges.

6.1 Prototype Temperature Prediction

Prediction of temperatures in the vicinity of a specific discharge configuration requires the parameters F_o, A, S_x, K/u_o, and V/u_o be specified in addition to ΔT_o, T_a, and the discharge channel area. The geometry of actual field configurations are rarely as simple as those assumed in the theoretical development and judgement must be exercised in the schematization of the discharge to a less complex form for which the dimensionless parameters may be given. This section is a discussion of the data requirements for treatment of a heated surface discharge by the theory of this study and of some schematization techniques.

The following are the physical data needed as input to the theoretical calculations:

The ambient temperature, T_a, is assumed in the theory to be constant in space and time. Actual ambient receiving water temperatures are often stratified vertically or horizontally and may be unsteady due to wind, tidal action or diurnal variations in solar heating. The natural stratification of the ambient water may be increased by accumulation of heat at the water surface if the discharge is in a semi-enclosed region. The value of the ambient temperature, for a given initial temp-

erature rise, ΔT_o, determines the initial density difference between the discharged and ambient water. Also the effectiveness of the entrainment of ambient water in reducing the discharge temperatures is a function of the ambient stratification.

If the temperature differences resulting from ambient stratification in the vicinity of the discharge are the same magnitude as the initial discharge temperature rise, the theoretical model of this study should not be applied without further development to account for the stratification. The theory is valid if an ambient temperature, T_a, may be chosen which is representative of the receiving water temperatures, that is, if the temporal or spatial variations in ambient temperature do not differ from T_a by more than a few degrees Fahrenheit.

The initial discharge temperature rise, ΔT_o, is determined from the discharge temperature, T_o, and the chosen ambient temperature, T_a. The value of ΔT_o will be equal to the temperature rise through the condensers only if the intake temperature is equal to T_a. Actual discharge temperatures should be relatively steady unless the power plant has several different condenser designs in which case the discharge temperature will vary with the plant load. Use of the theory requires that a constant value of ΔT_o be specified, the choice being based on the likely steady value of the discharge temperature.

The discharge channel geometry is important since the theory uses one half the square root of the discharge channel flow area as a scaling length. Calculation of the discharge densimetric Froude number, F_o, requires specification of the initial depth, h_o, and the aspect

ratio, A, requires both h_o and the initial width, b_o. Rectangular and circular discharge geometries are discussed in Chapter 5. The following procedure is suggested for any channel shape:

a) Let h_o be the actual maximum discharge channel depth so that calculation of F_o is not affected by the schematization.

b) Let b_o be such that the correct discharge channel area is preserved:

$$b_o = \frac{\text{channel area}}{2h_o} \tag{6.1}$$

Then the aspect ratio is given by:

$$A = \frac{h_o}{b_o} = \frac{2h_o^2}{\text{channel area}} \tag{6.2}$$

The discharge channel geometry may vary with time if the elevation of the receiving water changes due to tidal motion or other causes. In this case separate calculations for each elevation of the receiving water must be made, assuming that the steady state theory predicts the instantaneous temperature distribution.

The initial condenser water discharge velocity, u_o is a function of the power plant condenser water pumping rate and the channel area.

The bottom slope, S_x is usually not uniform as the theory assumes. The average value used as input to the theory should be close to the value of the slope near the discharge point since it is the initial

portion of the discharge jet which is most affected by the bottom slope.

The surface heat loss coefficient, K, may be determined from meteorological data as discussed by Brady (3) who gives several useful diagrams for estimation of K.

The cross flow velocity, V, in the receiving water may be measured by drogue surveys or estimated from current records or flow measurements in the case of a river. The theory accepts as input (see Appendix I) any analytical function which gives V as a function of x.

The dimensionless parameters $\mathbb{F}_o$, A, S_x, K/u_o, and V/u_o are functions of the above physical variables. The initial density difference $\Delta\rho_o$ does not appear explicitly in the theory but is represented by a T_o. In calculating the initial densimetric Froude number, $\mathbb{F}_o$, the actual value of $\Delta\rho_o$ should be used to minimize the error in the assumption that the coefficient of thermal expansion, a, is constant. This choice of $\Delta\rho_o$ is equivalent to choosing an average value of a over the temperature range T_a to $T_a + \Delta T_o$.

When the discharge channel densimetric Froude number, $\mathbb{F}_o$, is less than unity, a wedge of ambient water intrudes into the discharge channel as discussed in Chapter 2 and the heated flow will be forced to obtain a densimetric Froude number of unity at the discharge point (see Figure 2-4). The depth of the heated flow in the presence of a wedge, h_o^*, is given by: (12)

$$\frac{h_o^*}{h_o} = \mathbb{F}_o^{2/3} \tag{6.3}$$

where h_o and F_o are based on the channel dimensions. A flow area may be calculated based on the depth h_o^* and the aspect ratio calculated as described previously in this section. The actual discharge may be directed parallel to a wall which will effectively cut off lateral entrainment from one side of the jet. In this case the discharge may be schematized by assuming that the solid boundary is the centerline of a jet whose discharge channel is twice the width of the actual discharge (see Figure 6-1). The width b_o is then twice the width calculated by the procedure discussed previously.

More complicated arrangements of the discharge channel relative to the boundaries of the ambient receiving waters are beyond the capabilities of the theory of this study. If the discharge channel is nearly at right angles to the solid boundaries, the theory may be used as developed, or if the discharge is directed parallel to a straight boundary, the schematization described above may be used (see Figure 6-1). However, if it is not clear whether the jet will entrain water from one or both sides or if irregularly shaped solid boundaries will deflect the jet or distort it from the form assumed in the theory, a meaningful schematization is not possible.

Once the schematization of the discharge configuration is achieved, the theoretical calculation is performed by the computer program described in Appendix I. The inputs to the program for each calculation are F_o, A, S_x, K/u_o and V/u_o (as a function of $x/\sqrt{h_o b_o}$). The program outputs the values of $\Delta T_c/\Delta T_o$, u_c/u_o, $b/\sqrt{h_o b_o}$, $h/\sqrt{h_o b_o}$, $r/\sqrt{h_o b_o}$, $s/\sqrt{h_o b_o}$, θ, and the position of the jet centerline as a function of the distance along the centerline.

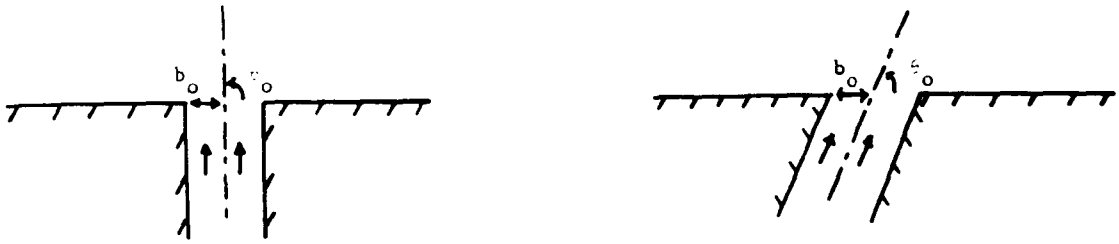

Discharges with Entrainment from Both Sides

Discharges with Entrainment from One Side

Schematization Possible

Schematization not Possible
Because of Irregular Geometry

Discharges with Obstructions

Figure 6-1. Discharge Channel Schematization

6.2 Modeling Heated Discharges

Laboratory scale models are used when the determination of temperatures in the vicinity of a prototype heated discharge is beyond the capability of analytical temperature prediction techniques. The theory of buoyant discharges developed in this study makes the construction of a model unnecessary if the region of interest is within the scope of the theory and if the prototype may successfully be schematized as discussed in the previous section.

Many prototype situations may be divided into a near field and a far field region. In the near field region the temperature distribution is controlled by jet entrainment, buoyant spreading and the local ambient cross flow. The theory of this study is a treatment of the near field. In the far field region ambient turbulent dispersion, convection, and surface heat loss determine the temperature distribution. The far field and near field are not independent of each other; the near field local ambient conditions are a function of the far field temperature and flow distribution and the input of heat to the far field is controlled by the near field characteristics.

Information may be needed about the near field or the far field or about both. Thermal pollution regulations may be such that maximum temperature levels must be met within the near field. On the other hand, an evaluation of the effects of the heated discharge upon the natural environment requires information about the far field temperature distribution. Recirculation studies may involve either of the regions, depending upon the relative location of the intake and discharge.

The theory of this study may be used to analyze the prototype temperature distribution if the near field temperatures are of interest. Schematization of the prototype near field is possible within the limitations discussed in the previous section. In general the theory may be applied if the far field ambient temperature is independent of the near field structure and if the geometry in the vicinity of the discharge is relatively simple.

In the case that the prototype does not yield to schematization or the far field conditions may not be estimated and may be a desired result of the analysis, a model study is required. If the far field temperature distribution is of interest the model must reproduce not only the far field physical phenomena but also the manner in which the near field inputs heat to the far field. In a heated discharge, this input is characterized by the dilution and corresponding temperature of the stable region. A model which is to reproduce the prototype far field temperature distribution must as a minimum requirement have a near field stable region with the same temperature rise and total flow at the same location as in the prototype.

The physical dimensions and fluid flows in a model of a heated discharge must be scaled from the prototype in a manner which insures similarity of the temperature distribution between model and prototype. Analytical statements of the proper scaling are commonly called "model laws" and will be different depending upon which physical process dominates the distribution of heat.

The characteristics of the near field behavior of buoyant jets

are discussed in Chapter 5. The dimensionless centerline controlling parameters are F_o, A, S_x and V/u_o, surface heat loss being unimportant in the near field. For similitude of model and prototype near field temperature distribution it is sufficient that F_o, A, S_x and V/u_o be the same in model and prototype. If the following scale ratios are defined:

z_r = ratio of vertical lengths in model and prototype

L_r = ratio of horizontal lengths in model and prototype

u_r = ratio of velocities in model and prototype

ΔT_r = ratio of temperature rises in model and prototype

$\Delta\rho_r$ = ratio of density differences in model and prototype

then the similarity requirements for the near field become:

$$F_{or} = 1.0 \text{ or } u_r = (\Delta\rho_r z_r)^{1/2} \tag{6.4}$$

$$A_r = S_{xr} = 1.0 \quad \text{or} \quad L_r = z_r \tag{6.5}$$

Thus the model must be undistorted (Equation 6.5) with the velocity ratio related to the length scale ratio and the density ratio by the well-known densimetric Froude model law (Equation 6.4). In most cases $\Delta\rho_r$ is not much different from unity because of the problems of working with very large or very small temperature differences in the laboratory.

The temperature and dilution in the stable region of a heated discharge are functions of F_o and A (see Figure 5-25). Thus even if

the detailed structure of the near field region is not of interest, similarity of near field heat input to the far field requires an undistorted, densimetric Froude model.

Distorted models have some distinct advantages over undistorted models especially in regard to laboratory space requirements. For a model to reproduce a large horizontal area of the prototype, making $z_r > L_r$ results in more workable water depths and higher model Reynolds numbers than if $z_r = L_r$. Distortion may be required by model laws for similarity of heat loss (14) or frictional effects (13) in the far field. If a distorted model is constructed, the aspect ratio and bottom slope will be different in the model than in the prototype even if $\mathbb{F}_o$ is the same. If this were the only effect of distortion, one might attempt to adjust the model values of $\mathbb{F}_o$ to compensate for the distortion of S_x and A. However, the ratios of dimensionless horizontal and vertical distances in model and prototype are:

$$\left[\frac{x}{\sqrt{h_o b_o}}\right]_r = \left[\frac{y}{\sqrt{h_o b_o}}\right]_r = \sqrt{\frac{L_r}{z_r}} \tag{6.6}$$

$$\left[\frac{z}{\sqrt{h_o b_o}}\right]_r = \sqrt{\frac{z_r}{L_r}} \tag{6.7}$$

The distortion thus tends to make the dimensionless x and y values of any physical position less in the model and the dimensionless z distances more. The model temperature distribution would be wider, longer, and

shallower than the prototype by a factor of $\sqrt{z_r/L_r}$. Varying F_o in the model arbitrarily may produce the same stable temperature or flow as the prototype but will not counteract the vertical and horizontal distortion of the temperature field. To compensate for a larger A in the model the value of F_o must be lowered in the model, which will produce an even wider and shallower model temperature distribution. It is concluded that it is impossible to build a distorted scale model which reproduces correctly the minimum required characteristics of the near field region of a heated surface discharge.

This result has been generally realized in the past. In certain cases a separate undistorted near field model has been constructed and the results used to adjust the discharge configuration in a distorted far field model to reproduce the stable region as observed in the near field model. The theory of this study should make it possible to circumvent the construction of near field models except in cases where geometrical complications are extreme and the theory cannot be used.

6.3 A Scale Model Case Study

A laboratory study of a heated discharge was described by Harleman and Stolzenbach (14) in 1968. The power plant is located on the coast of Massachusetts near Plymouth (see Figure 6.2). The primary discharge configuration under consideration was a surface discharge from a trapezoidal open channel into a coastal region having a relatively uniform bottom slope. The ambient cross current in the coastal zone was primarily due to wind-driven circulation. The intake was directly downwind of the discharge and was protected by two breakwaters (see Figure 6-2).

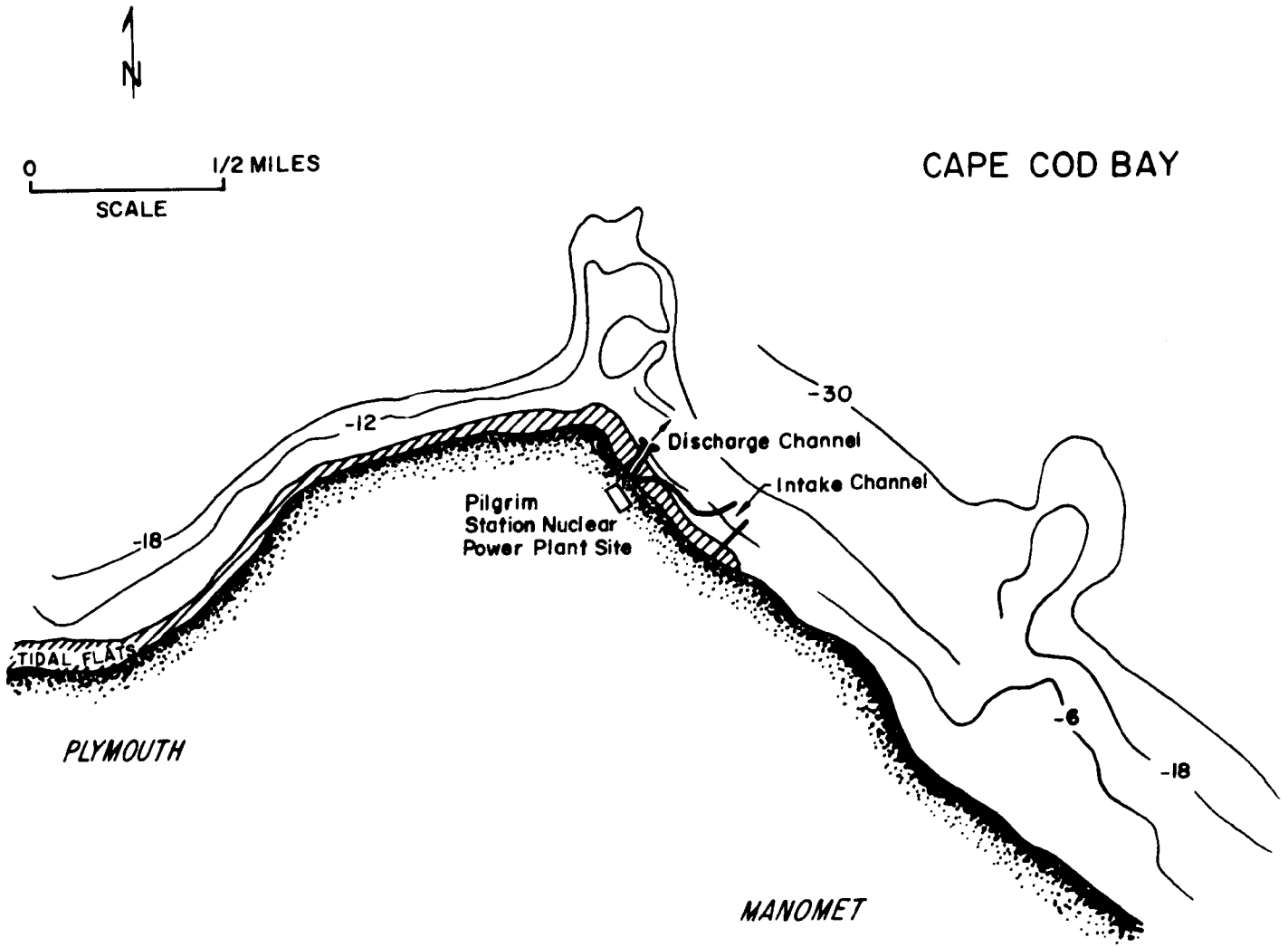

FIGURE 6.2 LOCATION OF POWER PLANT

The purpose of the model study was twofold: to determine the extent of far field recirculation of the heated water into the intake and to evaluate the near field temperature distribution. Thus both far and near field regions were of interest. Any analytical approach to predicting the near field temperatures would have been frustrated by the impossibility of determining whether the discharge jet entrainment would be cut off laterally by the breakwaters protecting the intake. This was a particularly strong possibility because the prevailing current would deflect the discharge toward the breakwaters.

In the model study $(\Delta T_o)_r$ was determined from the arbitrarily chosen condition $(\Delta\rho)_r = 1.0$. The horizontal length scale was $L_r = 1/240$ to allow reproduction of a sufficient length of coastline in the experimental basin. A vertical scale ratio was chosen as $z_r = 1/40$ on the basis of far field surface heat loss similarity (see Ref. 14). Harleman and Stolzenbach justified the 6 to 1 distortion in the model on the basis of Wiegel's data for bottom slopes with A = 1/5 (see Figure 5-23). This data indicated that the effects of the bottom slope and aspect ratio distortions tended to counteract each other with respect to ΔT_c. Figure 6-3 shows the temperature distribution measured in the model for a typical tide and current condition. The temperature distribution and observed current patterns in the model indicated that the discharge jet does entrain water from both sides.

With the knowledge that the entrainment in the jet is not laterally inhibited and using the theoretical results of the present study, the model and prototype may be schematized as discussed in the previous

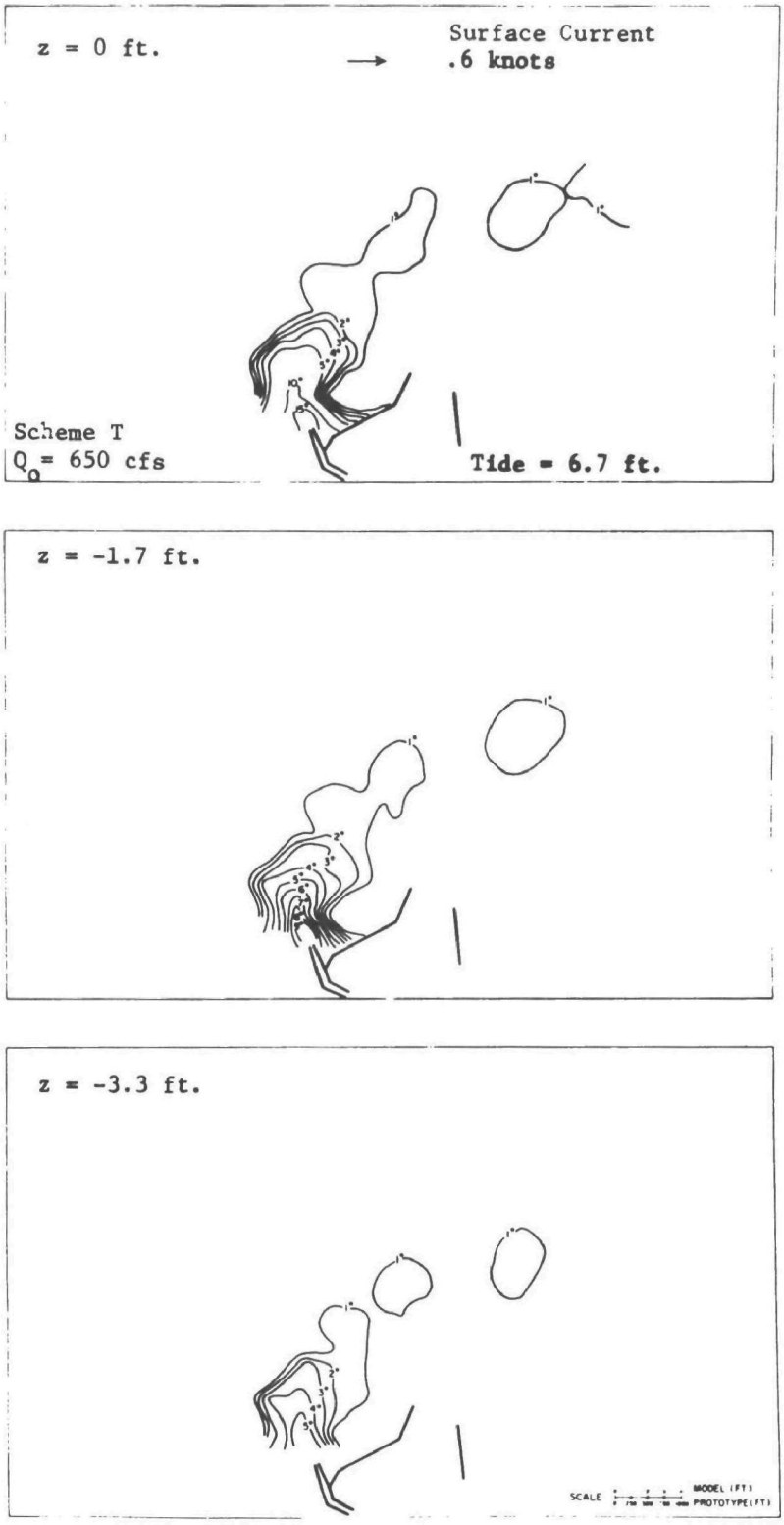

Figure 6-3. Temperature Rise Contours Measured in the Pilgrim Plant Model Study

section. The relevant parameters are:

	Prototype	Model
T_a	65°F	77°F
ΔT_o	28.7°F	25°F
Q_o	720 cfs	5.2 gpm
h_o	6.7 ft	.17 ft
b_o	26.0 ft	.11 ft
u_o	2.0 ft/sec	.32 ft/sec
V	1.0 ft/sec	.16 ft/sec
K	3.6×10^{-5} ft/sec (200 BTU/ft^2-day°F)	2×10^{-5} ft/sec (110 BTU/ft^2-day°F)
S_x	1/60	1/10
F_o	2.0	2.0
A	.26	1.5
K/u_o	1.8×10^{-5}	6×10^{-5}
V/u_o	.5	.5

The centerline surface temperatures observed in the model are shown in Figure 6-4. The model data is plotted in prototype distances (ft.) by scaling the model distances with the horizontal scale ratio $L_r = 1/240$. A theoretical calculation using the theory of this study with the tabulated model parameters is also shown. In the theoretical calculation $V/u_o = 0$ and $S_x = \infty$ since the cross flow in the model was not significant in the near field region and the large value of S_x(1/10) in the distorted model had little effect on such a low densimetric

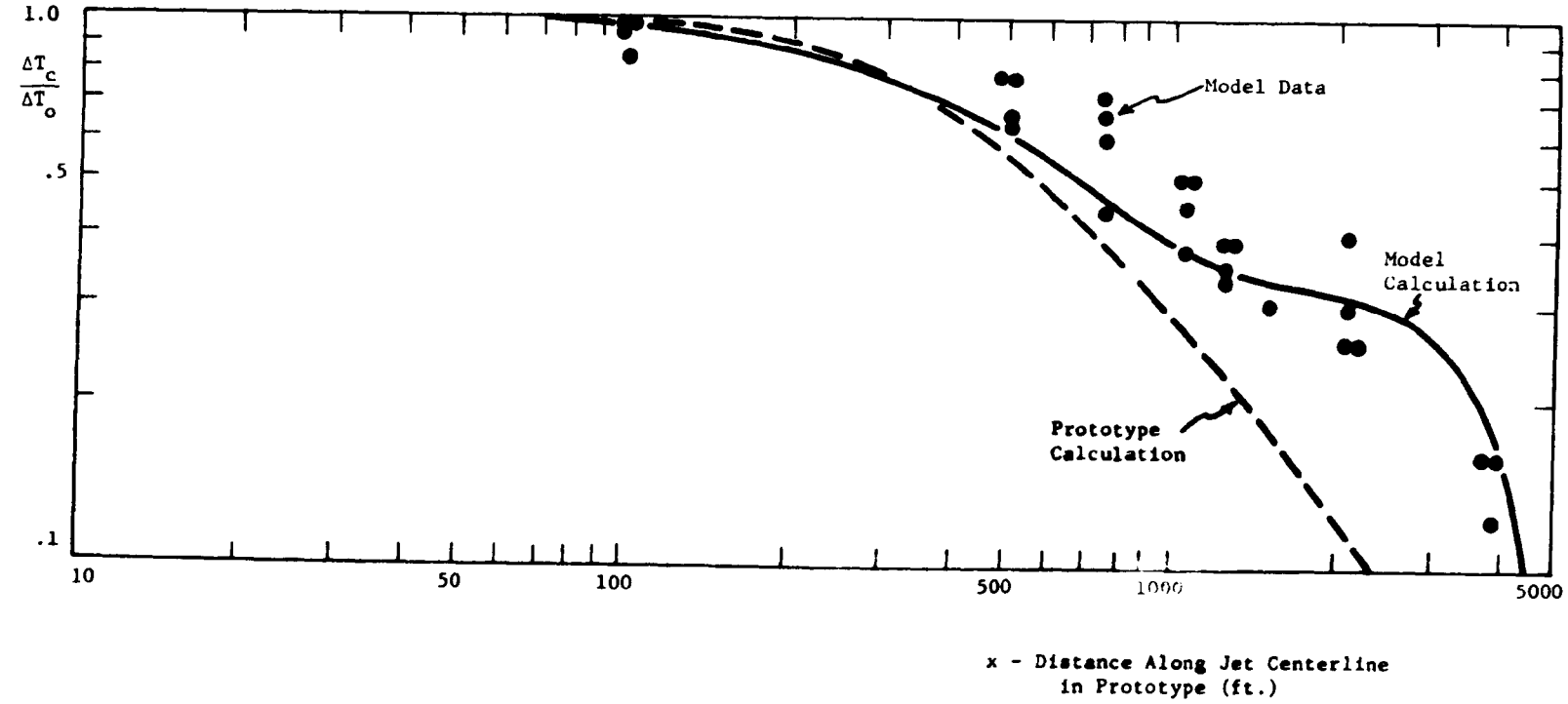

Figure 6-4. Theoretical Calculations and Model Data for Pilgrim Station Power Plant Model Study

Froude number discharge. The agreement between the model data and the theoretical calculation plotted in prototype distances (ft.) is good. It should be kept in mind that the schematization of the model for input to the theory is based upon the observed two-sided entrainment in the model. Figure 6-4 also shows the theoretical calculation for the prototype parameters. The model and prototype curves are close together up to about 500 ft. from the discharge, but the curves diverge from that point on. The argument based on Wiegel's data is obviously limited by the fact that the F_o in Wiegel's runs was 25 rather than 2. The model case shows the formation of a stable region which is apparently not present in the prototype although the limitations of the theory with respect to discharges with bottom slopes must be kept in mind. The model temperature distribution extends farther from the discharge than that of the prototype by roughly a factor of 2 to 3 which is what Equation 6.6 predicts for $z_r = 6L_r$ as was the case for this model.

This case study indicates that the distorted model does not reproduce the prototype temperature distribution although the results are conservative since the model showed higher temperature rises at corresponding distances from the discharge channel. Also the agreement of model results and theoretical calculations is a verification that the theory could be substituted for the construction and operation of the model as far as near field temperatures are concerned.

VII. Summary and Conclusions

7.1 Objectives

The use of natural waterways for disposal of power plant rejected heat necessitates prediction of the induced temperature distribution in the receiving water for:

a) Evaluation of thermal effects upon the natural environment.

b) Prevention of recirculation.

c) Design of discharge structures to meet temperature standards.

d) Scale model design.

This study treats a three-dimensional horizontal surface discharge of heated water from a rectangular open channel at the surface of a large ambient body of water which may have a bottom slope and a cross flow at right angles to the discharge. Of interest is the dependence of the temperature distribution in the vicinity of the discharge point upon the initial temperature difference between the ambient and discharged water, the initial discharge velocity, the discharge channel dimensions, the bottom slope, the ambient cross flow, and surface heat loss to the atmosphere. The primary objective is the prediction of the temperature distribution within the near field region dominated by turbulence generated by the discharge. Temperature distributions in the far field region where ambient processes dominate are beyond the scope of the study.

7.2 Theory and Experiments

Previous knowledge related to heated discharges consists of established theories for isothermal turbulent jets, measurements of the

physical properties of turbulent jets, experimental work on stratified turbulent flows, and a small number of laboratory experiments on heated surface jets. Previous attempts by others to develop a theory for heated three-dimensional surface discharges have been limited by failure to consider all the factors affecting the temperature distribution in the discharge.

The theory of this study has the following structure:

a) The discharge is basically a three-dimensional turbulent jet with a well defined turbulent region in which velocity and temperature are related to centerline values by similarity functions. Entrainment of ambient fluid into the turbulent region is proportional to the centerline velocity by an entrainment coefficient determined from non-buoyant jet theory. Unsheared core regions are accounted for in the theory.

b) The effect of buoyancy on the discharge is to reduce vertical entrainment and to promote lateral spreading of the of the jet as a density current. A major contribution of this study is the incorporation of these buoyancy effects into the turbulent jet theory.

c) Surface heat loss is assumed to be proportional to the surface temperature rise above ambient in the discharge and is accounted for throughout the entire discharge length.

d) The jet is deflected in the presence of an ambient

cross flow by entrainment of lateral momentum.

e) A bottom slope is assumed to inhibit vertical entrainment and buoyant lateral spreading as long as the discharge jet remains attached to the slope.

The theoretical development synthesizes the results of previous investigations of turbulent jets and stratified flows. No new empirical constants are introduced in the theory and the comparison of the theory with experiments does not involve any "fitting" of the theory to the data.

Experiments are performed in which all the controlling parameters are varied. Care is taken to insure establishment of fully turbulent steady state conditions in the discharge and accurate three-dimensional temperature measurements are taken. The data reduction results in centerline temperatures, discharge depths and widths, and centerline position in the case of an ambient cross current.

7.3 Results

A comparison of experimental data from this study and others with the theoretical calculations indicates that the theory reproduces the centerline temperature rise, the jet width and depth, and the centerline position. When a bottom slope is present good agreement is achieved for centerline temperature rises although the theory does not predict correctly the lateral spreading of the heated discharge.

Particular theoretical results are:

a) For nonbuoyant jets ($\mathbf{F}_o = \infty$) the discharge spreads linearly with distance from the origin. The centerline temperature

beyond the core region is given by:

$$\frac{\Delta T_c}{\Delta T_o} = 13.4 \frac{(1/2 \times \text{Area of Discharge Channel})^{1/2}}{x} \quad (7.1)$$

This expression is valid for discharges in which $F_o > 15$.

b) Buoyant jets ($1 < F_o < 10$) consist of a core region, an entrainment region, a stable region, and a heat loss region which marks the end of the jet and the beginning of the far field which is dominated by ambient processes.

c) Entrainment increases with increasing initial densimetric Froude number, F_o, and with discharge channel aspect ratio, $A = h_o/b_o$. The temperature and diluted flow in the jet in the stable region are functions of F_o and A (see Figure 5-25).

d) The vertical spread of the jet is inhibited and the lateral spread increased by the buoyancy of the discharge. Spreading increases with decreasing F_o and the maximum vertical penetration of the jet is a function of F_o (see Figure 5-26).

e) Surface heat loss has no significant effect on the behavior of the discharge in the core region, the entrainment region or the stable region.

f) Ambient cross flows whose velocities are small relative to the initial discharge velocity deflect the discharge centerline but do not greatly affect the temperature distribution.

g) Bottom slopes tend to inhibit vertical entrainment for heated discharges in which F_o is greater than about 5. Discharges with smaller values of F_o tend to separate from the bottom close to the discharge point and show little dependence on S_x, the value of the slope. There is some indication that in the region where the jet is attached to the bottom, the increased lateral area actually promotes increased entrainment in low F_o discharges.

This study of heated surface discharges satisfies its broad objectives to the following extent:

a) Evaluation of thermal effects: The theoretical model predicts the limits of the near field temperature distribution in which temperature rises are significant. The diversion of natural flows by jet entrainment is also a result of the theoretical calculations.

b) Recirculation: The dependence of the maximum vertical discharge depth on F_o (Figure 5-26) enables design of skimmer wall structures which require a knowledge of the depth of the heated layer at the intake. The calculated dimensions and position of the discharge jet aids in the location of an intake for prevention of recirculation.

c) Discharge design: The temperature and shape of the heated discharge is directly related to the densimetric Froude number, F_o, and the aspect ratio, A, of the discharge channel by the theory. Theoretical calculations may be

used to evaluate the success of discharge configurations in meeting temperature standards.

d) Scale models: The theory indicates that near field temperature distributions are not reproduced in distorted models. If the prototype discharge configuration may be schematized as input to the theory, the theoretical calculations will make construction of an undistorted near field model unnecessary.

7.4 Future Work

The immediate need is for incorporation into the theory of some of the more complex aspects of heated discharges:

a) Stratified receiving water: This requires more complicated assumptions for heat transfer within the jet and for buoyant spreading rates.

b) Accumulation of heat in the far field: If the far field is of finite size, the rejected heat will cause the far field surface temperature to rise until equilibrium with surface heat loss is achieved. The resulting stratification must be described and its interaction with the discharge entrainment and buoyant spreading accounted for as in (a) above.

c) A far field model: Buoyant plume theories (4) (28) have already been postulated. A complete picture of the temperature distribution in the near and far field regions awaits the development of a theory for the transition region between the near and far fields.

Much of the field data on temperatures in the vicinity of actual prototype discharges is either unavailable to researchers or is of such poor quality that it is unusable. Improvements in the theory of this study and the development of extensions as described above depend crucially upon the availability of accurate, complete field data for power plant heated discharges.

BIBLIOGRAPHY

1. Abramovich, G. N., The Theory of Turbulent Jets, The M.I.T. Press, M.I.T. Cambridge, Massachusetts, 1963.

2. Batchelor, G. K., An Introduction to Fluid Dynamics, Cambridge University Press, 1967.

3. Brady, D. K. and others, "Surface Heat Exchange at Power Plant Cooling Lakes", Edison Electric Institute, Publication No. 69-901, November 1969.

4. Brooks, N. H., "Diffusion of Sewage Effluent in an Ocean Current", in Waste Disposal in the Marine Environment, Pergamon Press, 1960.

5. Carter, H. H., "A Preliminary Report on The Characteristics of a Heated Jet Discharged Horizontally into a Traverse Current Part I - Constant Depth", Technical Report 61, Chesapeake Bay Institute, Johns Hopkins University, November 1969.

6. Cootner, P. H. and G. O. G. Lof, Water Demand for Steam Electric Generation, Resources for the Future, Inc., The Johns Hopkins Press, Baltimore, Maryland, 1965.

7. Deissler, R., "Turbulence in the Presence of a Vertical Body Force and Temperature Gradient", Journal of Geophysical Research, Vol. 67, No. 8, July 1962.

8. Edinger, J. E. and E. M. Polk, Jr., "Initial Mixing of Thermal Discharges into a Uniform Current", Report No. 1, Department of Environmental and Water Resources Engineering, Vanderbilt University, October 1969.

9. Ellison, T. H. and J. S. Turner, "Turbulent Entrainment in Stratified Flows", Journal of Fluid Mechanics, Vol. 6, Part 3, October 1959.

10. "Environmental Effects of Producing Electric Power", Hearings before the Joint Committee on Atomic Energy, Congress of the United States, U. S. Government Printing Office, 1969.

11. Fan, Loh-Nien, "Turbulent Buoyant Jets into Stratified or Flowing Ambient Fluids", W. M. Keck Laboratory of Hydraulics and Water Resources, California Institute of Technology, Report No. KH-R-15, June 1967.

12. Harleman, D. R. F., "Stratified Flow", in Handbook of Fluid Dynamics, V. L. Streeter, Ed., McGraw Hill Book Company, Inc., 1961.

13. Harleman, D. R. F. and K. D. Stolzenbach, "A Model Study of Thermal Stratification Produced by Condenser Water Discharge", M.I.T. Hydrodynamics Laboratory Technical Report No. 107, October 1967.

14. Harleman, D. R. F. and K. D. Stolzenbach, "A Model Study of Proposed Condenser Water Discharge Configurations for the Pilgrim Nuclear Power Station at Plymouth, Massachusetts", M.I.T. Hydrodynamics Laboratory Technical Report No. 113, May 1969.

15. Hayashi, T. and N. Shuto, "Diffusion of Warm Water Jets Discharged Horizontally at the Water Surface", IAHR Proceedings, Ft. Collins, Colorado, September 1967.

16. Hayashi, T. and N. Shuto, "Diffusion of Warm Cooling Water Discharged from a Power Plant", Proceedings of the 11th Conference on Coastal Engineering, London, 1968.

17. Hinze, J. O., Turbulence, McGraw Hill Book Company, Inc., 1959.

18. Hoopes, J. A. and others, "Heat Dissipation and Induced Circulations from Condenser Cooling Water Discharges into Lake Monona", Report No. 35, Engineering Experiment Station, University of Wisconsin, February 1968.

19. Industrial Waste Guide on Thermal Pollution, U. S. Department of the Interior, Federal Water Pollution Control Administration, Corvallis, Oregon, September 1968.

20. Ippen, A. T. and D. R. F. Harleman, "Steady-State Characteristics of Subsurface Flow", U. S. Department of Commerce, NBS Circular 521, "Gravity Waves", 1952.

21. Jen, Y. and others, "Surface Discharge of Horizontal Warm Water Jet", Technical Report HEL-3-3, University of California, December 1964.

22. Kato, H. and O. M. Phillips, "On the Penetration of a Turbulent Layer into Stratified Fluid", Journal of Fluid Mechanics, Vol. 37, Part 4, July 1969.

23. Lofquist, K., "Flow and Stress Near an Interface Between Stratified Liquids", The Physics of Fluids, Vol. 3, No. 2, March-April 1969.

24. Pai, Shih-I, Fluid Dynamics of Jets, D. Van Nostrand Company, Inc., 1954.

25. Parker, F. L. and P. A. Krenkel, Engineering Aspects of Thermal Pollution, Vanderbilt University Press, 1969.

26. Pearce, A. F., "Critical Reynolds Number for Fully-Developed Turbulence in Circular Submerged Water Jets", National Mechanical Engineering Research Institute, Council for Scientific and Industrial Research, CSIR Report MEG 475, Pretoria, South Africa, August 1966.

27. Phillips, O. M., The Dynamics of the Upper Ocean, Cambridge University Press, Cambridge, England, 1966.

28. Prych, E. A., "Effects of Density Differences on Lateral Mixing in Open-Channel Flows", W. M. Keck Laboratory of Hydraulics and Water Resources, California Institute of Technology, Report No. KH-R-21, May 1970.

29. Schlichting, H., Boundary-Layer Theory, Translated by J. Kesten, Sixth Edition, McGraw Hill Book Company, Inc., 1968.

30. Stefan, H. and F. R. Schiebe, "Experimental Study of Warm Water Flow Part I", Project Report No. 101, St. Anthony Falls Hydraulic Laboratory, University of Minnesota, December 1968.

31. Stefan, H. and F. R. Schiebe, "Experimental Study of Warm Water Flow into Impoundments Part III", Project Report No. 103, St. Anthony Falls Hydraulic Laboratory, University of Minnesota, December 1968.

32. Tamai, N. and others, "Horizontal Surface Discharge of Warm Water Jets", ASCE Journal of the Power Division, No. 6847, PO 2, October 1969.

33. Townsend, A. A., "The Mechanism of Entrainment in Free Turbulent Flow", Journal of Fluid Mechanics, Vol. 26, Part 4, 1966.

34. Townsend, A. A., The Structure of Turbulent Shear Flow, Cambridge University Press, Cambridge, England, 1956.

35. Wada, A., "Studies of Prediction of Recirculation of Cooling Water in a Bay", Proceedings of the 11th Conference on Coastal Engineering, London, 1968.

36. Webster, A. G., "Experimental Study of Turbulence in a Density-Stratified Shear Flow", Journal of Fluid Mechanics, Vol. 19, Part 2, June 1964.

37. Wiegel, R. L. and others, "Discharge of Warm Water Jet over Sloping Bottom", Technical Report HEL-3-4, University of California, November 1964.

38. Yevdjevich, Vujica M., "Diffusion of Slot Jets with Finite Length-Width Ratios", Hydraulic Papers, Colorado State University, Ft. Collins, Colorado, No. 2, 1966.

LIST OF FIGURES AND TABLES

LIST OF SYMBOLS

A - the discharge channel aspect ratio = h_o/b_o

a - the coefficient of thermal expansion = $-\frac{\partial \rho}{\partial T}$

b - horizontal distance from the jet centerline to the jet boundary

b_o - one half the width of a rectangular discharge channel

$b_{1/2}$ - horizontal distance from the jet centerline to the point where the temperature or velocity, as defined, is one half the centerline value

D - the ratio of flow in the jet to the initial discharge flow = dilution

D_{stable} - the dilution in the stable region of a heated discharge

$\left(\frac{db}{dx}\right)_{NB}$ - the spread of a non-buoyant jet

F - the densimetric Froude number = $\frac{u}{\sqrt{\frac{\Delta\rho}{\rho} gh}}$

F_o - the densimetric Froude number of the discharge channel = $\frac{u_o}{\sqrt{\frac{\Delta\rho_o}{\rho_a} gh_o}}$

F_L - the local densimetric Froude number in the jet = $\frac{u_c}{\sqrt{\frac{a\Delta T_c gh}{\rho_a}}}$

f - the similarity function for velocity = $\left[1 - (\zeta)^{3/2}\right]^2$

G_o - the turbulent integral time scale in a homogeneous flow

G_s - the turbulent integral time scale in a stratified flow

H - the ratio of heat flow in the jet to the initial discharge heat flow

h - vertical distance from the jet centerline to the jet boundary

h_o - depth of the discharge channel

h_o^* - depth of the heated flow at the point of discharge if a cold water wedge is present

$h_{1/2}$ - vertical distance from the jet centerline to the point where the temperature or velocity, as defined, is one half the centerline value

h_{max} - the maximum value of h obtained in a heated discharge

I_1 - $\int_o^1 f(\zeta)d\zeta = .4500$

I_2 - $\int_o^1 f^2(\zeta)d\zeta = .3160$

I_3 - $\int_o^1 t(\zeta)d\zeta = .6000$

I_4 - $\int_o^1 \int_\zeta^1 t(\zeta)d\zeta d\zeta = .2143$

I_5 - $\int_o^1 f(\zeta)\zeta^{1/2}\, d\zeta = .2222$

I_6 - $\int_o^1 f^2(\zeta)\zeta^{1/2} = .1333$

I_7 - $\int_o^1 f(\zeta)t(\zeta)d\zeta = .3680$

K - the surface heat loss coefficient

k - the thermal conductivity of water

L_r - the scale ratio for horizontal lengths between model and prototype

N - the Brunt-Vaisala frequency = $\left[-\frac{g}{\rho}\frac{\partial \rho}{\partial z}\right]^{1/2}$

p - the pressure

p_d - the dynamic pressure

p_a - the hydrostatic pressure

Q_o - the discharge channel flow

q_e - the entrainment flow into the jet per unit length of jet

R - the Eulerian time coefficient of a turbulent flow

R_i - the Richardson number = $\dfrac{\frac{g}{\rho}\frac{\partial \rho}{\partial z}}{\left[\frac{\partial u}{\partial z}\right]^2}$

R_H - the hydraulic radius of the discharge channel flow

R_o - the radius of a circular discharge pipe

$\mathbb{R}$ - the jet Reynolds number = $\dfrac{4u_o R_H}{\nu}$

r - the vertical distance from the jet centerline to the boundary of the core region

S_x - the bottom slope

s - the horizontal distance from the jet centerline to the boundary of the core region

T - the temperature

T_a - the ambient temperature

T_e - the equilibrium temperature

T_c - the jet surface centerline temperature

T_o - the temperature of the heated flow in the discharge channel

T_s - the temperature at the water surface

ΔT - temperature rise above ambient in the jet = $T - T_a$

ΔT_c - the surface temperature rise above ambient at the jet centerline $T_c - T_a$

ΔT_o - the temperature difference between the discharge and the ambient water = $T_o - T_a$

ΔT_r - the scale length for temperature rises between model and prototype

t - the similarity function for temperature = $1 - \zeta^{3/2}$

u,v,w - the velocity components in the fixed coordinate system

$\tilde{u},\tilde{v},\tilde{w}$ - the velocity components in the coordinate system relative to the centerline of a deflected jet

u_o - the velocity in the discharge channel

u_o^* - velocity of the heated flow at the point of discharge if a cold water wedge is present

u_c - the surface centerline jet velocity

u_r - the scale ratio for velocities between model and prototype

V - the ambient cross flow velocity

v_e - the lateral velocity of the entrained flow at the jet boundary

v_h - the lateral velocity in the jet at $y = s$ and $-h < z < -r$

v_s - the lateral velocity in the jet at $y = s$ and $-r < z < \eta$

w_b - the vertical velocity in the jet at $z = -r$ and $s < y < b$

w_e - the vertical velocity of the entrained flow at the jet boundary

w_r - the vertical velocity in the jet at $z = -r$ and $0 < y < s$

x,y,z - the fixed coordinate directions

$\tilde{x},\tilde{y},\tilde{z}$ - the coordinate directions relative to the centerline of a deflected jet

x_s - the distance from the jet origin to the point where $s = 0$

x_r - the distance from the jet origin to the point where $r = 0$

z_r - the scale ratio for vertical lengths between model and prototype

α - the entrainment coefficient

α_o - the entrainment coefficient in a homogeneous flow

α_s - the entrainment coefficient in a stratified flow

α_y - the lateral entrainment coefficient in non-buoyant and buoyant jets

α_z - the vertical entrainment coefficient in a non-buoyant jet

α_{sz} - the vertical entrainment coefficient in a buoyant jet

δ - a scaling quantity one order of magnitude less than unity

ε - the spread, $\frac{db}{dx}$, of the turbulent region in an undeflected non-buoyant jet

η - the water surface elevation

θ - the angle between the jet centerline ($\tilde{x}$ axis) and the y axis

θ_o - the angle between the discharge channel centerline and the y axis

ρ - the density of water

ρ_a - the density of the ambient water

ρ_o - the density of the heated discharge

$\Delta\rho$ - the difference between the density and the ambient water density = $\rho - \rho_a$

$\Delta\rho_o$ - the difference between the density of the heated flow in the discharge channel and the ambient density = $\rho_o - \rho_a$

$\Delta\rho_r$ - the scale length for density differences between model and prototype

Φ - viscous generation of heat

ν - the kinematic viscosity of water

Superscript * - indicates a characteristic magnitude of the variable

Superscript ' - indicates a turbulent fluctuating quantity

Appendix I. The Computer Program for Theoretical Calculations of Heated Discharge Behavior

The computer program is written in Fortran IV, G level, Mod 3 and the calculations for this study are done on an IBM 360-65 computer. The program consists of a main program and five subroutines:

MAIN: This program reads the input data for the theoretical calculations, sets up the initial conditions for each calculation, and calls the subroutine SRKGS which performs the actual calculations.

Input Data		Format
Number of Calculations		I3
One Set for Each Calculation	$\mathbb{F}_o$, S_x, A, K/u_o, θ_o, x_F, ERR, b_i	8F10.5
	I_1, I_2, I_3, I_4, I_5, I_6, I_7, ε	8F10.5
	V_1, V_2, V_3, V_4, V_5, V_6, V_7, V_8	8F10.5

where: $\mathbb{F}_o$ = initial densimetric Froude number = $\dfrac{u_o}{\sqrt{\dfrac{\Delta\rho_o}{\rho_a} g h_o}}$

S_x = bottom slope

A = channel aspect ratio = h_o/b_o

K/u_o = surface heat loss coefficient parameter

θ_o = initial angle of the discharge with the boundary of the ambient region

x_F = The value of $x/\sqrt{h_o b_o}$ at which the program should terminate for this calculation. In this study, x_F varies from 50 to 200.

ERR = Maximum allowable numerical truncation error in each dependent variable at each time step. In this study a value of ERR = .01 is used.

b_i = Initial value of $h/\sqrt{h_o b_o}$ and $b/\sqrt{h_o b_o}$ to be used in this calculation. The mathematical formulation of the theory sets h = b = 0 at x = 0 but in the numerical scheme a finite value must be given. A value of $b_i = 10^{-8}$ is used in this study. The calculations are found to be independent of the choice of b_i as long as it is small.

$I_1 - I_7$ = Integrations of similarity functions as given in Table 3-1.

ϵ = Spreading rate of the turbulent region of a non-buoyant jet.

$V_1 - V_8$ = Input constants describing the cross flow - (see description of subroutine CROSS).

SRKGS: This subroutine is a modified version of the IBM Scientific Subroutine Package routine DRKGS. It is a fourth order Runge-Kutta solution to a system of first order differential equations.

The form of the equation is:

$$\left[a_{ij} \right] \frac{dy_j}{dx} = c_i \qquad \text{(I-1)}$$

where a_{ij} is a coefficient matrix, y_j is a vector of the independent variables and c_i is a vector of the constants in the i equations.

The program MAIN provides the initial values y_{jo} and the subroutine SRKGS advances the solution by calling subroutine FCT (described below) which calculates the values of a_{ij}, c_i, and $\frac{dy_j}{dx}$ at each step. The solution is terminated when $x = x_f$. The results of each step are output by subroutine OUTP.

FCT: This routine takes the current values of x and y_j and computes the values a_{ij} and c_i according to the theory of this study, the system of equations in (I-1) are then solved by an IBM Scientific Subroutine DGELG which returns the values of $\partial y_j / \partial x$ to FCT which returns them to SRKGS.

OUTP: The independent variables y_j and u/u_o, $\Delta T_c/\Delta T_o$, $h/\sqrt{h_o b_o}$, $b/\sqrt{h_o b_o}$, $r/\sqrt{h_o b_o}$, $s/\sqrt{h_o b_o}$, db/dx, $x/\sqrt{h_o b_o}$, $y/\sqrt{h_o b_o}$, and θ . The values of these variables are output after each step of the calculation. The value of the dilution D and the heat flow H (see Chapter 5) are also calculated and printed. Each page of output displays the input variables for that particular calculation on the page heading.

CROSS: This subroutine is called whenever the velocity of the cross flow is required. The subroutine uses the values of V_1 - V_8 to compute the cross flow as a function of $x/\sqrt{h_o b_o}$. For each particular application of the theory, the subroutine may be different. The only requirements are as follows:

a) The subroutine returns the value of V/u_o at the given $x/\sqrt{h_o b_o}$.

b) V_8 is reserved for return of $\frac{1}{V/u_o} \frac{d(V/u_o)}{d(x/\sqrt{h_o b_o})}$ to the main program.

In this study the following algorithm is used;

$$V/u_o = V_3 \exp\left\{ - V_2 \left[V_4 \left(\frac{x}{\sqrt{h_o b_o}} \right) - V_1 \right]^2 \right\} \qquad \text{(I-2)}$$

$$V_8 = - 2V_4V_2 \left[V_4 \left(\frac{x}{\sqrt{h_o b_o}} \right) - V_1 \right] \qquad \text{(I-3)}$$

Note: The program may generate numerical underflows in certain calculations and corresponding error messages may be printed out. The result of an underflow calculation is set to zero automatically.

```
C       MAIN PROGRAM
        REAL I1,I2,IT,I5,I6
        DOUBLE PRECISION PRMT,Y,AUX,DERY,TH,XP,YP,B,U,G,H,BX,S,R,X,XLIM
        INTEGER RR
        EXTERNAL FCT,OUTP
        EQUIVALENCE (Y(1),TH),(Y(2),XP),(Y(3),YP),(Y(4),B),(Y(5),U)
        EQUIVALENCE (Y(6),G),(Y(7),H),(Y(8),BX),(Y(9),S),(Y(10),R)
        DIMENSION PRMT(5),Y(14),AUX(16,14),DERY(14),VEL(8)
        COMMON NPAGE,NLINE,FR,FI,AS,E,I1,I2,IT,T1,T2,EPS,I5,I6,SX,THI,VEL
        COMMON ERR
        RR=5
        READ (RR,1  ) KK
        DO 1 K=1,KK
        READ (RR,1  1) FR,SX,AS,E,THI,XLIM,ERR,BI
        READ (RR,1  1) I1,I2,T1,T2,I5,I6,IT,EPS
        READ (RR,1  1) (VEL(I), I=1,8)
-191-
  1     FORMAT (I3)
  1  1  FORMAT (8F1 .5)
        R=AS   5
        S=1./R
        B=BI
        H=BI
        U=1.
        G=1.
        BX=EPS
        TH=THI
        XP=
        YP=
        NPAGE=
        NLINE=5
        FI=(1./(FR  2))*S
        PRMT(1)=
        PRMT(2)=XLIM
        PRMT(3)=,000 1
        PRMT(4)=ERR
        DO 2 N=1,1
```

```
      DERY(N)=.1
    2 CONTINUE
      NDIM=10
      CALL SRKGS(PRMT,Y,DERY,NDIM,IHLF,FCT,OUTP,AUX)
    1 CONTINUE
      CALL EXIT
      END
```

```
      SUBROUTINE SRKGS(PRMT,Y,DERY,NDIM,IHLF,FCT,OUTP,AUX)                DRKG1070
      DOUBLE PRECISION PRMT,Y,DERY,AUX,A,B,C,X,XEND,H,AJ,BJ,CJ,R1,R2,     DRKG1110
     1DELT,DABS
      DIMENSION Y(14),DERY(14),AUX(8,14),A(4),B(4),C(4),PRMT(5)
      DO 1 I=1,NDIM                                                       DRKG1130
    1 AUX(8,I)=.0666666666666666667D0*DERY(I)                             DRKG1140
      X=PRMT(1)                                                           DRKG1150
      XEND=PRMT(2)                                                        DRKG1160
      H=PRMT(3)                                                           DRKG1170
      PRMT(5)=0.D0                                                        DRKG1180
      CALL FCT(X,Y,DERY)                                                  DRKG1190
C                                                                         DRKG1200
C     ERROR TEST                                                          DRKG1210
      IF(H*(XEND-X))38,37,2                                               DRKG1220
C                                                                         DRKG1230
C     PREPARATIONS FOR RUNGE-KUTTA METHOD                                 DRKG1240
    2 A(1)=.5D0                                                           DRKG1250
      A(2)=.29289321881345248D0                                           DRKG1260
      A(3)=1.7071067811865475D0                                           DRKG1270
      A(4)=.16666666666666667D0                                           DRKG1280
      B(1)=2.D0                                                           DRKG1290
      B(2)=1.D0                                                           DRKG1300
      B(3)=1.D0                                                           DRKG1310
      B(4)=2.D0                                                           DRKG1320
      C(1)=.5D0                                                           DRKG1330
      C(2)=.29289321881345248D0                                           DRKG1340
      C(3)=1.7071067811865475D0                                           DRKG1350
      C(4)=.5D0                                                           DRKG1360
C                                                                         DRKG1370
C     PREPARATIONS OF FIRST RUNGE-KUTTA STEP                              DRKG1380
      DO 3 I=1,NDIM                                                       DRKG1390
      AUX(1,I)=Y(I)                                                       DRKG1400
      AUX(2,I)=DERY(I)                                                    DRKG1410
      AUX(3,I)=0.D0                                                       DRKG1420
    3 AUX(6,I)=0.D0                                                       DRKG1430
      IREC=0                                                              DRKG1440
```

```
      H=H+H                                                          DRKG1450
      IHLF=-1                                                        DRKG1460
      ISTEP=0                                                        DRKG1470
      IEND=0                                                         DRKG1480
C                                                                    DRKG1490
C                                                                    DRKG1500
    4 IF((X+H-XEND)*H)7,6,5                                          DRKG1520
C     START OF A RUNGE-KUTTA STEP                                    DRKG1510
    5 H=XEND-X                                                       DRKG1530
    6 IEND=1                                                         DRKG1540
C                                                                    DRKG1550
C     RECORDING OF INITIAL VALUES OF THIS STEP                       DRKG1560
    7 CALL OUTP(X,Y,DERY,IREC,NDIM,PRMT)                             DRKG1570
      IF(PRMT(5))40,8,40                                             DRKG1580
    8 ITEST=0                                                        DRKG1590
    9 ISTEP=ISTEP+1                                                  DRKG1600
C                                                                    DRKG1610
C                                                                    DRKG1620
C     START OF INNERMOST RUNGE-KUTTA LOOP                            DRKG1630
      J=1                                                            DRKG1640
      DO 91 I=1,NDIM
      AUX(3,I)=0.D0
   91 AUX(6,I)=0.D0
   10 AJ=A(J)                                                        DRKG1650
      BJ=B(J)                                                        DRKG1660
      CJ=C(J)                                                        DRKG1670
      DO 11 I=1,NDIM                                                 DRKG1680
      R1=H*DERY(I)                                                   DRKG1690
      R2=AJ*(R1-BJ*AUX(6,I))                                         DRKG1700
      Y(I)=Y(I)+R2                                                   DRKG1710
      R2=R2+R2+R2                                                    DRKG1720
   11 AUX(6,I)=AUX(6,I)+R2-CJ*R1                                     DRKG1730
      IF(J-4)12,15,15                                                DRKG1740
   12 J=J+1                                                          DRKG1750
      IF(J-3)13,14,13                                                DRKG1760
   13 X=X+.5D0*H                                                     DRKG1770
```

```
   14 CALL FCT(X,Y,DERY)                                                    DRKG1780
      GOTO 10                                                               DRKG1790
C     END OF INNERMOST RUNGE-KUTTA LOOP                                     DRKG1800
C                                                                           DRKG1810
C                                                                           DRKG1820
C     TEST OF ACCURACY                                                      DRKG1830
   15 IF(ITEST)16,16,20                                                     DRKG1840
C                                                                           DRKG1850
C     IN CASE ITEST=0 THERE IS NO POSSIBILITY FOR TESTING OF ACCURACY       DRKG1860
   16 DO 17 I=1,NDIM                                                        DRKG1870
   17 AUX(4,I)=Y(I)                                                         DRKG1880
      ITEST=1                                                               DRKG1890
      ISTEP=ISTEP+ISTEP-2                                                   DRKG1900
   18 IHLF=IHLF+1                                                           DRKG1910
      X=X-H                                                                 DRKG1920
      H=.500*H                                                              DRKG1930
      DO 19 I=1,NDIM                                                        DRKG1940
      Y(I)=AUX(1,I)                                                         DRKG1950
      DERY(I)=AUX(2,I)                                                      DRKG1960
   19 AUX(6,I)=AUX(3,I)                                                     DRKG1970
      GOTO 9                                                                DRKG1980
C                                                                           DRKG1990
C     IN CASE ITEST=1 TESTING OF ACCURACY IS POSSIBLE                       DRKG2000
   20 IMOD=ISTEP/2                                                          DRKG2010
      IF(ISTEP-IMOD-IMOD)21,23,21                                           DRKG2020
   21 CALL FCT(X,Y,DERY)                                                    DRKG2030
      DO 22 I=1,NDIM                                                        DRKG2040
      AUX(5,I)=Y(I)                                                         DRKG2050
   22 AUX(7,I)=DERY(I)                                                      DRKG2060
      GOTO 9                                                                DRKG2070
C                                                                           DRKG2080
C     COMPUTATION OF TEST VALUE DELT                                        DRKG2090
   23 DELT=0.D0                                                             DRKG2100
      DO 24 I=1,NDIM                                                        DRKG2110
   24 DELT=DELT+AUX(8,I)*DABS(AUX(4,I)-Y(I))                                DRKG2120
      IF(DELT-PRMT(4))28,28,25                                              DRKG2130
```

```
C                                                                       DRKG2140
C       ERROR IS TOO GREAT                                              DRKG2150
   25 GO TO 26
   26 DO 27 I=1,NDIM                                                    DRKG2170
   27 AUX(4,I)=AUX(5,I)                                                 DRKG2180
      ISTEP=ISTEP+ISTEP-4                                               DRKG2190
      X=X-H                                                             DRKG2200
      IEND=0                                                            DRKG2210
      GOTO 18                                                           DRKG2220
C                                                                       DRKG2230
C       RESULT VALUES ARE GOOD                                          DRKG2240
   28 DO 50 K=1,10
      IF (Y(K)) 25,50,50
   50 CONTINUE
  281 CALL FCT(X,Y,DERY)                                                DRKG2250
      DO 29 I=1,NDIM                                                    DRKG2260
      AUX(1,I)=Y(I)                                                     DRKG2270
      AUX(2,I)=DERY(I)                                                  DRKG2280
      AUX(3,I)=AUX(6,I)                                                 DRKG2290
      Y(I)=AUX(5,I)                                                     DRKG2300
   29 DERY(I)=AUX(7,I)                                                  DRKG2310
      CALL OUTP(X-H,Y,DERY,IHLF,NDIM,PRMT)                              DRKG2320
      IF(PRMT(5))40,30,40                                               DRKG2330
   30 DO 31 I=1,NDIM                                                    DRKG2340
      Y(I)=AUX(1,I)                                                     DRKG2350
   31 DERY(I)=AUX(2,I)                                                  DRKG2360
      IREC=IHLF                                                         DRKG2370
      IF(IEND)32,32,39                                                  DRKG2380
C                                                                       DRKG2390
C       INCREMENT GETS DOUBLED                                          DRKG2400
   32 IHLF=IHLF-1                                                       DRKG2410
      ISTEP=ISTEP/2                                                     DRKG2420
      H=H+H                                                             DRKG2430
   33 IMOD=ISTEP/2                                                      DRKG2450
      IF(ISTEP-IMOD-IMOD)4,34,4                                         DRKG2460
   34 GO TO 35
```

```
   35 IHLF=IHLF-1                                                        DRKG2480
      ISTEP=ISTEP/2                                                      DRKG2490
      H=H+H                                                              DRKG2500
      GOTO 4                                                             DRKG2510
C                                                                        DRKG2520
C                                                                        DRKG2530
C     RETURNS TO CALLING PROGRAM                                         DRKG2540
   36 IHLF=11                                                            DRKG2550
      CALL FCT(X,Y,DERY)                                                 DRKG2560
      GOTO 39                                                            DRKG2570
   37 IHLF=12                                                            DRKG2580
      GOTO 39                                                            DRKG2590
   38 IHLF=13                                                            DRKG2600
   39 CALL OUTP(X,Y,DERY,IHLF,NDIM,PRMT)                                 DRKG2610
   40 RETURN                                                             DRKG2620
      END
```

```
      SUBROUTINE FCT(X,Y,DERY)
      INTEGER P
      INTEGER FLAG,SLOPE
      DOUBLE PRECISION A,DERY,X,Y,C,ERS,TH,XP,YP,B,U,G,H,BX,S,R,DABS
      REAL I1,I2,IT,I5,I6
      DIMENSION A(14,14),DERY(14),Y(14),VEL(8)
      COMMON NPAGE,NLINE,FR,FI,AS,E,I1,I2,IT,T1,T2,EPS,I5,I6,SX,THI,VEL
      COMMON ERR
      P=6
      TH=Y(1)
      XP=Y(2)
      YP=Y(3)
      B=Y(4)
      U=Y(5)
      G=Y(6)
      H=Y(7)
      BX=Y(8)
      S=Y(9)
      R=Y(10)
      IF (H) 700,700,701
  700 H=1.0D-7
  701 CONTINUE
      SLOPE=1
      FLAG=1
      CALL CROSS(XP,V)
      IF(V) 75,75,76
   75 EPSB=EPS
      FLAG=2
   76 IF (R-.00001) 80,80,81
   80 R=0.
      WINF=I1*U*EPS/2
      GO TO 811
   81 WINF=(I1-I2)*EPS*U
  811 IF (S-.00001) 82,82,83
   82 S=0.
      VINF=-I1*U*EPS/2
```

```
      GO TO 831
   83 VINF=-(I1-I2)*EPS*U
  831 VCT=DCOS(TH)*V
      VST=DSIN(TH)*V
      WINFS=WINF
      FIS=FI
      B1=S+B*I1
      B2=S+B*I2
      B3=B*I6
      B4=B*I5
      BG=S+B*T1
      BT=S+B*IT
      H1=R+H*I1
      H2=R+H*I2
      HGG=R*R*.5+T1*H*R+T2*H*H
      HT=R+H*IT
      HG=R+H*T1
      UM2=U*I2*I2+2.*VCT*I1*I1
      UM1= U*I2+2.*VCT*I1
  888 DO 1 N=1,14
      DO 1 NN=1,14
      A(N,NN)=0.
    1 CONTINUE
      GO TO (300,301), FLAG
  300 FI=.0000001
      GO TO 6
  301 ARG= 5*G*H/(U*U*FR*FR)
      IF(ARG)302,303,303
  302 ARG=0.
  303 IF (ARG-10.) 30,30,40
   40 WINF=0.
      GO TO 6
   30 WINF=WINF*EXP(-ARG)
    5 A(1,1)=U*U*B2*H2+2.*U*VCT*B1*H1+                    VCT*VCT*(S+B)*(R+H)
      A(2,2)=1.0
      A(3,3)=1.0
```

```
      A(4,4)=1.0
      DERY(4)= BX
      A(5,1)=-H*B*VST
      A(5,4)=I1*U*H*I1+H*VCT
      A(5,5)=I1*H*B*I1
      A(5,7)=I1*U*B*I1+B*VCT
      A(5,9)=U*H*I1+H*VCT
      A(5,10)=U*B*I1+B*VCT
      A(5,11)=-H*I1
      A(5,12)=B*I1
      A(6,1)=-2.*H*B*(U*I1*I1+VCT)*VST
      A(6,4)=U*H*UM2+T1*T2*H*H*G*FI+H*VCT*VCT
      A(6,5)=2.*H*B*(U*I2*I2+VCT*I1*I1)
      A(6,6)=T1*T2*H*H*B*FI
      A(6,7)=U*B*UM2+B*VCT*VCT    +T1*T2*2.*G*H*B*FI
      A(6,9)=U*H*UM1+H*VCT*VCT+T2*G*H*H*FI
      A(6,10)=U*B*UM1+B*VCT*VCT+T1*T1*G*H*B*FI
      A(6,11)=-H*UM1
      A(6,12)=B*UM1
      A(7,1)=-G*HG*BG*VST
      A(7,4)=G*(U*IT*HT+T1*VCT*HG)
      A(7,5)=G*HT*BT
      A(7,6)=U*HT*BT+VCT*BG*HG
      A(7,7)=G*(U*IT*BT+T1*VCT*BG)
      A(7,9)=G*(U*HT+VCT*HG)
      A(7,10)=G*(U*BT+VCT*BG)
      GO TO (304,305), FLAG
  304 A(8,8)=1.0
      DERY(8)=0.
      A(4,7)=-1.0
      DERY(4)=0.
      GO TO 306
  305 GO TO (3051,3052), SLOPE
 3051 A(8,1)=-(BX-EPSB)*VST*2.*(U*H1*B4+VCT*(R+H)*B)
      A(8,4)=(BX-EPSB)*(U*U*I6*H2+2.*VCT*U*H1*I5+VCT*VCT*(R+H))
      A(8,5)=(BX-EPSB)*2*(U*H2*B3+VCT*H1*B4)
```

```
      A(8,7)=(BX-EPSB)*(U*U*I2*B3+2.*VCT*B4*I1*U+VCT*VCT*B)
      A(8,8)=U*U*B3*H2+U*2.*VCT*B4*H1+VCT*VCT*(R+H)*B
      A(8,10)=(BX-EPSB)*(U*U*B3+2.*VCT*B4*U+VCT*VCT*B)
      DERY(8)=    G*HGG*FI
      GO TO 306
 3052 DERY(8)=0.
      A(8,8)=1.0
      DERY(4)= SX*DSIN(TH)
      A(4,4)=0.0
      A(4,7)=1.0
      A(4,10)=1.0
  306 IF (R) 50,50,51
   50 A(11,10)=1.0
      A(12,12)=1.0
      A(13,13)=1.0
      A(14,14)=1.0
      GO TO 60
   51 A(11,1)=-R*B*VST
      A(11,4)= I1*R*U+R*VCT
      A(11,5)= I1*R*B
      A(11,9)= U*R+R*VCT
      A(11,12)= -I1*B
      A(11,14)= -R
      A(12,1)=-2.*B*R*(U*I1+VCT)*VST
      A(12,4)=R*U*UM1+R*VCT*VCT+T1*G*FI*(.5*R*R+R*H*T1)
      A(12,5)=R*B*2.*(U*I2+VCT*I1)
      A(12,6)= T1*B*(.5*R*R+R*H*T1)*FI
      A(12,7)=T1*T1*B*R*G*FI
      A(12,9)=R*(U*U+2.*U*VCT+(R*.5+H*T1)*G*FI)+R*VCT*VCT
      A(12,10)=A(12,7)/T1
      A(12,12)= -B*UM1
      A(12,14)= -R*(U+VCT)
   60 IF (S) 61,61,62
   61 A(9,9)=1.0
      A(10,11)=1.0
      A(13,13)=1.0
```

```
      A(14,14)=1.0
      GO TO 70
   62 A(9,1)=-S*H*VST
      A(9,5)=I1*S*H
      A(9,7)=I1*S*U+S*VCT
      A(9,10)=S*U+S*VCT
      A(9,11)=I1*H
      A(9,13)=S
      A(10,1)=-2.*S*H*(U*I1+VCT)*VST
      A(10,5)=S*H*2.*(U*I2+VCT*I1)
      A(10,6)= I2*H*H*S*FI
      A(10,7)=S*U*UM1+S*VCT*VCT+T2*2.*H*G*S*FI
      A(10,10)=S*(U*U+2.*U*VCT+G*H*T1*FI+VCT*VCT)
      A(10,11)=H*UM1
      A(10,13)=S*(U+VCT)
      IF (R) 71,70,63
   63 A(13,1)=-R*S*VST
      A(13,5)= R*S
      A(13,13)= -S
      A(13,14)= R
      A(14,1)=-2.*R*S*(U+VCT)*VST
      A(14,5)=R*S*2.*(U+VCT)
      A(14,6)=(H*T1+R/2)*FI*R*S
      A(14,7)=G*T1*FI*R*S
      A(14,10)= G*FI*R*S
      A(14,13)=-S*(U+VCT)
      A(14,14)=R*(U+VCT)
   70 DERY(1)=-VST*(WINF*B1-VINF*H1)
      DERY(2)=DSIN(TH)
      DERY(3)=DCOS(TH)
      DERY(5)=(WINF*B-VINF*H)*I1
      DERY(6)=VCT*DERY(5)
      DERY(7)=-E*G*BG
      DERY(9)=S*WINF
      DERY(10)= VCT*DERY(9)
      DERY(11)=-R*VINF
```

```
      DERY(12)= VCT*DERY(11)
      DERY(13)= 0.
      DERY(14)=0.
      IF (V) 73,73,71
   71 VR=VCT*VEL(8)/VST
      DO 72 I=2,14
      DERY(I)=DERY(I)+A(I,1)*VR
   72 CONTINUE
   73 CONTINUE
      DO 20 I=1,14
      AMAX=0.0
      DO 21 J=1,14
      DA=DABS(A(I,J))
      IF (DA-AMAX) 21,21,22
   22 AMAX=DA
   21 CONTINUE
      IF (AMAX) 20,20,24
   24 DO 23 J=1,14
      A(I,J)=A(I,J)/AMAX
   23 CONTINUE
      DERY(I)=DERY(I)/AMAX
   20 CONTINUE
      ERS = .1D-16
      CALL DGELG(DERY,A,14,1,ERS,IER)
      IF (IER) 9,8,7
    9 WRITE (P,500) IER,FLAG,SLOPE
      WRITE (P,501) ((A(I,J),J=1,14),DERY(I),I=1,14)
      CALL EXIT
    7 WRITE (P,500) IER,FLAG,SLOPE
  500 FORMAT (1X,18HERROR IN MATRIX = ,I2,I4,I4)
  501 FORMAT (15(D8.2))
    8 GO TO (320,321), FLAG
  320 FLAG=2
      EPSB=DERY(4)
      FI=FIS
      GO TO 888
```

```
  321 GO TO (322,323),SLOPE
  322 SJ=DERY(7)+DERY(10)
      SXC=SX*DSIN(TH)
      IF (SXC-SJ) 3221,3221,323
 3221 SLOPE=2
      WINF=0.
      FI=.0000001
      GO TO 888
  323 FI=FIS
      VEL(8)=0.
      RETURN
      END
```

```
      SUBROUTINE OUTP(X,Y,DERY,IHLF,NDIM,PRMT)
      INTEGER P
      DOUBLE PRECISION DERY,Y,PRMT,X,TH,XP,YP,U,B,G,H,BX,S,R,XLIM
      REAL I1,I2,IT,I5,I6,M
      DIMENSION DERY(14),PRMT(5),Y(14),VEL(8)
      COMMON NPAGE,NLINE,FR,FI,AS,E,I1,I2,IT,T1,T2,EPS,I5,I6,SX,THI,VEL
      COMMON ERR
      TH=Y(1)
      XP=Y(2)
      YP=Y(3)
      U=Y(5)
      B=Y(4)
      G=Y(6)
      H=Y(7)
      BX=Y(8)
      S=Y(9)
      R=Y(10)
      P=6
      CALL CROSS(XP,V)
      IF (NLINE-50) 10,11,11
   11 NPAGE = NPAGE +1
      NLINE = 3
      WRITE (P,202) NPAGE
  202 FORMAT (1H1,24HBUOYANT JET CALCULATIONS,10X,5HPAGE ,I2)
      WRITE (P,2021)
 2021 FORMAT(/2X,2HFR,8X,2HSX,7X,2HAS,8X,1HE,6X,3HEPS,6X,3HTHI,7X
     1,2HI1,7X,2HI2,7X,2HI3,7X,2HI4,7X,2HI5,7X,2HI6,7X,2HI7,7X,3HERR)
      WRITE (P,203)FR,SX,AS,E,EPS ,THI,I1,I2,T1,T2,I5,I6,IT,ERR
  203 FORMAT (14(1X,F8.5)//)
      WRITE (P,300) (I,VEL(I), I=1,8)
  300 FORMAT (8(3X,3HVEL,I1,1H=,F8.3)//)
      WRITE (P,199)
  199 FORMAT (5X,1HX,8X,1HU,8X,1HT,8X,1HH,8X,1HB,8X,1HR,8X,1HS,7X
     1,2H M,8X,1HQ,8X,1HV,7X,2HHT,7X,2HXP,7X,2HYP,7X,2HTH/)
   10 NLINE = NLINE +1
      FC=(G*H/(U**U))
```

```
      FC=ABS(FC)
      FC=FC**.5
      FC=FR/FC
      Q=U*(S+B*I1)*(R+H*I1)+V*DCOS(TH)*(S+B)*(R+H)
      M=U*U*(S+B*I2)*(R+H*I2)+Q*V*DCOS(TH)
      M=M+U*V*DCOS(TH)*(S+B*I1)*(R+H*I1)
            M=M+(R*R*.5+T1*H*R+T2*H*H )*(S+B*T1)*G*FI
      HT=U*G*(S+B*IT)*(R+H*IT)+G*V*DCOS(TH)*(S+B*T1)*(R+H*T1)
      WRITE (P,200) X,U,G,H,B,R,S,M ,Q,V,HT,XP,YP,TH,IHLF
  200 FORMAT (3(1X,D8.3),1X,D9.3,10(1X,D8.3),1X,I3)
      IF (U-V*DCOS(TH)) 500,500,501
  500 PRMT(5)=1
  501 RETURN
      END
```

```
      SUBROUTINE CROSS(XP,V)
      REAL I1,I2,IT,I5,I6
      DOUBLE PRECISION XP
      DIMENSION VEL(8)
      COMMON NPAGE,NLINE,FR,FI,AS,E,I1,I2,IT,T1,T2,EPS,I5,I6,SX,THI,VEL
      A=XP*VEL(4)
      A= A-VEL(1)
      VEL(8)=-A*VEL(2)*2.0*VEL(4)
      A=A*A
      A=VEL(2)*A
      V=VEL(3)*EXP(-A)
      RETURN
      END
```

Appendix II. Deflected Jet in a Cross Flow:

Integration of the $\tilde{x}$ and $\tilde{y}$ Momentum Equations over the Entire Jet

This appendix considers the $\tilde{x}$ and $\tilde{y}$ momentum equations (3.108 and 3.109) for a deflected jet as given in Section 3.5.1. These equations will be integrated over the entire jet to give equations 3.122 and 3.123 which are used in Section 3.5.1 to develop the governing equations for deflected jets. The basic assumptions of the derivation are:

1) The velocity distributions within the jet are symmetrical about the $\tilde{y} = 0$ plane i.e. the cross flow does not greatly distort the jet from the structure defined for the undeflected jet in Chapter 3.

2) The flow outside the jet is irrotational.

Both of the above assumptions require that the cross flow velocity is small with respect to the initial jet velocity as discussed in Section 3.5.1.

The $\tilde{x}$ and $\tilde{y}$ equations (3.108 and 3.109) are:

$$\frac{\partial \tilde{u}^2}{\partial \tilde{x}} + \frac{\partial \tilde{u}\tilde{v}}{\partial \tilde{y}} + \frac{\partial \tilde{u}\tilde{w}}{\partial \tilde{z}} + 2\tilde{u}\tilde{v}\frac{\partial \theta}{\partial x} = \frac{ag}{\rho_a}\int_{\tilde{z}}^{-\infty} \frac{\partial \Delta T}{\partial \tilde{x}}\, d\tilde{z} - \frac{\partial \tilde{u}'\tilde{v}'}{\partial \tilde{y}} - \frac{\partial \tilde{u}'\tilde{w}'}{\partial \tilde{z}} - 2\tilde{u}'\tilde{v}'\frac{\partial \theta}{\partial x} \qquad \text{(II-1)}$$

$$\frac{\partial \tilde{u}\tilde{v}}{\partial \tilde{x}} + \frac{\partial \tilde{v}^2}{\partial \tilde{y}} + \frac{\partial \tilde{v}\tilde{w}}{\partial \tilde{z}} - \frac{\partial \theta}{\partial x}(\tilde{u}^2 - \tilde{v}^2) = \frac{ag}{\rho_a}\int_{\tilde{z}}^{-\infty} \frac{\partial \Delta T}{\partial \tilde{y}}\, d\tilde{z} - \frac{1}{\rho_a}\frac{\partial p_d}{\partial \tilde{y}} - \frac{\partial \tilde{v}'^2}{\partial \tilde{y}} - \frac{\partial \tilde{v}'\tilde{w}'}{\partial \tilde{z}}$$

$$+ (\tilde{u}'^2 - \tilde{v}'^2)\frac{\partial \theta}{\partial x} \qquad \text{(II-2)}$$

Figure II-1 shows a local section of the jet in which the shape of the jet cross section, A, is arbitrary except for symmetry about the $\tilde{y} = 0$ plane and in which the distribution of entrainment flow around the jet section circumference, C, is also arbitrary.

Equations II-1 and II-2 are integrated over the entire jet area, A, taking advantage of basic scale relationships introduced in Chapter 3, the symmetry of the jet, and the boundary conditions at the jet boundary as given in Chapter 3.

$$\frac{d}{d\tilde{x}} \iint_A \tilde{u}^2 \, d\tilde{y}d\tilde{z} = \frac{ag}{\rho_a} \iint_A \int_{\tilde{z}}^{-\infty} \frac{d\Delta T}{dx} \, d\tilde{z}' d\tilde{y}d\tilde{z} + \oint_C \tilde{u}(\tilde{w}d\tilde{y} - \tilde{v}d\tilde{z}) \qquad \text{(II-3)}$$

$$-\frac{d\theta}{d\tilde{x}} \iint_A \tilde{u}^2 \, d\tilde{y}d\tilde{z} = -\oint_C \frac{p_d}{\rho_a} \, d\tilde{z} + \oint_C \tilde{v}(\tilde{w}d\tilde{y} - \tilde{v}d\tilde{z}) \qquad \text{(II-4)}$$

It is assumed that everywhere on the jet boundary (see Figure II-1):

$$\tilde{u} = V \cos \theta \qquad \text{(II-5)}$$

Noticing that the total entrainment per unit length of jet, q_e, is given by:

$$q_e = \oint_C (\tilde{w}d\tilde{y} - \tilde{v}d\tilde{z}) \qquad \text{(II-6)}$$

then the integrated $\tilde{x}$ equation (II-3) becomes:

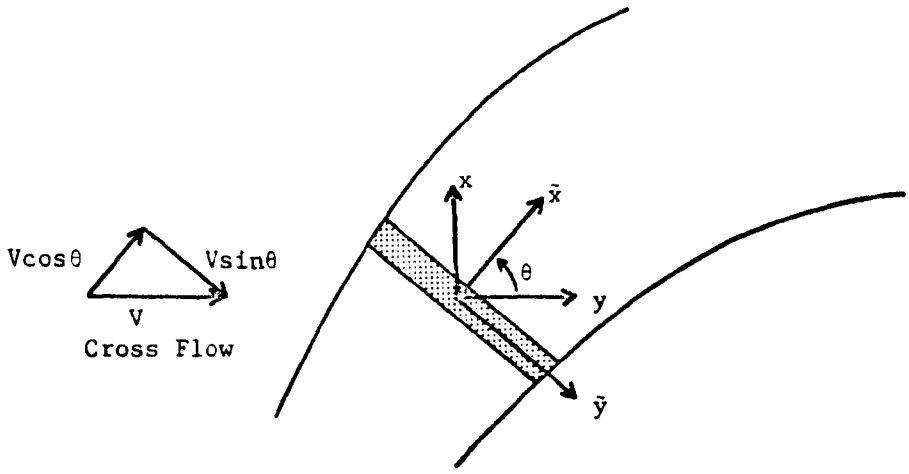

Top View of Deflected Jet

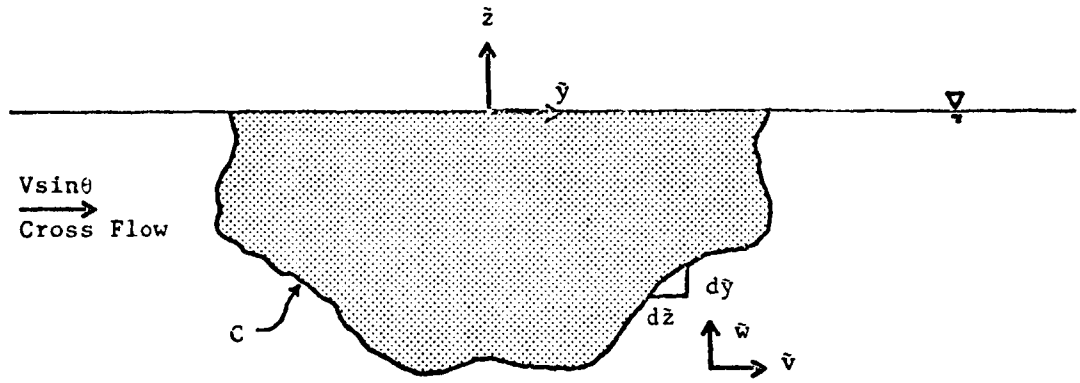

Cross Section of Jet

Total Entrainment/Unit Length = q_e

Figure II-1. Generalized Cross Section of a Deflected Jet

$$\frac{d}{d\tilde{x}} \oiint_A \tilde{u}^2 \, d\tilde{y}d\tilde{z} = \frac{ag}{\rho_a} \oiint_A \int_z^{-\infty} \frac{d\Delta T}{d\tilde{x}} \, d\tilde{z}'d\tilde{y}d\tilde{z} + q_e V \cos\theta \qquad \text{(II-7)}$$

The above equation, when the integrations are written in terms of the jet geometry defined in Chapter 3, is the desired result i.e. Equation 3.113.

The $\tilde{y}$ momentum Equation (II-4) is not so easily dealt with since the velocities on the boundary are not known without determining the flow of the ambient fluid around the jet. The assumption of irrotational flow makes it possible to use several properties of potential flows to evaluate the terms in II-4.

A Bernoulli equation is written from a point far from the jet to the jet boundary:

$$\frac{\rho_a V^2}{2} + p_{d\infty} = \left| p_d + \frac{1}{2} \rho_a [\tilde{u}^2 + \tilde{v}^2 + \tilde{w}^2] \right|_{\text{on C}} \qquad \text{(II-8)}$$

where $p_{d\infty}$ is the dynamic pressure far from the jet. This may be written:

$$p_d = H - \frac{1}{2} \rho_a [\tilde{v}^2 + \tilde{w}^2] \quad \text{on C} \qquad \text{(II-9)}$$

$$\text{where} \quad H = \frac{\rho V^2}{2} + p_{d\infty} - \rho V^2 \cos^2\theta \qquad \text{(II-10)}$$

is constant and will not contribute to the pressure integral over the

circumference of the jet.

Then Equation II-4 becomes:

$$-\frac{d\theta}{d\tilde{x}} \iint_A \tilde{u}^2 \, d\tilde{y}d\tilde{z} = \oint_C \left[\frac{1}{2} (\tilde{w}^2 - \tilde{v}^2) \, d\tilde{z} + \tilde{v}\tilde{w}d\tilde{y} \right] \qquad \text{(II-11)}$$

Defining a complex coordinate system in the $\tilde{y}$-$\tilde{z}$ plane

$$\zeta = \tilde{y} + i\,\tilde{z} \qquad \text{(II-12)}$$

and a complex potential, Ω, for which the velocities $\tilde{v}$ and $\tilde{w}$ are given by

$$\frac{d\Omega}{d\zeta} = \tilde{v} - i\,\tilde{w} \qquad \text{(II-13)}$$

Equation II-11 becomes

$$-\frac{d\theta}{d\tilde{x}} \iint_A \tilde{u}^2 \, d\tilde{y}d\tilde{z} = \text{Real} \quad \frac{i}{2} \oint_C \left(\frac{d\Omega}{d\zeta} \right)^2 d\zeta \qquad \text{(II-14)}$$

Batchelor (2) shows that for an arbitrary shaped cylinder in the presence of a cross flow, V sin θ, and having a total mass flux per unit length into the cylinder q_e the above integral may be easily evaluated and the integrated $\tilde{y}$ equation becomes simply:

$$\frac{d\theta}{d\tilde{x}} \iint_A \tilde{u}^2 \, d\tilde{y}d\tilde{z} = - q_e \, V \sin \theta \qquad \text{(II-15)}$$

which is the desired result.